

CARDIFF UNIVERSITY



**Time-Resolved Spectroscopy of Colour
Centres in Diamond**

by

Amber May Wassell

A thesis presented for the degree of
Doctor of Philosophy

School of Physics and Astronomy

May 2021

Abstract

Diamond is an extraordinary crystalline material which exhibits many extreme material properties. It is one of the hardest materials known, and it has unrivalled transparency to light across the ultraviolet, visible, infrared and THz bands. Its relatively high refractive index enhances internal reflections and gives diamond its signature sparkle. The high-value of natural diamond necessitates robust investigation of a gemstone's provenance. This was the motivation behind the research described in this thesis.

Spectroscopy provides a way to characterise defects and impurities that have been incorporated into the diamond lattice, and which may reveal clues about the growth conditions. With the increased prevalence of synthetic diamond material in the gemstone market, there is a growing need for better screening. Given that it is becoming common practice for less experienced diamond appraisers to carry out this task, it is important there are simple assistive technologies which are both trustworthy and time-efficient to aid appraisers in grading.

A bespoke diamond imaging rig was constructed to investigate the spectroscopic properties of suspect defects within the diamond lattice that might help differentiate between natural and synthetic gemstones. The imaging system revealed an unusual photoluminescent spectral signature with a wavelength of 499 nm. This signature had not previously been observed in natural diamond. This spectral feature became the major focus of this work.

A systematic study of synthetic material of known composition led to the hypothesis that this signature is indicative of silicon incorporation during growth. Natural growth conditions preclude the incorporation of this element. A key refinement of the hypothesis was that the coexistence of nitrogen in addition to silicon was necessary for the formation of the defect associated with this spectral signature. Furthermore, the 499 nm spectral feature was only observed in samples that had been post-growth annealed in a restricted temperature window where nitrogen vacancies are known to be mobile. Based on these observations, it is proposed that the possible structure of the 499 nm colour centre is narrowed to a small family of $\text{Si}_x \text{N}_y \text{V}_z$ complexes.

This is an important result because the observation of this 499 nm photoluminescence feature in a gemstone of unknown provenance can potentially be used to identify whether the material is synthetic in origin.

Acknowledgements

Firstly, I would like to thank my supervision team, Dr Colin McGuinness, Dr Chris Hodges and Dr Steven Lynch. Colin, thank you for going out of your way time and time again to help me, your kindness never failed to surprise me, I hope you enjoy all your newfound spare time now I am out of your hair. Chris, your support throughout has been incredible, you have taught me so many lab skills and you were always there with the emergency Jaffa cakes when things got hard. Steve, thank you for helping me learn theory I never thought I could master and for supervising me during this PhD.

I would like to thank De Beers Technologies for their financial support for this PhD. Also, to the friendly members of staff who helped me during my time there.

I thank all my friends who have supported me through this journey and kept things fun and entertaining even when things were not always going so well. Olivia, you have supported me from the start and cheered me on all the way, I could not ask for a better cheerleader. Georgie, thank you for always making me focus and picking me up (literally) when I'd had enough. Jess, thank you for being my lab partner in crime, these last few years would not have been half as much fun without you. Bethan & Sam thanks for all the PhD advice over the years, I'm not sure what Devon will be like without a PhD or two to discuss.

Dave, this thesis could not have been completed without you, thanks for your continued love and support during this process and for all the help you have given me throughout my countless years at university. They say diamonds are forever, well so are you.

Last and by no means least, I would like to thank my family for all their love and support over my many years of education, especially to Anne for never getting tired of reading my thesis. Special thanks go to my mom, Julie Wassell, and dad, Mark Wassell, who have worked tirelessly over the years to help me get where I am today. If it were not for all the cue cards I don't know if I would ever have gotten here. It is to them I dedicate this thesis.

Publications

Published papers

Amber M Wassell, Colin D McGuinness, Chris Hodges, Peter MP Lanigan, David Fisher, Philip M Martineau, Mark E Newton, and Stephen A Lynch. Anomalous green luminescent properties in cvd synthetic diamonds. *physica status solidi (a)*, 2018.

Colin D McGuinness, Amber M Wassell, Peter MP Lanigan, and Stephen A Lynch. Separation of natural from laboratory-grown diamond using time-gated luminescence imaging. *Gems & Gemology*, 56(2), 2020.

Presentations

De Beers 68th Diamond Conference, The University of Warwick. Poster presentation. ‘Time resolved spectroscopy of the 499 nm feature in CVD diamond samples’

Hasselt Diamond Workshop SBDD XXIII. Poster presentation. ‘Time-resolved luminescence spectroscopy of the 499 nm spectral feature in synthetic CVD single crystal diamond’

De Beers 69th Diamond Conference, The University of Warwick. Poster presentation. ‘Anomalous Green Luminescent Properties in CVD Synthetic Diamonds’

Hasselt Diamond Workshop SBDD XXIV. Poster presentation. ‘Prompt and delayed luminescence properties of natural and laboratory grown diamonds’

Contents

Abstract	i
Acknowledgements	ii
Publications	iii
List of Figures	vii
List of Tables	xvi
1 Motivation	1
1.1 History of Diamond	1
1.2 Diamond: A Miraculous Material	2
1.3 The Diamond Market	2
1.3.1 The Synthetic ‘Problem’	3
1.4 Diamond for quantum technologies	4
1.5 Thesis Overview	5
2 Background Theory	7
2.1 Introduction	7
2.2 Diamond Structure	7
2.2.1 Diamond’s Extreme Properties	8
2.2.2 Natural Diamond Formation	9
2.3 Synthetic Diamond Production	10
2.3.1 High Pressure High Temperature Diamond Synthesis (HPHT)	11
2.3.2 Chemical Vapour Deposition Diamond Synthesis (CVD)	12
2.4 Diamond Treatments	12
2.4.1 Heat treatment	13
2.4.2 Irradiation treatment	14
2.5 Defects in Diamonds	14
2.5.1 Nitrogen Defects	15
2.5.1.1 Isolated Nitrogen	15
2.5.1.2 Aggregated Nitrogen	16
2.5.1.3 Nitrogen Vacancy centre	17

2.5.2	Silicon Vacancy	18
2.5.3	Boron	20
2.6	Luminescence Mechanism	20
2.6.1	Fluorescence/Rapid Luminescence	21
2.6.2	Phosphorescence/Delayed Luminescence	21
2.7	Optical Techniques for Synthetic Diamond detection	22
2.7.1	Ultra Violet-Visible Spectroscopy	22
2.7.2	Photoluminescence (below bandgap)	24
2.7.3	Deep UV excited surface luminescence	25
2.7.4	Fourier Transform Infra-Red spectroscopy	27
2.8	Motivation	29
3	Experimental theory	31
3.1	Introduction	31
3.2	Dispersive Spectrometers	31
3.2.1	Grating geometry: Czerny-Turner	32
3.2.2	Resolution	32
3.3	Time-resolved Imaging	34
3.4	Experimental equipment	35
3.4.1	Spectrometer	35
3.4.2	Light Source	36
3.4.3	Detector	38
3.4.3.1	Spectroscopy detectors	38
3.4.3.2	Imaging detectors	39
3.5	Cryogenics	40
3.6	Samples and post processing	40
3.7	Conclusion	41
4	Time-Gated Luminescence Imaging of Natural and Synthetic Diamonds	43
4.1	Background and Motivation	43
4.1.1	UV excitation of diamond	44
4.1.2	Other relaxation paths	44
4.1.3	Fermi's Golden Rule	45
4.1.4	Atomic Systems	45
4.1.5	Molecular Systems	45
4.1.6	Penetration depth	48
4.1.7	Diamond types	48
4.1.8	Motivation	49
4.2	Time-Resolved Imaging Rig	50
4.2.1	Sample Selection	50
4.3	Natural Diamond Samples	51
4.3.1	Type IIa	51
4.3.2	Type Ia	53
4.3.3	Type IIb	55
4.3.4	Unusual natural diamond	57
4.4	CVD Diamond Samples	59
4.4.1	As grown CVD	59

4.4.2	Commercially sourced LINPO CVD	61
4.4.3	Commercially sourced Gemesis CVD	63
4.4.4	Commercially available Diamond Foundry CVD	65
4.4.5	Commercially available CVD of unknown origin	67
4.5	HPHT Diamond Samples	69
4.5.1	Colourless HPHT	69
4.6	Discussion	71
4.7	Conclusion	72
5	Anomalous Green Luminescent Properties in CVD Synthetic Diamond	73
5.1	Background and Motivation	73
5.2	Experimental Details	75
5.3	Prompt Luminescence	75
5.4	Delayed Luminescence	76
5.5	Annealing Sequence	82
5.6	Discussion	86
5.7	Conclusion	87
6	Temperature Dependent Studies of three CVD synthetic diamond sam- ples	88
6.1	Background and Motivation	88
6.2	Experimental Techniques and Sample Selection	89
6.3	Sample 3: 499 nm containing CVD synthetic sample	91
6.4	Intentionally nitrogen doped CVD synthetic	94
6.5	High purity CVD synthetic sample	97
6.6	Comparison of Prompt Luminescence	100
6.7	Comparison of Delayed Luminescence	102
6.8	Sample 3: Intensity vs Temperature	104
6.9	NV sample: Intensity vs Temperature	106
6.10	High purity sample: Intensity vs Temperature	109
6.11	Comparison of defect features in samples	110
6.12	Sample 3: Lifetime studies	114
6.13	Discussion	116
6.14	Conclusion	119
7	Conclusion and Future Work	120
7.1	Conclusion	120
7.2	Future Work	122

List of Figures

2.1	Diamond lattice, comprised of two inter-penetrating face centred cubic lattices, that are displaced from one another by $a_0(1/4,1/4,1/4)$, where a_0 is the lattice constant.	8
2.2	Carbon phase diagram.[27]	10
2.3	Schematic of a HPHT belt press.	11
2.4	Schematic drawing of two different types of CVD reactors. On the left-hand side is a hot filament CVD reactor, on the right-hand side is a microwave plasma CVD reactor.	13
2.5	Diamond lattice showing the NV centre. Single substitutional nitrogen shown in blue.	18
2.6	Diamond lattice showing the SiV centre, the Si atom (red) can be seen between two vacant lattice sites.	19
2.7	Jablonski diagram showing both singlet and triplet states responsible for fluorescence and phosphorescence respectively.	22
2.8	UV-Vis Spectra of natural diamond samples taken by Lu et al. Showing a sharp emission around 300 nm aswell as weaker emissions at 415 and 475 nm [60].	24
2.9	Photoluminescence spectrum by Palyanov et al. of diamond crystals synthesized in Mg-based systems. Spectra a and b were taken with an excitation of 395 nm and spectra c was taken with an excitation of 532 nm. The spectrum shows the NV^0 centre at 637 nm, the NV^- centre at 575 nm and the SiV^- centre at 737 nm [62].	25
2.10	Diamondview TM images of a CVD diamond sample (left), a natural diamond sample (middle) and a HPHT diamond sample (right). The CVD sample exhibits closely spaced events due to step growth, striations, steps and risers and also has the orange luminescence typically associated with as-grown CVD samples. The natural diamond shows a polygonised dislocation pattern and blue luminescence commonly associated with natural diamond. Finally, the HPHT stone has a cubo-octahedral grown pattern and a long-lived turquoise luminesce that is usually associated with HPHT diamonds.	27
2.11	Schematic diagram of a Michelson interferometer.	28
2.12	Spectrum by Ferrer et al. of a brilliant cut diamond without impurities. The spectrum shows three different zones, a central zone from 2675 cm^{-1} to 1500 cm^{-1} and two smaller broadbands at 3633 cm^{-1} and 3215 cm^{-1} [57].	28
3.1	Schematic drawing of a Czerny-Turner grating geometry.	32

3.2	Photograph of the time resolved imaging set-up, showing the xenon flash lamp, lens system, cryostat, sample holder and camera.	35
3.3	Schematic drawing of the Horiba Fluorolog, made up of three sections: the inbuilt excitation source optics, the collection optics and the Horiba IHR320 spectrometer.	36
3.4	Photograph of the sample holder used within the fluorolog spectrometer, based on the De Beers DiamondView 3 design.	37
3.5	Spectral throughput of the bespoke band-pass filter from Laser components.	37
4.1	Schematic diagram showing the experimental imaging rig. The source is a xenon flash lamp spectrally filtered to 190-227 nm, the camera is a Basler Ace aca1920-40uc area scan camera, the two have been synchronised to account for the difference in latency.	50
4.2	CMOS image of the prompt (top) and delayed (bottom) luminescence of a typical Type IIa natural diamond. Both the prompt and delayed luminescence are blue in colour. However, the prompt luminescence is a brighter more violet blue whereas the delayed is a duller paler blue. The prompt luminescence also shows a clear dislocation structure in the centre of the image (it is this that causes the bright blue colour) whereas in the delayed luminescence no structure can be seen in this area. The delayed luminescence was recorded with a delay of 100 μ s after the rising edge of the UV pump pulse and integrated for 30 ms.	52
4.3	Spectral data showing both the prompt and delayed luminescence produced by a Type IIa natural diamond. The prompt luminescence is made up of a broadband centred at 435 nm whereas the delayed luminescence is made up of a broadband centred at 455 nm. This explains why the images of both the prompt and delayed luminescence showed different shades of blue.	53
4.4	CMOS image of the prompt (top) and delayed (bottom) luminescence of a Type Ia natural diamond. Overall, the prompt luminescence is turquoise in colour, this is made up of a green component attributed to the H3 defect and a blue component attributed to the N3 defect. The delayed luminescence is blue in colour suggesting the green component of the prompt luminescence decays faster than the blue component which is still visible. The delayed luminescence was recorded with a delay of 100 μ s after the rising edge of the UV pump pulse and integrated for 30 ms.	54
4.5	Spectral data showing both the prompt and delayed luminescence produced by a Type Ia natural diamond. The prompt luminescence shows the N3 defect at 415 nm along with its vibronic sideband and the H3 defect at 503 nm along with its vibronic sideband. The delayed luminescence is made up of a broadband centred at 455 nm, the origin of which is unknown.	55
4.6	CMOS image of the prompt (top) and delayed (bottom) luminescence of a Type IIb natural diamond. The prompt luminescence is violet blue in colour and the dislocation pattern can be clearly seen. The delayed luminescence differs as it is turquoise in colour and does not have the visible dislocation structure. The delayed luminescence was recorded with a delay of 100 μ s after the rising edge of the UV pump pulse and integrated for 30 ms.	56

- 4.7 Spectral data showing both the prompt and delayed luminescence produced by a Type IIb natural diamond. The prompt luminescence is made up of a broadband centred at 425 nm attributed to the dislocation luminescence and the delayed luminescence is made up of a broadband centred at 480 nm, the origin of which is unknown. 57
- 4.8 CMOS image of the prompt (top) and delayed luminescence of an unusual natural diamond, the delayed luminescence was taken at two delays, 100 μ s (middle) and 2 ms (bottom) after the rising edge of the UV pump pulse and both integrated for 30 ms. The prompt luminescence was the same violet blue as in previous stones caused by the dislocation luminescence. The delayed luminescence with a delay of 100 μ s was turquoise in colour, this is not a common luminescence colour for the delayed luminescence of a natural diamond and could cause confusion when identifying the diamond. Lengthening the delay to 2 ms showed the duller blue luminescence which is commonly associated with diamond the origin of which remains unknown. 58
- 4.9 Spectral data showing both the prompt and delayed (100 μ s delay) luminescence produced by an unusual natural diamond. The prompt luminescence consists of a broadband at 435 nm due to the dislocation luminescence. The delayed luminescence produces a turquoise colour due to the broadband centred around 450 nm and the green component at 503 nm due to the H3 defect (shown by line drawn at 503 nm), the H3 defect is also present in the prompt luminescence but overshadowed by the large blue broadband. 59
- 4.10 CMOS image of the prompt (top) and delayed (bottom) luminescence of a typical as grown CVD synthetic diamond. Both the prompt and delayed luminescence are orange in colour, however the prompt luminescence is a much brighter red. The red colour is attributed to the NV⁰ defect in both cases. However, as the delay increases the brightness decreases due to being further through the lifetime of the NV⁰ centre. The delayed luminescence was recorded with a delay of 100 μ s after the rising edge of the UV pump pulse and integrated for 60 ms. 60
- 4.11 Spectral data showing both the prompt and delayed luminescence produced by an as grown CVD synthetic diamond. In both cases the NV⁰ centre at 575 nm can be seen in conjunction with its vibronic side band. The prompt luminescence also shows two defined peaks at 503 nm (attributed to the H3 defect) and 533 nm (origin unknown). 61
- 4.12 CMOS image of the prompt (top) and delayed (bottom) luminescence of a commercially available LINPO CVD synthetic diamond. The prompt luminescence was bright blue in colour with some growth structure patterning, quite similar to that seen in natural diamonds. The prompt luminescence also has a vague red component running through it as well as some discrete red narrow bands of luminescence due to the NV⁰ defect. The delayed luminescence was, however, not like that seen in natural diamond as it was green in colour, due to the H3 defect. The delayed luminescence was recorded with a delay of 100 μ s after the rising edge of the UV pump pulse and integrated for 30 ms. 62

- 4.13 Spectral data showing both the prompt and delayed luminescence produced by a commercially sourced LINPO CVD synthetic diamond. The prompt luminescence consists of a broadband centred around 440 nm. The delayed luminescence shows a broadband centred around 540 nm, the H3 centre can be seen at 503 nm, a peak of unknown origin is seen at 533 nm, as well as the NV⁰ defect at 575 nm in conjunction with its vibronic side band. 63
- 4.14 CMOS image of the prompt (top) and delayed (bottom) luminescence of a commercially available Gemesis CVD synthetic diamond. Much like the LINPO stone, the prompt luminescence is bright blue in colour with a growth pattern structure that could potentially be mistaken as natural diamond. The delayed luminescence once again is green in colour. However, this time the luminescence is not due to the H3 defect and is instead caused by a defect found at 499 nm. The delayed luminescence was recorded with a delay of 100 μ s after the rising edge of the UV pump pulse and integrated for 30 ms. 64
- 4.15 Spectral data showing both the prompt and delayed luminescence produced by a commercially sourced Gemesis CVD synthetic diamond. The prompt luminescence consists of a broadband at 435 nm, there is also a peak at 575 nm due to the NV⁰ centre, as well as a peak at 737 nm attributed to the SiV⁻ centre. The delayed luminescence is comprised of the 499 nm peak in conjunction with its vibronic side band. In addition, this there is a broadband at 340 nm, the NV⁰ centre is also present in the delayed luminescence but it is harder to see as it sits on top of the 499 nm feature's vibronic side band. 65
- 4.16 CMOS image of the prompt (top) and delayed (bottom) luminescence of a commercially available Diamond Foundry CVD synthetic diamond. Both the prompt and delayed luminescence are a similar green in colour. The delayed luminescence was recorded with a delay of 100 μ s after the rising edge of the UV pump pulse and integrated for 30 ms. 66
- 4.17 Spectral data showing both the prompt and delayed luminescence produced by a commercially sourced Diamond Foundry CVD synthetic diamond. The 499.6 nm line can be seen in both the prompt and delayed luminescence in conjunction with its vibronic side band. The delayed luminescence also has a small broadband centred at 360 nm. 67
- 4.18 CMOS image of the prompt (top) and delayed (bottom) luminescence of a commercially available CVD synthetic diamond of unknown origin. The prompt luminescence was green in colour, in contrast the delayed luminescence was bright turquoise. The delayed luminescence was recorded with a delay of 100 μ s after the rising edge of the UV pump pulse and integrated for 60 ms. 68
- 4.19 Spectral data showing both the prompt and delayed luminescence produced by a commercially sourced diamond of unknown origin. The prompt luminescence is dominated by a broadband centred around 535 nm upon which sits the 499nm feature in conjunction with its vibronic band. The delayed luminescence consists of a broadband at around 480 nm; as well as a small broadband centred around 340 nm, a similar small broadband is seen in the prompt luminescence centred at 350 nm. 69

4.20	CMOS image of the prompt (top) and delayed (bottom) luminescence of a colourless HPHT synthetic diamond. The prompt luminescence is quite hard to distinguish as a colour but is made up of a green/red colour the origin of which is unknown, the delayed luminescence is bright blue in colour. The delayed luminescence was recorded with a delay of 100 μ s after the rising edge of the UV pump pulse and integrated for 10 ms.	70
4.21	Spectral data showing both the prompt and delayed luminescence recorded for a typical HPHT synthetic. The prompt luminescence consists of a broadband centred at around 510 nm and the delayed luminescence consists of a broadband centred around 480 nm. As both spectra are broad and featureless not much information can be gained as to the origin of both the prompt and delayed luminescence.	71
5.1	Schematic diagram showing the difference in prompt and delayed luminescence of a natural diamond sample (top) and a CVD synthetic diamond sample (bottom). The natural diamond displays a prompt luminescence signal at 425 nm and a delayed luminescence signal at 455 nm whereas the prompt luminescence for the CVD sample is seen at 435 nm and the delayed luminescence at 499 nm.	74
5.2	CMOS image of the prompt blue luminescence signal recorded for Sample 3 of the Gemesis synthetic CVD diamond gemstones. The left-hand image shows the side of the gemstone, the right-hand side shows the table (top) of the gemstone.	76
5.3	CMOS image of the prompt blue luminescence signal, recorded from a natural diamond gemstone. The dislocation structure in the stone can be clearly seen, and is attributed most commonly to the blue luminescence.	77
5.4	Comparing prompt blue luminescence spectra under UV illumination of the synthetic Gemesis diamond gemstone (Sample 3) and the natural Type IIa diamond gemstone. The natural Type IIa stone is dominated by a broadband at 425 nm, Sample 3 of the Gemesis CVD sample set is also dominated by a broadband found at 435 nm, the NV ⁰ centre is also present at 575 nm along with the SiV ⁻ centre at 737 nm.	77
5.5	CMOS image of the delayed 499 nm luminescence signal, recorded for Sample 3 of the Gemesis synthetic CVD diamond gemstone. The left-hand image shows the side of the gemstone, the right-hand side shows the table (top) of the gemstone.	78
5.6	shortcaption	78
5.7	CMOS images of the prompt and delayed luminescence of both Sample 1 and Sample 2 from the Gemesis CVD samples. The top left image shows the blue prompt luminescence of Sample 1; the top right image shows the delayed green luminescence of Sample 1; the bottom left image shows the prompt blue luminescence of Sample 2; the bottom right image shows the delayed green luminescence of Sample 2.	80

- 5.8 Spectra showing the prompt luminescence of all of the Gemesis sample set. All three samples show a broadband centred at 435 nm. All three samples also contain the NV^0 centre at 575 nm. However, it is in far greater concentration in Samples 1 and 2. Whereas Sample 3 also shows the SiV^- centre at 737 nm, the other two stones also contain the SiV^- centre but in a much smaller concentration which is not visible in this graph. There is also a peak at 533 nm in all 3 samples but most apparent in Samples 1 and 2; the origin of the 533 nm spectral line is unknown. 81
- 5.9 Spectra showing the delayed luminescence of the Gemesis sample set. Sample 1 has a broadband around 490 nm, whereas Samples 2 and 3 have a broadband centred around 520 nm. All 3 samples display a second broadband. In sample 1 this is centred around 345 nm, in Samples 2 and 3 this is centred at 340 nm. All 3 samples contain the 499.6 nm feature, although it is much harder to distinguish in Sample 1 due to the large broadband surrounding it. 81
- 5.10 Photoluminescence spectrum for a pump wavelength of 633 nm recorded at 77 K. The spectrum shows a sharp peak at 737 nm attributed to the SiV^- centre, it also shows a peak at 637 nm attributed to the NV^- centre, as well as a peak at 690 nm which is often attributed to radiative recombination between donor-acceptor pairs in CVD diamond. 83
- 5.11 Room temperature delayed luminescence spectra for the series of annealed E6 CVD diamond samples with comparatively higher silicon and nitrogen concentrations annealed at different temperatures. The 499 nm spectral line can only be observed in the temperature range 1600 - 2000 °C. The NV^0 centre at 575 nm is only observed in the delayed luminescence sample annealed up to 1600 °C, the temperature at which NV^0 centres are known to become mobile. 83
- 5.12 Composite CMOS image recording the luminescence from the 8 high concentration silicon-doped samples under UV illumination. This figure highlights a progressive colour change from red through green and then turquoise with increasing annealing temperature. 84
- 5.13 Composite CMOS image recording the luminescence from the 7 low concentration silicon-doped samples under UV illumination. This figure highlights a progressive colour change from red through green and then turquoise with increasing annealing temperature much like that seen in Figure 5.12. 85
- 5.14 Delayed luminescence spectrum for the Element 6 CVD diamond sample annealed at 1800°C with negligible silicon concentration. The H3 defect can be seen at 503 nm, shown by the vertical line on the graph. 85
- 6.1 Spectral data showing the prompt blue luminescence of Sample 3 over a range of different temperatures. A broadband can be seen at all temperatures centred around 435 nm. In the lower temperature spectra, a peak can be seen at around 460 nm, 499 nm, 575 nm (attributed to the NV^0 centre) and 737 nm (attributed to the SiV^- centre). 90

- 6.2 Spectral data showing the delayed luminescence of Sample 3 over a range of different temperatures. At lower temperatures a broadband is seen around 465 nm; as temperatures increase, this shifts to a broadband around 440 nm, followed by a split broadband at 440 nm and 465 nm, before finally at very hot temperatures a broadband centred at around 480 nm. A peak at 737 nm attributed to the SiV^- centre can be seen at all temperatures. The 499 nm feature can be seen in temperatures above 250 K. 90
- 6.3 Imaging of Sample 3 taken at 77 K (top row), 150 K (middle row) and 296 K (bottom row). The images were taken at 0 delay after excitation (1st column), 90 μs after excitation and 70000 μs after excitation. At 77 K and 150 K the luminescence at both prompt and delayed timescales was blue, at 296 K the prompt luminescence was also blue in colour but the delayed luminescence at both delays was green in colour; this is thought to be due to the 499 nm feature. 93
- 6.4 Spectral data showing the prompt luminescence of the nitrogen doped sample over a range of different temperatures. A sharp peak at 575 nm in conjunction with its vibronic side band is seen at all temperatures, this is due to the NV^0 centre. A sharp peak at 533 nm can also be seen at all temperatures the origin of which is unknown. 94
- 6.5 Spectral data showing the delayed luminescence of the nitrogen doped sample over a range of different temperatures. A peak at 575 nm is seen at all temperatures, at low temperatures a range of other sharp peaks emerged with the most prominent being at 419 nm, 455 nm and 498 nm, these sat on top of a broadband centred at around 460 nm. 94
- 6.6 Spectral data showing the photoluminescence recorded at 77 K with an excitation of 514 nm. Both the NV^0 centre at 575 nm and NV^- centre at 637 nm. 95
- 6.7 Imaging of the nitrogen containing sample taken at 77 K (top row), 150 K (middle row) and 296 K (bottom row). The images were taken at 0 delay after excitation (1st column), 90 μs after excitation and 70000 μs after excitation. At 77 K and 150 K the prompt luminescence was orange in colour and the delayed luminescence was blue in colour, at 296K the prompt and 90 μs delayed luminescence was orange in colour and the 70000 μs delayed showed no luminescence. The orange colour is associated with the NV^0 centre. 97
- 6.8 Spectral data showing the prompt luminescence of the high purity sample over a range of different temperatures. All temperatures show a broadband centred around 435 nm as well as two peaks with vibronic side bands at 485 nm and 530 nm; the origin of both is unknown. 98
- 6.9 Spectral data showing the delayed luminescence of the high purity sample over a range of different temperatures. A broadband is seen in all temperatures centred at 450 nm, a small peak is seen at 733 nm at 110 K; this is of unknown origin. 98
- 6.10 Image of the prompt luminescence of the high purity sample taken at room temperature, the sample does not exhibit delayed luminescence at room temperature. Unfortunately, at this time it was not possible to record an image of the prompt and delayed luminescence at any other temperature. 100

-
- 6.11 Spectral data for comparison of prompt luminescence between each stone, this is repeat spectra of Sample 3: Figure 6.1 (top), nitrogen containing sample: Figure 6.4 (middle) and the high purity sample: Figure 6.8 (bottom) shown together for ease of comparison. All three samples are overall quite different in shape; however, NV^0 can be seen in both Sample 3 and the nitrogen containing stone, a peak at 460 nm can be seen in both Sample 3 and the high purity stone. 101
- 6.12 Spectral data for comparison of delayed luminescence between each stone, this is repeat spectra of Sample 3: Figure 6.2 (top), nitrogen containing sample: Figure 6.5 (middle) and the high purity sample: Figure 6.9 (bottom) shown together for ease of comparison. All three stones have a similar blue broadband feature from 77 -150 K. The graphs differed alot from each other at mid-high temperatures. No high temperature data was recorded for the high purity stone as it did not exhibit delayed luminescence at high temperatures. 103
- 6.13 Spectra showing the prompt luminescence intensity vs temperature for a number of different wavelengths for Sample 3. The 435 nm, 465 nm, 500 nm and 737 nm wavelengths all share a similar profile, while 575 nm does not. Both the 575 nm and 737 nm profile can be seen more closely in the top left hand corner of the graph. 104
- 6.14 Spectra showing the delayed luminescence intensity vs temperature for a number of different wavelengths for Sample 3. The 435 nm and 465 nm followed a similar profile to each other, the 500 nm and 575 nm wavelengths followed a similar profile to each other and the 737 nm wavelength did not follow a similar profile to any of the other wavelengths. 105
- 6.15 Spectra showing the prompt luminescence intensity vs temperature for a number of different wavelengths for the nitrogen containing sample. The 575 nm wavelength dominates the spectra at all temperatures. 107
- 6.16 Zoomed in version of Figure 6.15 showing the prompt luminescence intensity vs temperature for a number of different wavelengths for the nitrogen containing sample. The 435 nm, 465 nm and 500 nm wavelengths all share a very similar profile while the 737 nm does not follow the same profile as any of the other wavelengths. 107
- 6.17 Spectra showing the delayed luminescence intensity vs temperature for a number of different wavelengths for the nitrogen containing sample. The 435 nm, 465 nm and 500 nm wavelengths all share a similar profile, the 575 nm wavelength and the 737 nm wavelength do not share a similar profile to each other or any of the lower wavelengths. 108
- 6.18 Spectra showing the prompt luminescence intensity vs temperature for a number of different wavelengths for the high purity sample. All the wavelengths share the same profile. 109
- 6.19 Spectra showing the delayed luminescence intensity vs temperature for a number of different wavelengths for the high purity sample. The 435 nm, 465 nm, 500 nm and 575 nm wavelengths all share a similar profile, the 737 nm wavelength does not share a similar profile with any of the wavelengths. 110

6.20	Comparison of the temperature dependence of the prompt luminescence between each stone, this is repeat spectra of sample 3: Figure 6.13 (top), nitrogen containing sample: Figure 6.15 (middle) and the high purity sample: Figure 6.18 (bottom) shown together for ease of comparison. . . .	111
6.21	Comparison of the temperature dependence of the delayed luminescence between each stone, this is repeat spectra of sample 3: Figure 6.14 (top), nitrogen containing sample: Figure 6.17 (middle) and the high purity sample: Figure 6.19 (bottom) shown together for ease of comparison. . . .	113
6.22	Spectra showing the decay traces seen for both the 450 nm and 510 nm spectral line at 290 K.	114
6.23	Spectral data of the decay trace taken at 290 K for the 450 nm line plotted on a log scale. If the spectral data was exponential you would expect a linear line once plotted on a log scale, this is not seen here.	114
6.24	Spectral data showing an example fit for the 450 nm time decay. The fit is made up of three exponentials.	115
6.25	Spectra showing the effect of temperature on the average decay time of wavelengths at 450 nm and 510 nm. Both wavelengths share a similar trend in average decay time in response to temperature, with the lowest overall lifetime of both wavelengths being at 190 K and the highest average decay time being seen around 270 -290 K.	116
6.26	Repeat spectral data of delayed luminescence data for Sample 3 taken at 250 K, showing the split broadband at 440 nm and 465 nm and the 499 nm feature all marked with a black line.	117
6.27	Schematic diagram of a proposed band structure for new defect level between the conduction band and valence band. Where the blue emission is from the 460 nm peak, the red is from the 440 nm peak and the green is from the 499 nm peak.	117
6.28	Schematic diagram of a proposed band structure allowing for the emission of the 499 nm feature on prompt timescales. Where the blue arrow represents the UV excitaton, grey arrow represents either phonons or potentially photons in the IR region and the green arrow the 499 nm emission.	118
6.29	Schematic diagram of a proposed band structures allowing for the emission of the 499 nm feature on delayed timescales. Where the blue arrows represent the UV excitation and intial emission from the CB, grey arrows represent the prescence of phonons and the green arrows represent the 499 nm emission.	118

List of Tables

2.1	Diamonds extreme properties taken from Synthetic Diamond: Emerging CVD science and technology [25].	9
3.1	International Gemological Institute grading results for the three synthetic CVD gemstones sourced from Gemesis	41
3.2	Annealing conditions, physical dimensions and carat weight for each of the samples cut from the original E6 CVD nitrogen-doped diamond plate with high silicon concentration and independently heat treated.	41
3.3	Annealing conditions, physical dimensions and carat weight for each of the samples cut from the original E6 CVD nitrogen-doped diamond plate with low silicon concentration and independently heat treated.	41
4.1	Showing what defects can commonly be found in different diamond types. Further detail: A-centres are comprised of a neutral nearest neighbour pair of nitrogen atoms. B-centres consist of a carbon vacancy surrounded by four nitrogen atoms. The N3 defect consists of three nitrogen atoms surrounding a vacancy.	48
4.2	Table as in Figure 4.2 describing natural diamond types, the most likely defect to be found in each type, the percentage of natural diamonds of each type with the addition of the luminescence observed for each type surveyed in this chapter. It is important to note that the luminescence recorded is not the only luminescence that can be observed for each diamond type: rather it is the most commonly seen.	71

Dedicated to my parents

Chapter 1

Motivation

1.1 History of Diamond

Diamond has always been of great interest to human kind due to its beauty, rarity and durability [1]. It was first mined in India around 800 BC, where it quickly became a religious icon due to its beauty and resilience [2]. Diamond was given its name from the Greek ‘adamas’, meaning invincible and unconquerable, and was quick to become treasured as a gemstone. One of its early uses was as a religious symbol; it was even carried into battle to offer protection to the bearer [1]. However, diamond was not only admired for its beauty. It was quickly realised how hard the material was, with some believing it to be indestructible, leading to its use as an engraving tool in early human history [1]. Since this time, diamond has grown in popularity due to increased supply and improvement in cutting and polishing techniques, resulting in the increased beauty of the gem [3]. Diamond is now synonymous worldwide with engagement rings, with much emphasis placed on its rarity in comparison with other stones, causing diamond to be the ‘symbol of eternal love’.

In 1772, it was confirmed by Antoine Lavoisier that diamond was, in fact, made from carbon. Lavoisier placed a diamond in a closed glass jar and used a lens to concentrate the rays of the sun onto the diamond sample, causing the diamond to burn and leave no visible trace it ever existed [4]. Lavoisier summarised that the product of the reaction must be a gas as the weight of the jar remained unchanged once the diamond had been burned. The same phenomenon was noted upon burning charcoal in a closed glass jar, leading Lavoisier to conclude that both diamond and charcoal were different forms of the same element. This element was given the name carbon. The product of the reaction was found to be carbon dioxide, due to the experiment taking place in the presence of oxygen.

As carbon is an easily accessible material many attempts have been made to turn cheap sources of carbon into diamond, many of which will be referenced later in this introduction [3, 5].

1.2 Diamond: A Miraculous Material

Diamond is not only a prized jewel it is also a miraculous material; the mechanical, thermal and electrical properties exhibited are superior to most other materials. The unique properties of diamond are primarily due to its face-centred cubic structure made up of carbon atoms. The tetragonal symmetry and high coordination number of cubic group IV elements impart unusual stiffness, strength and hardness due to the number and symmetry of the bonds and close packing light atoms [6]. It is these properties that have allowed diamond to make such an impact on both the scientific and industrial worlds. Most commonly diamond is known for its extreme hardness (receiving a 10 in the Mohs scale of hardness [7]); arguably this has led to its most common use as an abrasive, both in the form of abrasive powders and in drill bits. However, diamond has much more to offer than being an extremely hard material; it also has the highest thermal conductivity of any known material at temperatures above 100 K [8]. A pure natural diamond sample has been reported as having a thermal conductivity of 24-25 $\text{Wcm}^{-1}\text{K}^{-1}$ compared to 4 $\text{Wcm}^{-1}\text{K}^{-1}$ for copper and 1.5 $\text{Wcm}^{-1}\text{K}^{-1}$ for silicon [9]. This extremely high thermal conductivity makes it a great heat sink and opens up many applications in the electronics field for thermal management [10]. Furthermore, diamond is bio-inert meaning it can be used to interact with the body [11]. This started out with practical uses such as diamond drill bits and scalpels but far more options are now being explored such as targeted drug administration. The extreme properties don't stop there; some of diamond's most impressive properties are its optical properties. Diamond is an ideal material for multi-spectral optical applications as it is transparent from the UV to the far infra-red due to its bandgap of 5.45 eV [12], with only minor absorption bands existing from two phonon absorptions between 2.5 and 6.5 μm .

1.3 The Diamond Market

Considering these properties along with the rarity of diamond, the intrinsic value of natural diamond is unsurprisingly significant. Vast amounts of diamond are mined each year world-wide, the global diamond production in 2017 was estimated to be around 140 million carats with total value exceeding \$15 billion [13]. Some of the largest producing

countries of diamond are Australia, the Democratic Republic of Congo, South Africa, Canada and Russia, with estimated worldwide reserves of 1.3 billion carats [14].

The global diamond mining industry is largely dominated by a handful of companies with Alrosa, De Beers Rio Tinto and Dominion Diamond accounting for 78% of global mining revenue in 2012 [15]. The value of the diamond increases dramatically through processing from production to retail, in 2011 \$15 billion in rough diamond equated to an estimated \$24 billion in polished diamond and \$71 billion in retail value [16].

Diamonds also have high industrial value, primarily, but not limited to, their use as cutting and grinding tools. Around half of all diamonds mined are not of sufficiently high quality to be sold on as gemstones and are instead sold for industrial purposes. The rapid growth of the construction and automotive sectors are driving the projected growth in the industrial diamond market. The industrial diamond market is not only limited to diamonds mined from the ground but also includes synthetically grown diamond.

1.3.1 The Synthetic ‘Problem’

It is now possible to grow synthetic diamond gemstones through both the chemical vapour deposition technique (CVD) and the high temperature high pressure technique (HPHT). Such synthetic diamonds were predominantly produced for the use of the industrial diamond market. However, as the industry has improved it is now possible to grow synthetic gem-quality stones. Companies such as Gemesis have been producing synthetics for the gem market for a number of years; in recent years even the De Beers Group joined the synthetic market with its new collection of synthetic gems being marketed as a cheaper alternative to both much sort after natural gem and the synthetic gems already on the market [17, 18]. Other techniques have also been introduced allowing for the treatment of natural diamonds in order to improve their colour and clarity by heating and irradiation. Natural untreated diamonds have higher value than both treated and synthetic diamonds. Therefore, consumer confidence in the ability to detect undisclosed synthetics must be maintained. With the technology ever expanding and improving in the production of synthetic gemstones there is a risk of flooding the market. This does not pose a problem as long as synthetics are properly disclosed and sold at their true value. However, undisclosed synthetic diamonds are starting to infiltrate the natural diamond market. Due to the vast difference in the natural and synthetic market, with the average cost in 2018 of natural diamond being around \$6400 per carat, compared to a generic lab created diamond selling for \$3700 per carat (42 % lower) and DeBeers Lightbox selling synthetic diamond at \$800 per carat, it is of the upmost importance that consumers can be confident that undisclosed synthetics can be

detected with a high degree of accuracy [19, 20]. There are many unique characteristics within diamond that can be used to distinguish between naturals and synthetics. However, the properties of both natural and synthetic diamonds are inherently variable often making detection difficult. It is for this reason that new interrogation methods and further exploration into the differences between synthetic and natural diamonds must remain at the forefront of research, allowing consumers to have complete confidence when buying diamond.

1.4 Diamond for quantum technologies

Diamond is not only a miraculous material in terms of its beauty as a gemstone and its extreme hardness as a cutting tool but is also showing great promise in the role of host for quantum technologies.

The smallest unit of information in a classical computer is the bit, which can be either 0 or 1. The analogous object in quantum computing is the qubit. For a qubit to preserve the information it holds indefinitely, it needs to be isolated from all sources of noise that might cause decoherence. For example, a qubit based on cold atoms will be isolated from the environment by the vacuum. In the solid-state, the qubit will be surrounded by the host crystal lattice. Many of the most important sources of decoherence come from phonons travelling through the crystal, which can cause fluctuations in the local electric field. The elemental single crystals silicon and diamond can provide the optimum crystalline host because the bonds between atoms are perfectly covalent [21]. Consequently, there are no permanent dipoles between atoms, and the high-energy optical phonons associated with nearest neighbour atomic motion do not cause local fluctuations of the background electric field. Diamond is also transparent to the ultra-violet (UV), visible and infra-red (IR) spectral regions. Diamond's transparency in the UV region is attributed to its wide band gap. The transparency within the IR region is due to diamond being an elemental crystal with no electronegativity difference across the carbon-carbon bond, resulting in no dipole being present and therefore the lattice vibrations have no way to couple with the electromagnetic fields [6]. Its optical transparency band is the widest of all known solids, thus making it a perfect host material with only a small exception to its transparency caused by the intrinsic vibrational absorption band between 2.5 and 6 μm which disturbs diamonds transparency in the infrared region [6]. It is this optical transparency that allows lattice defects to reveal the optical activity of both their electronic and vibrational transitions [22]. It is these lattice defects which could become quantum bits (qubits), one of the most promising candidates for incorporating

into quantum technologies as a qubit is the nitrogen vacancy centre (NV). The main reason for this is its atom-like properties, its long-lived spin quantum states, its well-defined optical transitions and its near perfect dielectric environment [23]. When subjected to a strong magnetic field the NV centre's electronic spin can be up or down or in a superposition of the two, therefore acting as a qubit. The NV centre has proved superior to other candidates as it is an intrinsic feature of a physical structure - dispensing with complex hardware for trapping ions and natural light emitters - therefore, information can be relatively easily read from them. While NV^- has attracted most attention due to the length of time it can maintain quantum information, it is not the only candidate within the diamond host material; there is also much ongoing research into other defects such as silicon vacancy (SiV).

1.5 Thesis Overview

The ongoing occurrence of undisclosed synthetics within the diamond market has ensured the need for further interrogation methods when identifying natural and synthetic diamond. As the quality of synthetic diamond stones increases, the task of identifying such stones becomes more difficult. It is important new interrogation methods are implemented to allow for a growing understanding of the field. This thesis aims to explore a new interrogation method to learn more about diamond defects and their origins, with special attention paid to a defect observed in diamond at 499.6 nm. An outline of this thesis follows:

Chapter 2 - a review of diamond, specifically focussing on its structure, synthesis and defects found within the diamond lattice. This chapter also provides a brief insight into luminescence mechanisms, specifically fluorescence and phosphorescence. Optical techniques used to help classify defects and determine the origin of the diamond sample are explored. These optical methods will be drawn on and other similar methods explored within the results section of this thesis.

Chapter 3 - aims to provide the theory required for the interpretation of the results of the experimental studies, along with specific details into equipment used to produce the results. This will include the new imaging method produced for use within this thesis, which combines the use of delayed luminescence with imaging in order to explore the defects within diamond samples along with helping to determine their origin.

Chapter 4 - experimentation will be undertaken using the imaging rig outlined in Chapter 3. This includes testing the parameters of the rig using a range of well-known samples of both a natural and synthetic origin, allowing identification of 'finger-prints'

of natural, CVD synthetic and HPHT synthetic diamond. Identification of a sharp emission line observed at 499.6 nm was seen in a number of samples surveyed, this has led to further research being carried out into this feature.

Chapter 5 - pays close attention to the sharp emission feature found at 499.6 nm, a feature observed in the UV luminescence of a CVD diamond gemstone. Very little is currently known about this defect; it is thought that with the use of the imaging rig this defect could, in future, be recognised as a signature of a synthetic diamond. This chapter aims to use a number of interrogation methods in order to determine as much as possible about the origin and chemical make-up of the defect.

Chapter 6 - consists of a temperature dependence study carried out on three CVD gemstones. Focus is placed on a set of specific wavelengths on both prompt and delayed timescales in order to observe how those particular wavelengths are affected by temperature. The overall aim being to learn more about the 499 nm feature and its potential structure.

Chapter 7 - provides a conclusion of the results presented in this thesis along with a brief outlook on future work that could be carried out to compliment the work done within this PhD.

Chapter 2

Background Theory

2.1 Introduction

The intention in this chapter is to provide the reader with the relevant background theory to complement the work described later in the thesis. To begin with, I describe the crystalline structure of diamond, before moving on to some common growth techniques. The conversation then moves naturally to the discussion of lattice defects and the incorporation of impurities. The summary of common and useful defects in diamond will be focussed on defects that will be used within this thesis. The theory of luminescence will be discussed in order to provide background to the investigations into both prompt and delayed luminescence that will take place in this thesis. For perspective, I also provide a short review of interrogation methods currently used within the field of diamond identification. These methods are aimed at establishing the element composition and structural features that might reveal clues about the growth conditions of the diamond. I conclude the chapter by outlining the rationale behind the research undertaken during my PhD studies.

2.2 Diamond Structure

Diamond is an allotrope of carbon, with each carbon atom covalently bonded to its four nearest neighbour atoms in a tetrahedral arrangement. The carbon atoms are arranged in two inter-penetrating face centred cubic (FCC) lattices, that are displaced from one another by $a_0(1/4, 1/4, 1/4)$, where a_0 is the lattice constant [24]. A carbon atom contains six electrons and has a ground state configuration of $(1s)^2(2s)^2(2p)^2$. However, this is not energetically favourable, in order for the lowest energy to be achieved four

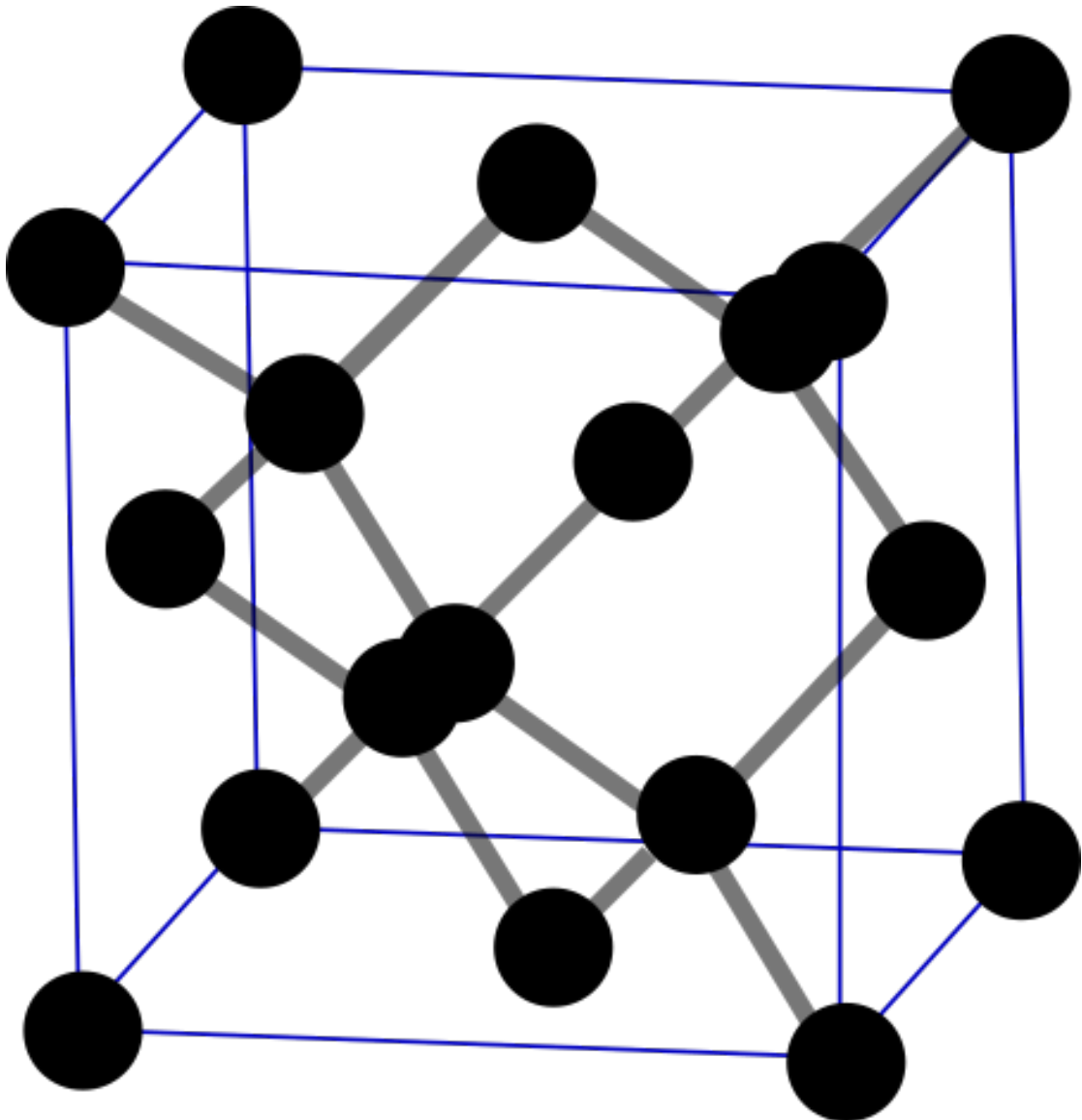


FIGURE 2.1: Diamond lattice, comprised of two inter-penetrating face centred cubic lattices, that are displaced from one another by $a_0(1/4, 1/4, 1/4)$, where a_0 is the lattice constant.

degenerate hybridised sp^3 orbitals are formed. It is the four equivalent bonds that causes the tetrahedral coordination of the atoms in the diamond lattice.

2.2.1 Diamond's Extreme Properties

The structure of pure diamond results in many extreme properties, a summary of these can be found in Table 2.1. It was diamond's extreme optical properties and its hardness that initially led to its position as the world's most popular gemstone. As a gemstone it is important that the diamond cannot be easily scratched; its extreme hardness of 1.0×10^4 kg/mm² prevents it from getting scratched and, therefore, becoming dull

overtime [25]. Diamond also has an unusually high refractive index of 2.41 compare with glass which has a refractive index of 1.52 [25, 26]. It is this refractive index that gives rise to multiple internal reflections when the gemstone is appropriately cut, overall giving diamond it's sparkling appearance. However, these extreme properties also mean that diamond has many uses in the industrial market. It is commonplace for properties such as diamond's extreme hardness to be exploited for use in industrial cutting and milling most commonly in the form of diamond drill bits. Furthermore, it is not only the extreme hardness that has valuable industrial uses, but also its thermal conductivity for uses such as heat sinks, its optical properties for use in lenses and its bioinert properties for uses such as medicine, to name but a few.

Property	Value	Units
Hardness	1.0×10^4	kg/mm ²
Strength, tensile	> 1.2	GPa
Strength, compressive	> 110	GPa
Coefficient of friction (Dynamic)	0.03	Dimensionless
Sound velocity	1.8×10^4	m/s
Density	3.52	g/cm ³
Young's modulus	1.22	GPa
Poisson's ratio	0.2	Dimensionless
Thermal expansion coefficient	1.1×10^{16}	K ⁻¹
Thermal conductivity	20.0	W/cm-k
Thermal shock parameter	3×10^8	W/m
Debye temperature	2200	K
Optical index of refraction (at 591 nm)	2.41	Dimensionless
Optical transmissivity (from nm to far IR)	225	Dimensionless
Loss tangent at 40Hz	6.0×10^{-4}	Dimensionless
Dielectric constant	5.7	Dimensionless
Dielectric strength	1.0×10^7	V/cm
Electron mobility	2200	cm ² /V-s
Electron saturated velocity	2.7×10^7	cm/s
Hole saturated velocity	1.0×10^7	cm/s
Work function	Negative	on [111] surface
Bandgap	5.45	eV
Resistivity	10^{13} - 10^{16}	Ω -cm

TABLE 2.1: Diamonds extreme properties taken from Synthetic Diamond: Emerging CVD science and technology [25].

2.2.2 Natural Diamond Formation

At atmospheric pressure and temperature diamond is the metastable state of carbon, with the stable state being graphite. Graphite is a crystalline form of carbon with sp² bonding, its atoms form in planes where each atom is attached to its 3 nearest neighbours; it is most commonly used as the lead in pencils. Natural diamond formation

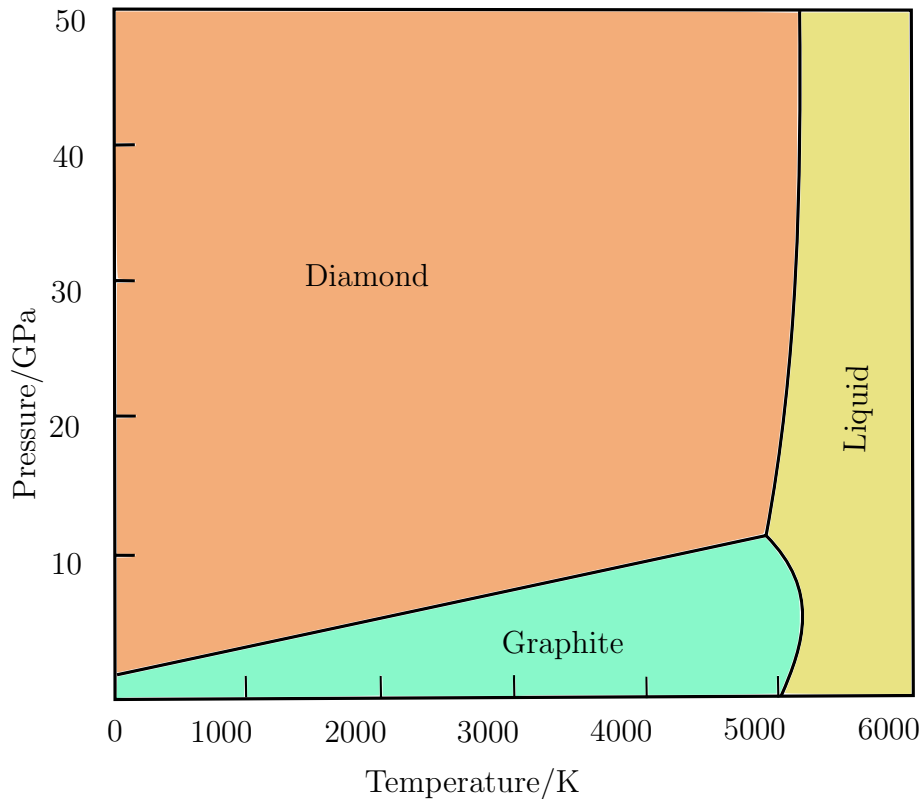


FIGURE 2.2: Carbon phase diagram.[27]

cannot occur unless the carbon source is in the diamond stable region of the phase diagram, as shown in Figure 2.2.

For natural diamond synthesis temperatures of 1000-1600 °C are needed in conjunction with pressures of 4.5-6 GPa. The conditions required for diamond formation are met in the lithospheric mantle which is found 140-190 km below the Earth's surface. However, changes in temperature at this distance below the Earth's surface vary greatly over different parts of the Earth. To find the correct combination of temperature and pressure the diamond formation occurs in the cratonic lithosphere (an old and stable part of the continental lithosphere). The longer the diamond crystal resides in the cratonic lithosphere the larger the crystal can grow. Diamond bearing rocks can be carried from the mantle to the surface of the Earth by deep-origin volcanic eruptions [28].

2.3 Synthetic Diamond Production

What was once thought to be a mystical crystal that required millions of years to form within the Earth's mantle can now be synthesised in a laboratory in a matter of hours. In 1955 General Electric produced the first verifiable and reproducible synthetic diamond. Bundy et al. used a carbon source and converted it to diamond by recreating the high

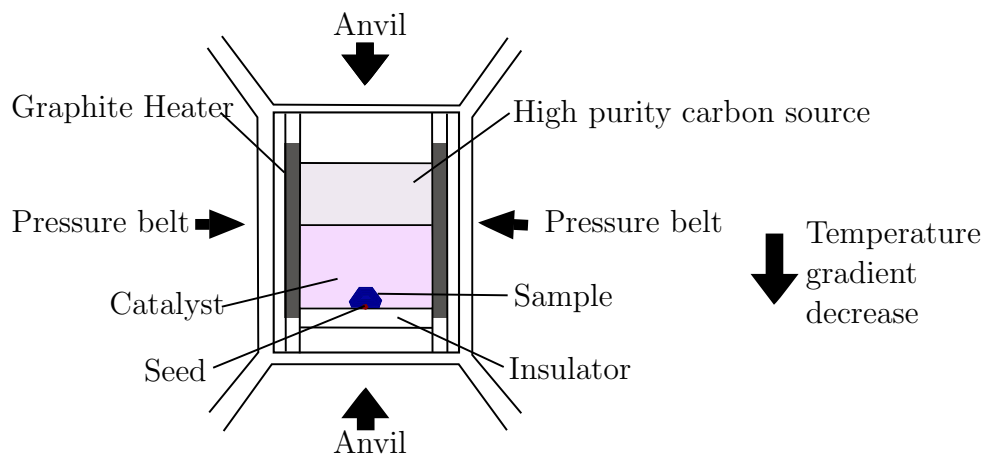


FIGURE 2.3: Schematic of a HPHT belt press.

temperatures and pressures found in the Earth's mantle [29]. This recreation of the Earth's environment has since gone on to be called high pressure high temperature synthesis and is not the only synthesis method currently used. The introduction of the synthetic diamond has gone on to revolutionise the use of diamonds in both industry and research. The synthetic market was initially used for industrial purposes but has now also moved into the gemstone/jewellery sector. The synthetic diamond industry has progressed greatly since 1955 and there are now two individual methods used to synthetically produce diamonds, which are detailed below [30–32].

2.3.1 High Pressure High Temperature Diamond Synthesis (HPHT)

HPHT aims to recreate the conditions found in the Earth's lithospheric mantle in order to produce synthetic diamond. These high temperatures ($\sim 2000^\circ\text{C}$) and pressures ($\sim 5\text{GPa}$) can be produced inside a press with the help of a metal solvent catalyst. The metal solvent is commonly iron, nickel or cobalt. It is used to lower the temperature needed for diamond to form as well as stabilising the molten carbon as it goes through a decreasing temperature gradient onto a diamond seed, which is held at a lower temperature. Once the carbon meets the diamond seed it condenses and allows for crystallisation of the diamond onto the seed crystal.

At present there are three main types of press thought to be capable of supplying the necessary temperature and pressure, known as the belt press (shown in Figure 2.3), the cubic press and the split-sphere press. All three produce the required conditions for diamond to be the stable form of carbon in the presence of a metal catalyst [30, 32].

2.3.2 Chemical Vapour Deposition Diamond Synthesis (CVD)

CVD synthesis has become a well-established field over the last three decades; this technique involves the growth of diamond from a hydrocarbon gas mixture. Unlike the original HPHT method, the temperatures and pressures required are lower and, therefore, more accessible. With the conditions used in CVD synthesis, the formation of graphite or another non-diamond form of carbon would conventionally be expected. Eversole and Kenmore proved this not to be the case and filed for a patent as a diamond growth method in 1958 [33]. The technique was further developed by Angus et al. in 1968, who noted that the presence of atomic hydrogen in the reactor resulted in preferential etching of graphitic material [34]. In line with these findings, CVD growth involves a sealed chamber heated to around 800 °C containing gaseous reactants, usually methane and hydrogen, which are activated by the use of hot filaments or plasmas. The methane provides a source of carbon while the hydrogen is used to prevent non-sp³ bonded carbon forming around the substrate [34]. The application of the hot filaments or plasmas causes molecular hydrogen to convert to atomic hydrogen, two chemical processes are caused when atomic hydrogen is present in the gas phase. The first process causes any non-diamond carbon (such as graphite) to react with the atomic hydrogen and evaporate into the newly formed gas phase. Secondly, the atomic hydrogen reacts with the hydrocarbon gas added to the chamber to form a highly reactive carbon-hydrogen species that, on decomposition, gives up the hydrogen leaving behind pure carbon in the form of diamond [30, 31, 35].

CVD synthesis allows for the production of very pure diamond. However, it can also be used to incorporate tailored defects into the lattice by controlling the growth temperature and source gases. For example, nitrogen is a commonly incorporated defect which increases growth rates but produces a yellowish-brown discolouration in the stone [36]. Silicon is also incorporated in CVD growth often by accident as many chambers have silica reactor windows. Therefore, when trying to produce high-purity intrinsic diamond care must be taken regarding the choice of growth chamber [37]. CVD synthesis can produce both single crystal and polycrystalline stones dependent on the substrate used and the growth conditions, it can also produce thin-film diamond or bulk diamond, making it a very versatile process [38].

2.4 Diamond Treatments

Heat and irradiation can both be used to treat diamond, either separately or a combination of both. Using these treatments can have a massive effect on the defects within

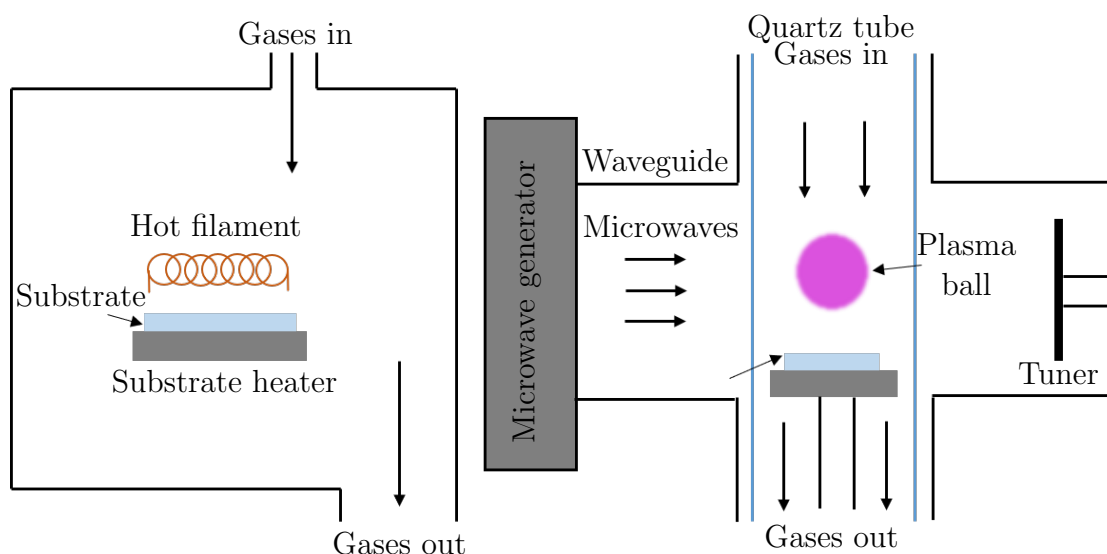


FIGURE 2.4: Schematic drawing of two different types of CVD reactors. On the left-hand side is a hot filament CVD reactor, on the right-hand side is a microwave plasma CVD reactor.

these diamonds and, therefore, an impact on the appearance of the diamond and its colour. Altering the optical properties of a diamond gemstone, from a less appealing colour (such as yellow) to a more appealing colour (such as colourless) can drastically affect the gemstone's value.

2.4.1 Heat treatment

When heat is applied to a diamond it provides energy to the defect structures within the lattice. If the energy is sufficiently high it can allow defects to migrate through the lattice, aggregate or dissociate.

Aggregation is a process commonly seen in natural diamonds; heat and pressure from the surrounding environment often result in diamond forming with predominantly aggregated forms of nitrogen. This process can be replicated using HTHP annealing; the annealing process can be seen to turn natural brown diamond into near colourless diamond, hugely increasing its desirability. Increasing the stone's desirability would, therefore, increase its value. For this reason, it must be distinguishable from an untreated natural stone. A number of interrogation methods can be used to distinguish between stones of this nature many of which will be explored later within this thesis. The same effect can be seen when CVD stones are HPHT annealed, a colour change from brown to near colourless occurs. However, the brown colour in CVD is not thought to be of the same origin as when it is found in natural diamond. It is this colour change from brown to colourless that is the most common reason to HPHT anneal a diamond.

There are other less common reasons to heat a diamond; for example, if a black diamond is desired, very high heat can be applied to turn the diamond black. This kind of process is not very common and usually only done with low quality stones.

2.4.2 Irradiation treatment

The irradiation process of diamond was first noted by Sir William Crookes who discovered that diamonds colour could be changed when exposed to radium salts [39]. The irradiation process now involves bombarding a diamond with radiation of sufficient energy to displace carbon atoms from their regular lattice sites. Upon displacing the carbon atoms, vacancies and interstitials are created (both of which will be discussed further in this introduction). As with heat treatment, irradiation is commonly used to enhance the colour of the diamond; colours produced by irradiation include blue, green, canary yellow and pink. These colours are often referred to as ‘fancy’ colours. High value is associated with fancy colours; as with heat treatment, it is important that they can be distinguished from untreated stones.

A combination of both heat treatment and irradiation is often used in order to produce desirable diamond stones. It is common practice to change the colour of the stone by the use of irradiation, followed by heat treatment to re-position the atoms within the lattice, thereby enhancing the colour created by irradiation. However, that is not the only combination. For example, pink diamonds are often produced by HPHT annealing first, followed by irradiation and then a follow-up HPHT treatment. It is important that these processes are carried out carefully otherwise stones can become too vivid in colour and, as a result, look too bright and unnatural.

2.5 Defects in Diamonds

Defects have always been apparent in natural diamonds and as synthesis methods have improved it is now possible to controllably add defects to synthetic diamonds. A defect is an interruption of the lattice periodicity of a crystal. Defects can either be extrinsic - originating from inclusions of foreign materials in diamond - or intrinsic meaning one or more of the carbon atoms has been displaced in the diamond’s lattice. These interruptions in the lattice can occur in either one, two or three dimensions and are therefore classed as surface (1D), line (2D) or point (3D) defects.

The emphasis in this report will be on point defects, which are split into three categories:

- Impurities: when a lattice site is occupied by an atom other than carbon.

- Vacancies: when a carbon atom is missing from one of the lattice sites.
- Interstitials: when an atom is located at a different site that is not a substitutional lattice site. (This atom could be carbon).

It is common for both natural and synthetic diamond to involve a combination of all three point defects. Even at very low concentrations, point defects can have a serious effect on the properties of diamond. There are a number of different impurities which can be incorporated into diamond, some of the most researched are nitrogen, hydrogen, silicon and boron. So far, more than 500 electronic and 150 vibrational optical centres have been detected in diamond in the spectral range of 20 to 0.17 μm . Impurities known to form optically active defects in diamond are H, He, Li, B, N, O, Ne, P, Si, As, Ti, Cr, Ni, Co, Zn, Zr, Ag, W, Xe and Tl [22]. This section will focus on defects that can be seen in the samples being studied, which are primarily nitrogen and silicon related defects.

2.5.1 Nitrogen Defects

The most common impurity in diamond is nitrogen [40]. Nitrogen can produce many different defects in the diamond lattice. As well as being present in natural diamond, nitrogen can be easily incorporated into HPHT and CVD grown diamond. Nitrogen is also one of the most technologically important defects in diamond in addition to being the most common. While there are many optical centres in diamond which include nitrogen, in this thesis I will mainly concentrate on the following centres: single substitutional nitrogen, A centres, B centres, N3 and the nitrogen vacancy defect.

Where nitrogen concentrations are high enough to be detected in diamond by infrared absorption, it is known as Type I diamond; this is further categorised into Type Ia diamonds which are those which contain mainly aggregated nitrogen and Type Ib diamonds which are those that contain mostly isolated nitrogen. This can be sub-categorised once more when taking into account if the diamond contains mostly A or mostly B centres known as Type IaA and Type IaB respectively.

2.5.1.1 Isolated Nitrogen

Single substitutional nitrogen N_s^0 (where the N_s is referring to a single unpaired nitrogen atom and the 0 referring to it's neutral charge state) was first identified using electron paramagnetic resonance studies (EPR) by Smith et al. in natural diamond [41]. The defect has since been observed in both HPHT and CVD synthetic diamond and can also be produced by HPHT annealing stones which contain A or B centres. Single

substitutional nitrogen atoms in diamond are also referred to as C centres [42]. The defect consists of a lone nitrogen atom in the place of one of the constituent carbon atoms, with the substitutional nitrogen bonding to each of the four neighbouring carbon atoms. The substitutional nitrogen results in an additional electron that is localised in an anti-bonding orbital. This orbital sits between the substitutional nitrogen and one of the carbon atoms. This unique nitrogen-carbon bond is extended by around 20-30% when compared with the other carbon-carbon bonds in the lattice. The other three carbon-nitrogen bonds are slightly shorter than the rest of the carbon-carbon bonds in the lattice, producing a C_{3v} symmetry.

The N_s^0 can be observed using absorption spectroscopy, the neutral charge state shows a range of optical absorptions before rapidly rising around 1.7 eV continuing until it meets the fundamental absorption edge at 5.5eV. With some sharp absorption lines around 4 eV and broadbands at 3.3, 3.9 and 4.6 eV, it is these broadbands that have been associated with the yellow colourisation associated with the N_s^0 centre. The concentration of the N_s^0 centre can be calculated using FTIR spectroscopy. The N_s^0 defect has absorption peaks at 1344 and 1130 cm^{-1} , the strength of these peaks is known to be proportional to the concentration of N_s^0 [43].

2.5.1.2 Aggregated Nitrogen

Nitrogen aggregates are typically only formed under HPHT conditions. These conditions can occur during natural post-grown annealing in the Earth's upper mantle or in a laboratory.

One such example of aggregated nitrogen is referred to as the A centre: the A centre consists of a neutral nearest neighbour pair of nitrogen atoms substituting for two neighbouring carbon atoms [44]. The A centre is measurable in around 98% of all natural diamonds [45]. The formation of A centres has been studied by HPHT annealing Type Ib diamond between 1600-2000 °C; at these temperatures the single substitutional nitrogen disperses allowing A centres to form. It was found that the formation of A centres was far more likely than nitrogen diffusing out of the diamond. The addition of nitrogen vacancies enhances the efficiency of aggregation, lowering the temperature needed for A centres to form to around 1500 °C. The concentration of A centres within the diamond can be calculated using IR spectra; there is an IR absorption peak associated with the feature 1282 cm^{-1} [43].

Another aggregated form of nitrogen is the B centre; it is more complex than the A centre and consists of a single vacancy surrounded by four substitutional nitrogen atoms in the place of the carbon atoms. The B centre occurs naturally in diamond but it can

also be created using extended HPHT annealing treatments at 2000-2500 °C. The B centre has an infrared absorption band at 1175 cm^{-1} [43].

The final aggregated defect discussed here is the N3 defect. The N3 defect is commonly seen in Type Ia diamond; it consists of a vacancy surrounded by three nearest neighbour nitrogen atoms and a carbon atom with a dangling bond. The N3 defect occurs in natural diamond; it has been reported that diamonds that contain the N3 defect are always accompanied by A centres [46]. The N3 defect can be seen optically at 415 nm in photoluminescence [43].

2.5.1.3 Nitrogen Vacancy centre

The predominant defect focused on in this report is the nitrogen vacancy (NV) centre. It is observed in both natural diamond and CVD grown diamond. It is also possible to form the NV defect by irradiating diamond in order to create vacancies and then annealing the diamond at around 900 K allowing the vacancies to migrate within the lattice. The NV centre is formed once a vacancy is caught by a single substitutional nitrogen centre. The nitrogen vacancy centre consists of a single substitutional nitrogen and a vacancy in the place of two carbon atoms, as shown in Figure 2.5. The nitrogen-vacancy defect has two charge states NV^0 and NV^- , which charge state is formed depends on the availability of electron donors. The NV centre anneals out at around 1800 °C; this often leads to aggregation of nitrogen atoms into A centres [47]. The NV centre was first reported optically at 637 nm; later work reported a line at 575 nm on stones that had undergone the same treatment as those showing the 575nm line [48]. It was suggested that the two optical observations made could be from two different charge states of the nitrogen vacancy centre, this was later confirmed by Mita [49]. It was confirmed that the 637 nm line was associated with the negatively charged nitrogen vacancy centre, NV^- , and the 575 nm line is associated with the neutral nitrogen vacancy centre, NV^0 [49]. As a diamond defect the nitrogen vacancy centre has attracted a lot of attention. With its atomic-like properties, long-lived spin quantum states and well-defined optical transitions, the nitrogen vacancy centre is one of the most promising candidates for use as a qubit in quantum mechanics [23].

The H3 centre, although potentially misleading in name, does not have any involvement with hydrogen and is instead another centre in diamond similar to the nitrogen vacancy centre. The H3 centre consists of two substitutional nitrogen atoms separated by a vacancy in a neutral charge state. The H3 defect is observed in natural diamond but is most commonly observed in irradiated diamonds that have undergone annealing. The irradiation produces vacancies which then become mobile when annealed above 500 °C,

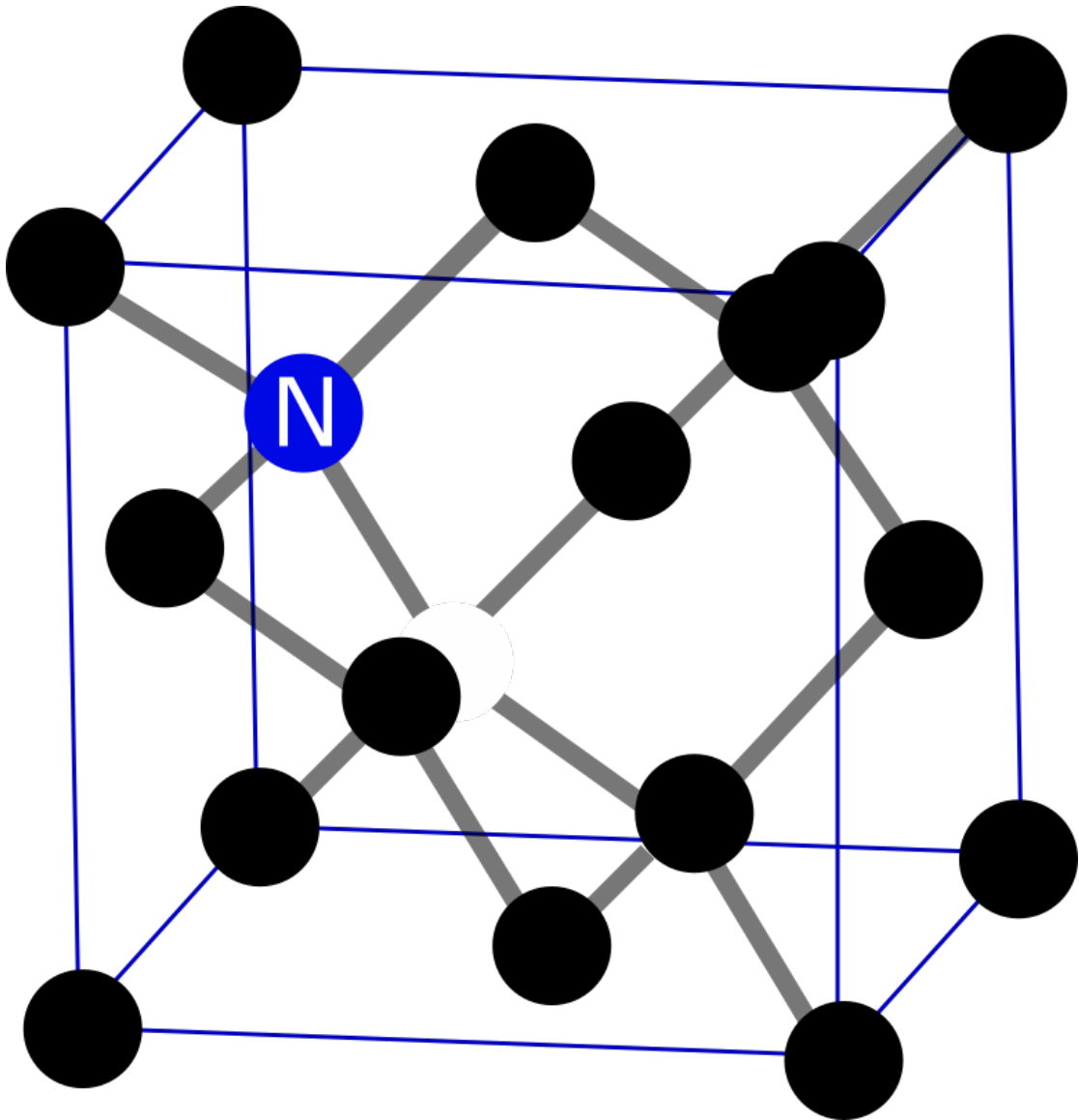


FIGURE 2.5: Diamond lattice showing the NV centre. Single substitutional nitrogen shown in blue.

allowing the vacancies to interact with the A centres producing the H3 centre [50]. The H3 defect shows a strong optical absorption at 503.2 nm [43].

2.5.2 Silicon Vacancy

A range of silicon defects have been reported in diamond; this is unexpected as from a thermodynamical perspective silicon is not soluble in diamond. Silicon defects commonly form as a result of non-equilibrium growth conditions. The silicon vacancy (SiV) centre is formed when a silicon atom replaces two neighbouring carbon atoms in the diamond lattice, the silicon atom is placed between the two vacated sites, as shown in Figure 2.6. As a result of this, a silicon atom with atomic radius around 60% higher than a carbon

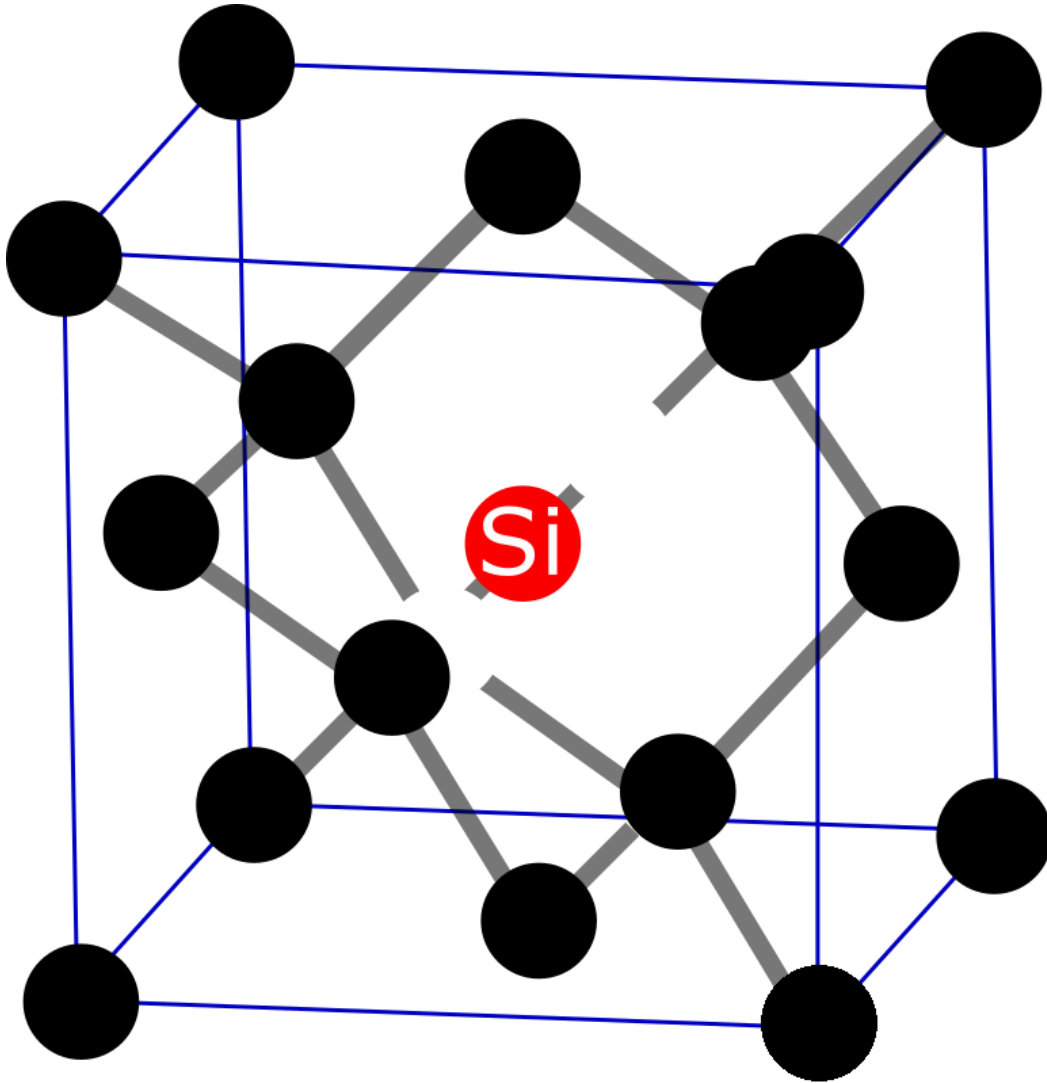


FIGURE 2.6: Diamond lattice showing the SiV centre, the Si atom (red) can be seen between two vacant lattice sites.

atom can be accommodated in the diamond lattice. SiV is commonly seen in CVD synthetic stones due to oxygen leaching from the silica windows used in the reactors. However, it can also be grown into HPHT diamond by Si doping. Silicon related impurities have only been reported in natural diamond after ion implantation or a combination of heat and irradiation treatments have taken place. Silicon vacancy dates back to the 1980's when it was discovered using cathodoluminescence spectroscopy [51], but is most commonly observed in photoluminescence experiments with SiV^- being observed at 737 nm. In 2011, a neutral form of silicon vacancy was reported by D'Haenens-Johansson et al. who first reported the defect after carrying out electron paramagnetic resonance studies [52]. The SiV^0 can also be observed in photoluminescence at 946 nm.

The silicon vacancy defect emerged as a promising competitor to the nitrogen vacancy centre in terms of quantum technologies due to its narrow zero phonon line transitions and weak phonon sidebands [53]. SiV centres are the only solid-state emitters for which indistinguishable photons have been created without spectral tuning of individual emitters [54].

2.5.3 Boron

Boron is a defect that is not commonly seen in natural diamonds: only around 1% of natural diamonds contain this defect. Boron is a very effective dopant in synthetic diamond growth due to the high level of boron solubility in diamond [55]. Diamonds that contain boron are classed as Type IIb diamonds. Boron atoms have one less available electron than carbon atoms allowing the boron to act as an acceptor. The acceptor state is situated 0.37eV above the valence band. The addition of boron to the diamond lattice allows the diamond to become a P-type semiconductor, opening up many electronic applications for diamond. Boron has a primary infrared absorption line at 2803 cm^{-1} [43].

The above summarises a brief list of impurities for use with this thesis. However, there are many other impurities seen in diamond many of which are still being characterised. One such impurity is a feature found at 499 nm in photoluminescence, much of the work carried out in this thesis is based on this impurity.

2.6 Luminescence Mechanism

Luminescence refers to the emission of light from a material following the absorption of energy from an external excitation source; in the context of this thesis that would be an ultra-violet source. Energy is absorbed from the excitation source and is then emitted in the form of light or heat; it is this emitted radiative energy that is recorded as the luminescence of the material.

Luminescence is split into two further categories, known as fluorescence and phosphorescence, and is formally described as the emission of light from excited singlet states and excited triplet states respectively [56].

2.6.1 Fluorescence/Rapid Luminescence

The process of fluorescence occurs when an excited electron relaxes in a light-emitting transition from an excited singlet state to the ground singlet state in a timeframe of around 10 ns to 10 μ s. A singlet state is defined when all the electron spins are paired in a molecular electronic state and the electronic energy states do not split when exposed to a magnetic field. Fluorescence is therefore often considered to be the luminescence that is recorded from the material immediately after excitation. Figure 2.7 is a Jablonski style diagram, showing the ground singlet state and the excited singlet state as S_0 and S_1 respectively. The excitation causes an electron to be excited from S_0 to S_1 ; this electron will then fall back to its ground-state and the difference in energy between the levels is dissipated via emission of a photon. The emitted photon will have lower energy and therefore higher wavelength than the original excitation due to the energy loss from vibrational relaxation. There are a variety of vibrational levels of the ground-state that the electron can relax back into, resulting in a bandwidth of possible wavelengths for photon emission. Before fluorescence emission takes place, excited electrons tend to decay by non-radiative processes to the lowest vibrational level of the lowest excited state. Therefore, the emitted wavelength and the excitation wavelength are independent of one another.

2.6.2 Phosphorescence/Delayed Luminescence

Phosphorescence differs from fluorescence: rather than being a singlet to singlet transition it is instead triplet to singlet transition. In excited singlet states, the electron in the excited orbital is paired (by opposite spin) to the second electron in the ground-state orbital, whereas in a triplet state the electrons in both the excited orbital and the ground-state have the same spin orientation. After excitation, intersystem crossing can allow an electron to move from an excited singlet state into an energetically favourable excited triplet state, causing the inversion of the electrons spin, thus making the spin parallel to that in the ground singlet state, as shown in 2.7. As the states have different spin multiplicity transitions from the excited triplet state to the ground singlet state are forbidden, due to the conservation of angular momentum. This restriction is relaxed as a result of spin-orbit coupling which allows the excited triplet state to radiatively transition to the single ground state. As this transition is forbidden it occurs on a much slower timescale. Due to the complex temporal characteristics of diamond luminescence the distinction between fluorescence and phosphorescence can be unclear, in this thesis the terms *prompt* luminescence and *delayed* luminescence will be used. Prompt luminescence will be used to describe the luminescence recorded contemporaneously with the

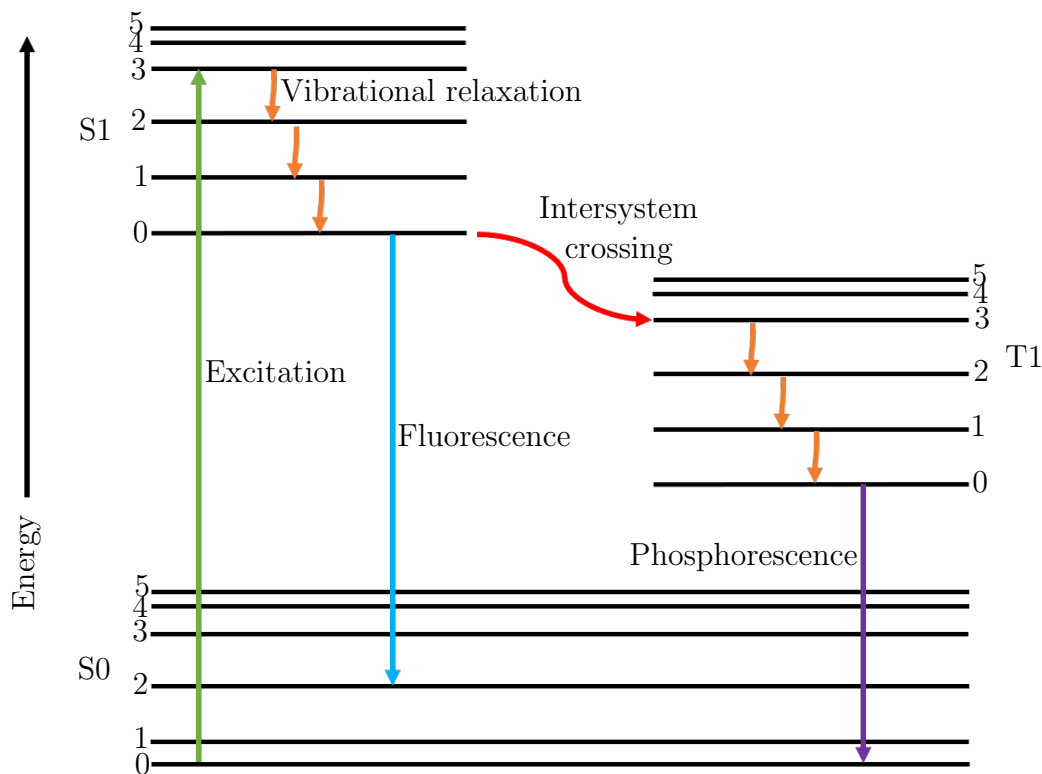


FIGURE 2.7: Jablonski diagram showing both singlet and triplet states responsible for fluorescence and phosphorescence respectively.

excitation and delayed luminescence will refer to the luminescence recorded a set delay after the excitation.

2.7 Optical Techniques for Synthetic Diamond detection

With increasing quantities of synthetic diamonds finding their way onto the gem market it has become more important than ever that such synthetic, or treated, diamonds can be distinguished from natural stones. Research into optical properties of diamond has been carried out for well over half a century and it has now become clear that this fundamental research underpins the work carried out into diamond classification [57]. The most common optical techniques used to identify and classify diamonds are listed below, with a brief insight in to how they work and features associated with diamond in each case.

2.7.1 Ultra Violet-Visible Spectroscopy

In ultraviolet-visible spectroscopy, UV-Vis, ultraviolet and visible light are used to illuminate the stone; it is an absorption technique where-by a wide range of colours are

illuminated on the sample [58]. An absorption spectrum is a measure of the amount of radiation absorbed by a sample as a function of energy, it is dependent on the atomic energy levels of the defects within the diamond sample. Radiation is absorbed when the energy of the radiation coincides with the energy difference between two electronic states. The absorbance of a spectral line is related to the number of defects in the sample.

Absorption spectroscopy requires two spectra to be taken; firstly, a background spectrum must be obtained by recording a spectrum of only the source. The sample can then be placed into the source beam and a second spectrum, can be recorded; this will show unique spectral lines which correspond to absorption by defects found within the diamond. The spectrum containing the spectral information can then be divided by the background spectrum to give a transmission spectrum, with $I(\lambda)$ referring to the intensity of the sample spectrum and $I_0(\lambda)$ referring to the intensity of the background spectrum [58]:

$$T(\lambda) = \frac{I(\lambda)}{I_0(\lambda)} \quad (2.1)$$

This transmission spectrum in turn can be converted into an absorbance spectrum by [58]:

$$A(\lambda) = -\log_{10}(T(\lambda)) \quad (2.2)$$

Absorption spectroscopy not only provides a scientific representation of the diamond's colour it can also indicate if a diamond has been heat treated or irradiated. Natural diamond samples exhibit a sharp absorption peak at around 300 nm, as well as weak absorptions at 415 nm and 475 nm both attributed to nitrogen. Nitrogen is a very widespread and abundant impurity found in diamond, it can be present in several optical defects all of which produce absorption towards the blue end of the spectrum between 415 and 478 nm [59].

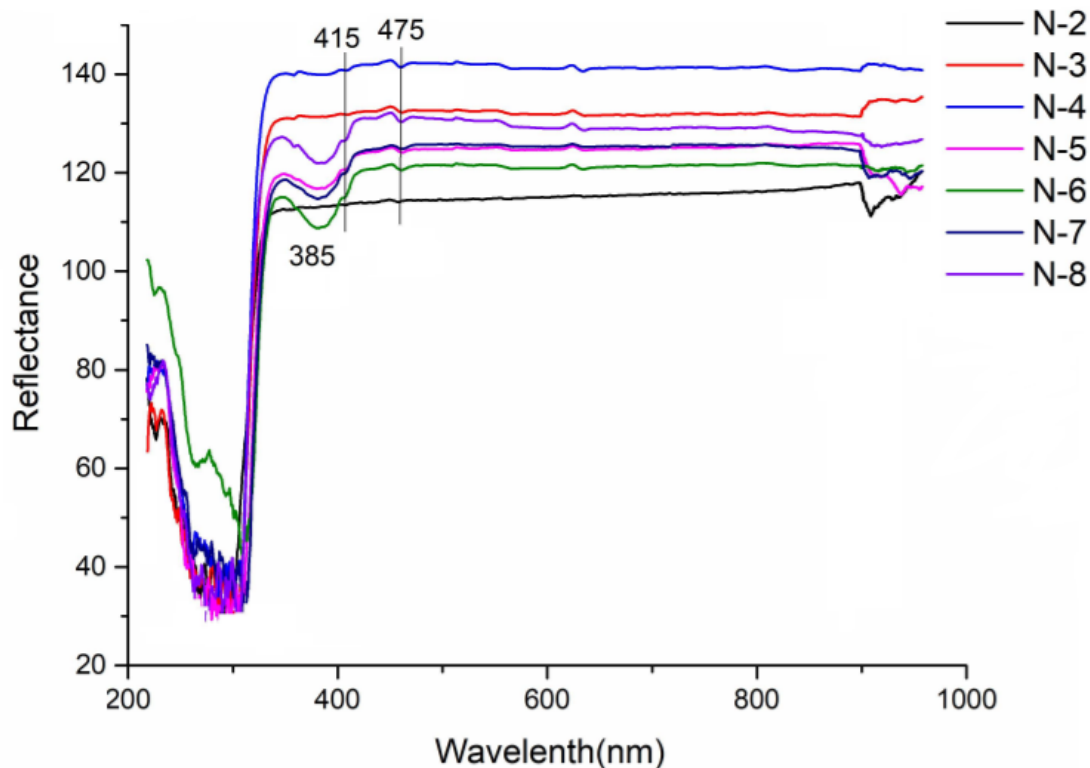


FIGURE 2.8: UV-Vis Spectra of natural diamond samples taken by Lu et al. Showing a sharp emission around 300 nm as well as weaker emissions at 415 and 475 nm [60].

2.7.2 Photoluminescence (below bandgap)

Photoluminescence with below band-gap light is a non-destructive analytical technique used in diamond characterisation. The use of below band-gap light allows the bulk of the diamond to be investigated as the light can propagate through the diamond without being absorbed. Photoluminescence works as described above in the luminescence mechanisms section. An electron is excited by an excitation source (e.g., a laser or UV lamp below diamond band-gap), this electron can then relax back down either through a fluorescent/prompt luminescent mechanism or a phosphorescent/delayed luminescent mechanism. Photoluminescence is a very sensitive technique that can measure defects even at low concentrations. It commonly shows sharp diagnostic peaks within its spectra along with some broadbands [61]. Only optically active defects can be detected by photoluminescence spectroscopy, fortunately most impurities in diamond are optically active in some manner. Commonly identified spectral features seen in photoluminescence are the NV^0 centre at 637 nm, the NV^- centre at 575 nm and the SiV^- centre at 737 nm [49, 52]. Photoluminescence spectroscopy is carried out within this thesis and further details of the equipment used can be found in Chapter 3.

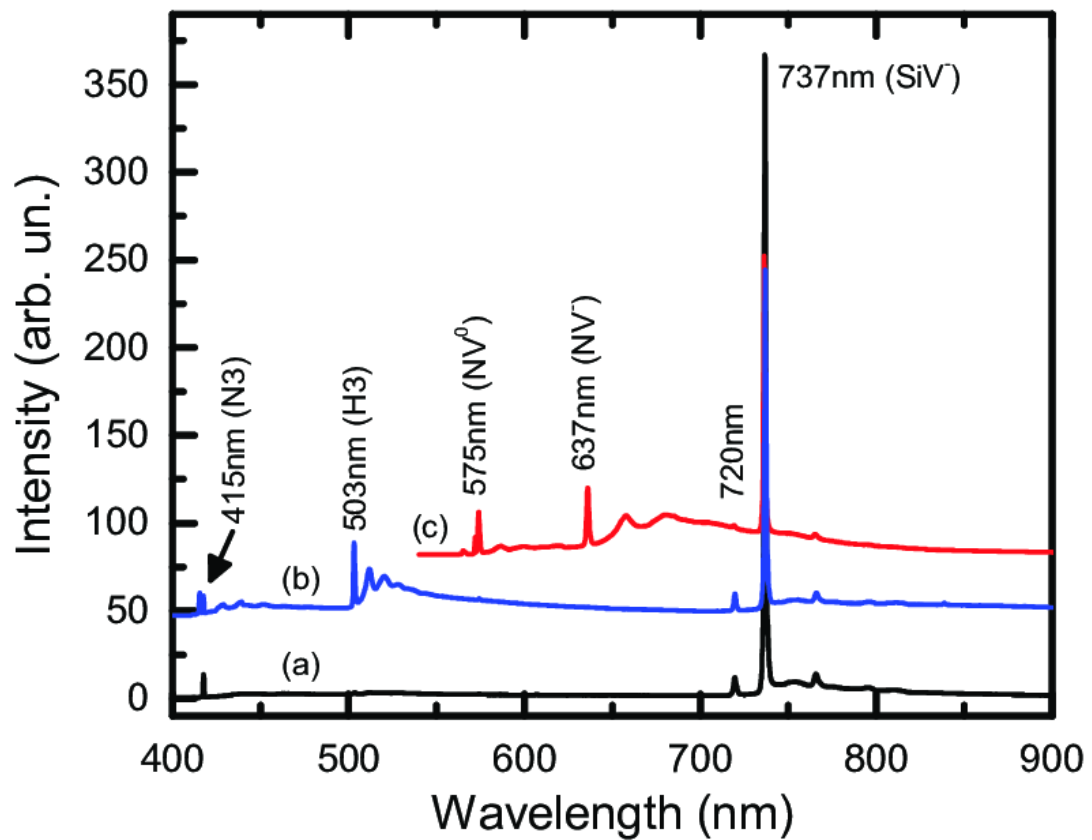


FIGURE 2.9: Photoluminescence spectrum by Palyanov et al. of diamond crystals synthesized in Mg-based systems. Spectra a and b were taken with an excitation of 395 nm and spectra c was taken with an excitation of 532 nm. The spectrum shows the NV^0 centre at 637 nm, the NV^- centre at 575 nm and the SiV^- centre at 737 nm [62].

2.7.3 Deep UV excited surface luminescence

Much like photoluminescence, deep UV excited surface luminescence studies the luminescence of a diamond when illuminated with light: in this case, specifically light of short wavelength Ultra-Violet light. Data is commonly recorded as spectra detailing the defects found in each stone. However, it can also be recorded as images showing the luminescence being emitted from the samples. One of the most widely used pieces of equipment employing this technique is the De Beers' DiamondViewTM.

The De Beers DiamondViewTM is a commercially available detection device that looks at the surface fluorescence of a diamond when the surface is irradiated with UV light of wavelength 225 nm or less. This type of below bandgap photoluminescence using deep UV light cannot propagate below the surface because of bandgap absorption, making this a surface technique. The energy of this light is equal or greater than that of the intrinsic energy band gap of diamond. The device displays an image of the stone which allows a user to determine whether a stone is of natural or synthetic origin. The diamond is

assessed by user interpretation, this is mainly down to the fluorescence, growth pattern and long-lived phosphorescence of the stone. Synthetic diamonds have different growth sectors through the body of the crystals, these growth sectors cause different growth patterns to be produced in the diamond, sectors of different growth types will luminesce with different colours [63]. Different sectors incorporate impurities as they go, at different rates from each other and in different ways, giving different spectroscopic properties. In unpolished stones, the presence of different growth sectors in synthetic diamond will produce characteristic growth faces on the surface of the diamond quite distinct from those formed on the surface of natural diamond. A skilled person can identify an unpolished synthetic diamond from a natural just by looking at it. However, all the surface information is removed when the stone is polished, illuminating with UV light and observing the luminescence will once again allow the user to observe the growth pattern. Implementing luminescence imaging in this way allows the user to see more than the human eye can detect and therefore establish the origin of the diamond. Growth sectors play a large part in identification between natural and synthetic diamonds with synthetic diamonds often having bundles of dislocations rather than the mosaic-like polygonised dislocations seen in natural diamonds [63]. Colour is also a factor used for identification with different defects causing different luminescence. For example, orange to orange-red shows nitrogen is present, blue-turquoise when boron is present and dark overall with blue dislocation luminescence indicates high purity samples [63, 64]. Figure 2.10 shows examples of natural, CVD and HPHT stones. The natural stone can be identified by its mosaic-like polygonised dislocation pattern and blue luminescence. The CVD stone exhibits closely spaced events from step flow growth, striations, steps and risers along with the orange luminescence that is often associated with as-grown CVD. Finally, the HPHT stone shows cubo-octahedral growth sectors and a long-lived turquoise luminescence commonly associated with HPHT grown diamonds.

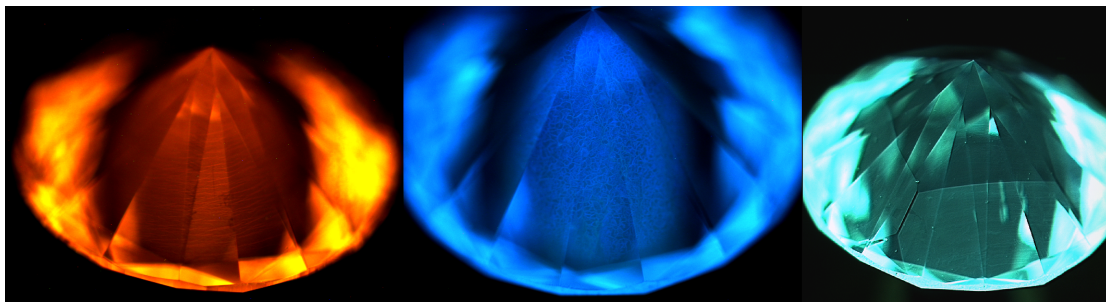


FIGURE 2.10: DiamondviewTM images of a CVD diamond sample (left), a natural diamond sample (middle) and a HPHT diamond sample (right). The CVD sample exhibits closely spaced events due to step growth, striations, steps and risers and also has the orange luminescence typically associated with as-grown CVD samples. The natural diamond shows a polygonised dislocation pattern and blue luminescence commonly associated with natural diamond. Finally, the HPHT stone has a cubo-octahedral grown pattern and a long-lived turquoise luminescence that is usually associated with HPHT diamonds.

2.7.4 Fourier Transform Infra-Red spectroscopy

Fourier transform infra-red spectroscopy (FTIR) is an analytical technique used to obtain infra-red spectra of absorption or emission of a material. It is a versatile, non-destructive technique which provides real-time measurements. FTIR is used for the identification and characterisation of materials based on their interaction with IR radiation [65]. The FTIR spectrometer gives results by producing an interferogram (defined as a photographic record of an interference pattern) which can then be Fourier transformed to construct a spectrum in the frequency domain.

An FTIR spectrometer is based on the Michelson interferometer, as shown in Figure 2.11. The interferometer is used to modulate the incoming optical radiation by changing the optical path difference between the two paths. This is achieved by moving one of the two mirrors inside the interferometer. Firstly, infra-red light is emitted by the source, this then passes through a beam splitter which allows half the light through to a mirror which is not fixed in position (Mirror 2) and reflects half the light to a fixed mirror (Mirror 1), when the light recombines there is a path length difference. The beam leaving the spectrometer then passes through the sample compartment before being focussed on to the detector. The detector measures the intensity of the combined IR beams as a function of the moving mirror displacement, some wavelengths interfere constructively and some destructively. When the path lengths are equal, all the wavelengths interfere constructively giving rise to the centre burst of the interferogram. A Fourier transform is used to turn this into a spectrum. A spectrum is recorded both with and without a sample in the beam, the difference is the sample spectrum.

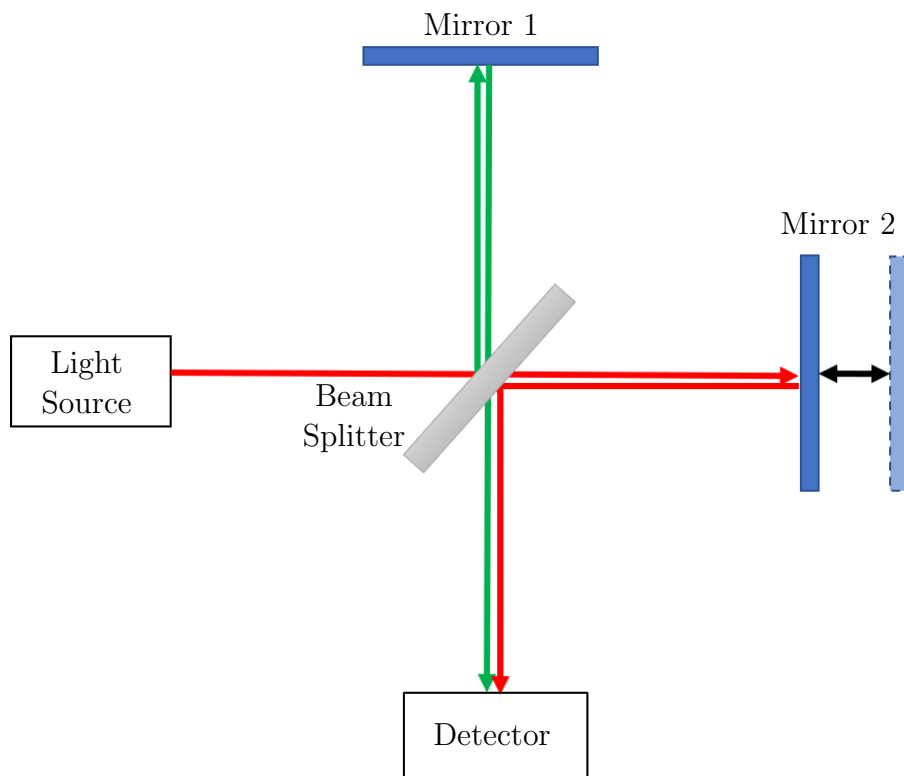
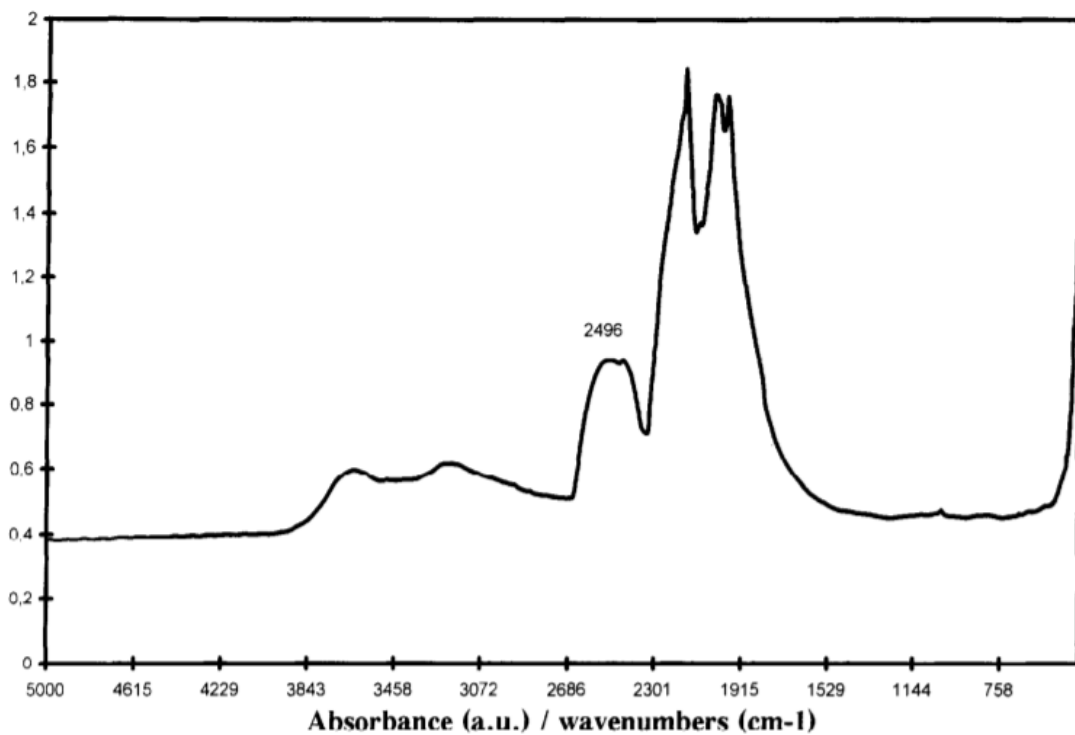


FIGURE 2.11: Schematic diagram of a Michelson interferometer.

FIGURE 2.12: Spectrum by Ferrer et al. of a brilliant cut diamond without impurities. The spectrum shows three different zones, a central zone from 2675 cm⁻¹ to 1500 cm⁻¹ and two smaller broadbands at 3633 cm⁻¹ and 3215 cm⁻¹ [57].

This technique is used frequently in diamond classification. The infrared spectrum of diamond is made up of three different zones, a central zone from 2675 cm^{-1} to 1500 cm^{-1} and two smaller broadbands at 3633 cm^{-1} and 3215 cm^{-1} as shown in Figure 2.12[57]. These absorptions are observed in the spectra of all diamonds, all other absorptions seen in diamond samples are dependent upon the impurities within the specific samples.

A few commonly seen defect absorptions in FTIR spectroscopy of diamonds are absorption in the region of $3100\text{-}3570\text{ cm}^{-1}$ which is associated with hydrogen defects and a spectral region containing complicated bands is seen between $1500\text{-}1000\text{ cm}^{-1}$ which is associated with nitrogen defects [66]. An absorption associated with synthetic growth is seen at 1050 cm^{-1} , it is known as the E centre and is observed in nitrogen containing diamonds. Two absorptions associated with HPHT synthesis are seen at 1344 cm^{-1} , associated with the C centre, and at 1128 cm^{-1} attributed to a defect centre with a single substituting nitrogen [67].

2.8 Motivation

There is considerable interest in research into defects found within the diamond lattice. These defects have significant impact on both the overall look and the physical properties of the diamond. This interest not only comes from the scientific community, but also from industrial companies, mining companies and jewellers alike, each with a different interest in what effect the defect has on the diamond but all of significant interest.

In terms of the gem industry it is extremely important that differentiation can be made between natural, synthetic and treated diamonds. As consumer confidence is needed when selling gems, it is of the utmost importance that undisclosed synthetics can be differentiated from natural diamonds with a high degree of certainty. Within the industrial community, the more information obtained about each defect and what effect that has on the diamond's physical properties, allows for tailor making the material required for the specific commercial application in mind.

In this thesis impurity complexes from natural, CVD and HPHT synthesis have been investigated using optical techniques. A further imaging investigation technique has been constructed in order to gather additional information into specific defects as well as providing a user friendly way of differentiating between natural and synthetic stones. The more advanced the synthesis process of diamond becomes the more important it is that investigation techniques continue to improve to allow for true identification of diamond samples. This thesis will focus on novel research to attempt to identify and

characterise defects within diamond; special attention will be paid to a defect seen at 499 nm in photoluminescence.

Chapter 3

Experimental theory

3.1 Introduction

Throughout this thesis several measurement techniques have been employed in order to obtain the results found in the subsequent chapters. This chapter will introduce these techniques along with the underlying theoretical principles linked to them and the results presented later in this thesis. This will include the imaging of diamonds, how to carry out the technique and what we hope to learn from the technique. Dispersive spectrometry will also be discussed along with its use in this thesis. A summary of specific experimental equipment used will also be given: for example, light sources, detectors and cryogenics.

3.2 Dispersive Spectrometers

The dispersive spectrometer is generally recognised as having been developed in the 1860's by Gustav Kirchhoff and Robert Bunsen [68]. It consisted of a sodium chloride prism which was used as an optical splitting system, later becoming known as the first generation of the spectrometer [69, 70]. The instrument required arduous sample preparation and the overall measurement region was extremely narrow due to the nature of the prism. This instrument was, therefore, too specialised for wide scale application.

Not long after, the second generation of the dispersive spectrometer - known as a monochromator spectrometer - was invented [71]. This spectrometer replaced the prism with an optical grating: a periodic structure for the diffraction of light. The monochromator is an optical sub-assembly that accepts polychromatic light and outputs monochromatic light, meaning it produces a beam of light with extremely narrow bandwidth. The

entrance ports tend to be geometrically fixed slits or optical fibres. The wavelength of the output light is determined by the angle of the diffraction grating inside, which can be rotated either manually or with a motor. The monochromator spectrometer is therefore a very versatile piece of equipment that produces a selectable monochromatic source of light. There are many different configurations of monochromator spectrometers one of the most common and the type used in this thesis is the Czerny-Turner configuration.

3.2.1 Grating geometry: Czerny-Turner

The Czerny-Turner monochromator is the classical type of optical monochromator, as shown in Figure 3.1 [71]. In this set-up input light is focussed onto the input slit, upon exiting the slit the light becomes divergent. The light is then collimated by a curved mirror (mirror 1) before hitting a diffraction grating that deflects the light in slightly different directions based on its wavelength. This light then meets a second curved mirror (mirror 2) which translates each different beam direction into different positions on the exit slit, meaning only light in a narrow wavelength can get through the slit. The set-up shown in Figure 3.1 is usually contained within a box with additional apertures and black shields in order to minimise the effect of stray light. It is also common practice to place the diffraction grating onto a motorised stage, allowing the centre wavelength of the pass band to be changed depending upon the position of the stage. Many monochromators contain several gratings of differing line spacings in order to study different wavelength regions, a motorised stage allows for switching between such gratings.

3.2.2 Resolution

The spectral resolution refers to the ability of a spectrometer to separate wavelengths, it determines the number of spectral peaks that the spectrometer can resolve. It is most

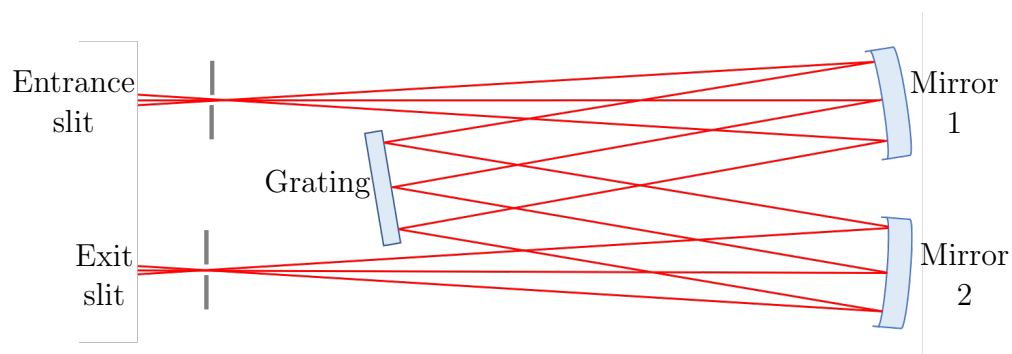


FIGURE 3.1: Schematic drawing of a Czerny-Turner grating geometry.

widely defined as the full width half maximum (FWHM) [72]. The spectral resolution of a spectrometer is dependent on the diffraction grating and the convolution of the entrance and exit slit (or detector).

The diffraction grating determines the total wavelength range of the spectrometer. The resolving power of a grating is a measure of ability to spatially separate adjacent spectral lines of average wavelengths [73]. The Rayleigh criterion states that two wavelengths are resolvable when the maxima of one wavelength coincides with the minima of a second wavelength, meaning they are identifiable as distinct spectral lines [73]. The chromatic resolving power (R) is defined in equation 3.1 [74].

$$R = \frac{\lambda}{\Delta\lambda} \quad (3.1)$$

Where $\Delta\lambda$ is the smallest difference in wavelength that can be distinguished at a wavelength of λ .

Diffraction gratings are available in various groove densities, the higher the groove density the higher the resolution is. However, as groove density is increased the spectral range of the system decreases. In most cases the resolution of the diffraction grating is greater than the resolution of the optical system, meaning it is not usually the resolution limiting factor.

The entrance slit width determines the spectral resolution and throughput of the spectrometer, as it determines the size of the image that can be formed on the detector plane. The entrance slit controls the spectral resolution by restricting the angle and the width of the beam of light entering the spectrometer. As the width of the slit decreases, light travelling at a large angle from the optical axis cannot enter the slit, meaning the light that does enter the spectrometer will be highly paraxial. In order to maximise the throughput of light into the spectrometer the entrance slit needs to be as large as possible, however the larger the entrance slit the lower the resolution, therefore it is important to limit the slit width to allow resolution requirements to be met.

In a spectrometer the entrance slit should be imaged perfectly onto the exit slit. In order to image the entrance slit onto the exit slit, the slits need to be the same size. This is important when using a point detector, as the spectrum is generated by scanning the angle of the grating, therefore the image on the exit slit will be specific wavelengths determined by the angle of the grating. If the exit slit is bigger than the entrance slit a larger range of diffracted wavelengths will be imaged on the detector, worsening the resolution. If the exit slit is smaller than the entrance slit, the resolution will be unaffected however the intensity of light reaching the detector will be decreased. It is

also commonplace to use an array detector or CCD, in which case the exit slit is no longer a factor involved in determining the resolution of the system and instead it is the pixel width of the detector. Ideally the pixel width would match the entrance slit width, if the detector pixels are larger than the resolution element then the resolution will instead be set by the size of the pixels.

3.3 Time-resolved Imaging

Time resolved imaging is a technique that is commonly used in biosciences, however, it has shown itself to be a useful tool for a range of samples including diamond. Time resolved imaging allows prompt and delayed surface luminescence of a material to be distinguishable.

To carry out time resolved imaging, a material is subjected to excitation from an excitation light source, the emission is then recorded by a camera. Unlike traditional imaging systems a delay can be placed on the camera before the image is taken, allowing both the prompt and delayed luminescence to be studied separately. A delay after the initial excitation can be placed at any time delay from the excitation pulse (within the parameters of the camera used).

The imaging system used within this thesis can be seen in Figure 3.2; this is made up of an excitation source, lens system, sample and detector the specifics of which will be discussed within the experimental equipment below.

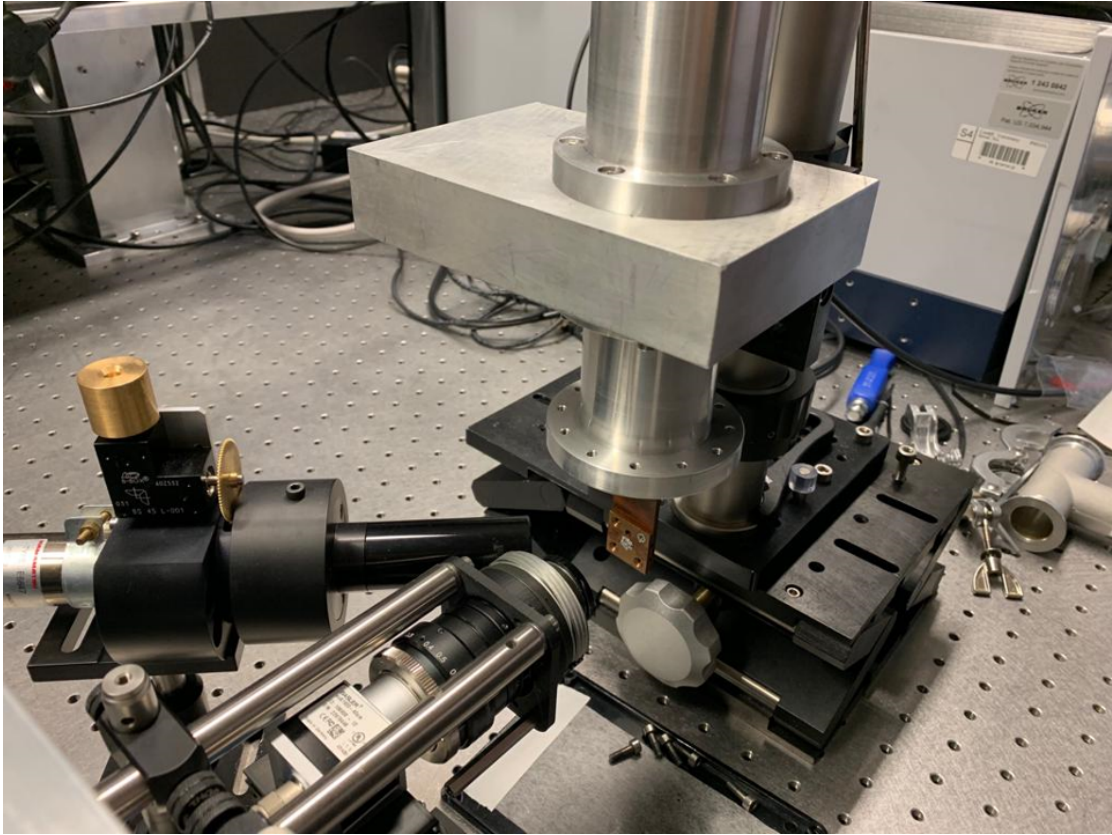


FIGURE 3.2: Photograph of the time resolved imaging set-up, showing the xenon flash lamp, lens system, cryostat, sample holder and camera.

3.4 Experimental equipment

3.4.1 Spectrometer

The dispersive spectrometer used to carry out spectroscopy in this thesis was a custom Horiba Fluorolog with a Horiba iHR-320 spectrometer attachment. Figure 3.3 shows the configuration of the spectrometer.

The spectrometer is made up of 3 blocks: the first being the inbuilt excitation source optics (containing two excitation sources), the second being the collection optics and the third being a Horiba IHR320 spectrometer. The inbuilt excitation sources found within the spectrometer have not been used for the purpose of this thesis and, therefore, specifics have not been included in Figure 3.3. The collection optics section of the spectrometer is where the light emitted by the diamond after excitation is collected. Within this section a diamond is placed on a sample holder; the sample holder used can be seen in Figure 3.4 and is based on the rotational design used in the De Beers DiamondView 3 [75]. The diamond is positioned in order that most light is directed at 90° to the excitation source where it is collimated by a mirror; a second mirror then focusses the

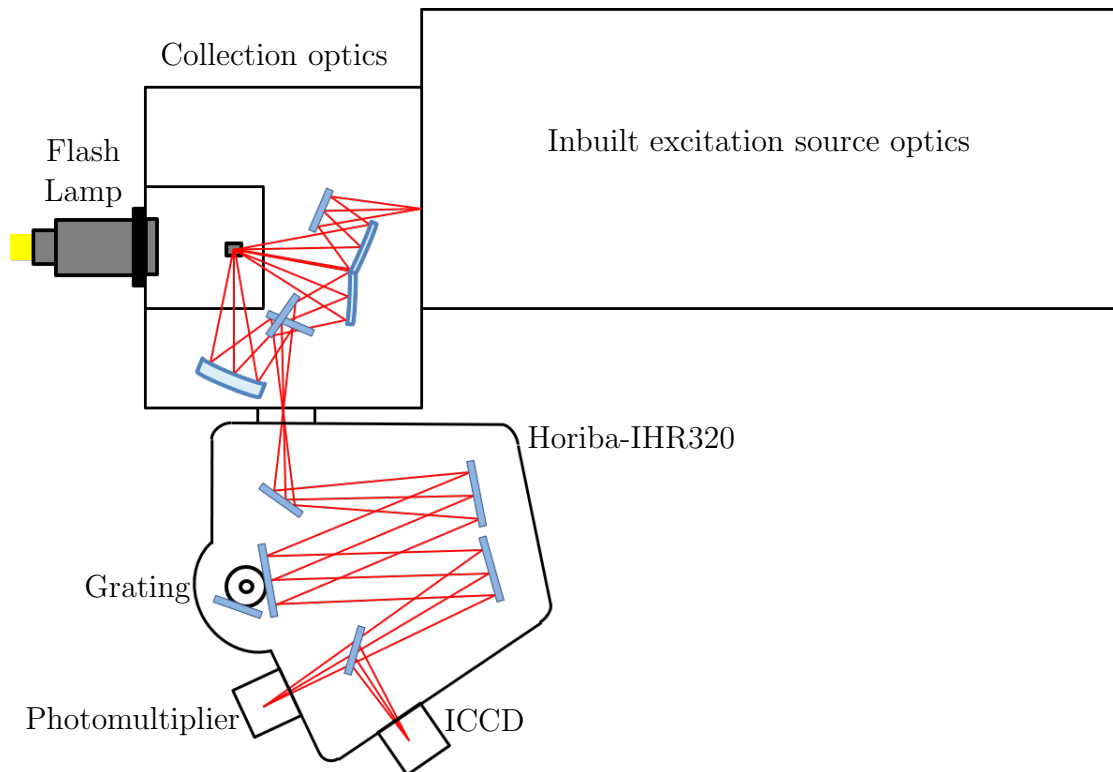


FIGURE 3.3: Schematic drawing of the Horiba Fluorolog, made up of three sections: the inbuilt excitation source optics, the collection optics and the Horiba IHR320 spectrometer.

emitted light into the Horiba IHR320. The Horiba IHR320 is the final section of the spectrometer and can be used as a stand-alone piece of equipment. Given the difficulty in collecting emitted light from a diamond gemstone, it is useful to use it in conjunction with the collection optics. The IHR-320 spectrometer has a 300 g/mm grating and has two different detectors attached to it. There is a moveable mirror which allows for switching between the two detectors: the Andor iStar DH320T-18U-E3 Intensified CCD and the IBH TBX-850C photomultiplier.

3.4.2 Light Source

The light source used for both spectroscopy and imaging was a Hamamatsu Photonics L7685 xenon flashlamp which was spectrally filtered to 190–227 nm output, with temporal pulse width of 2.9 μs at full width half maximum. The UV emission of the lamp was confined to 190–227 nm by a bespoke band-pass filter from Laser Components, the spectral throughput of the filter can be seen in Figure 3.5. The light source was synchronised with all the detectors using TTL signals, as discussed below.

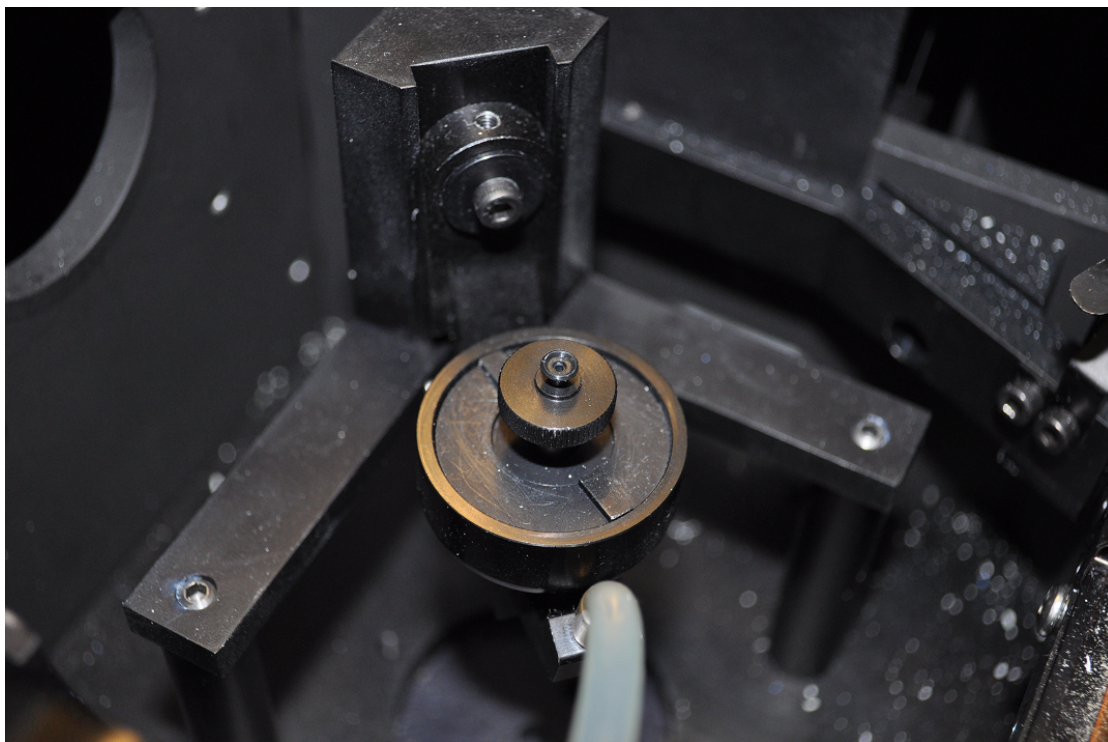


FIGURE 3.4: Photograph of the sample holder used within the fluorolog spectrometer, based on the De Beers DiamondView 3 design.

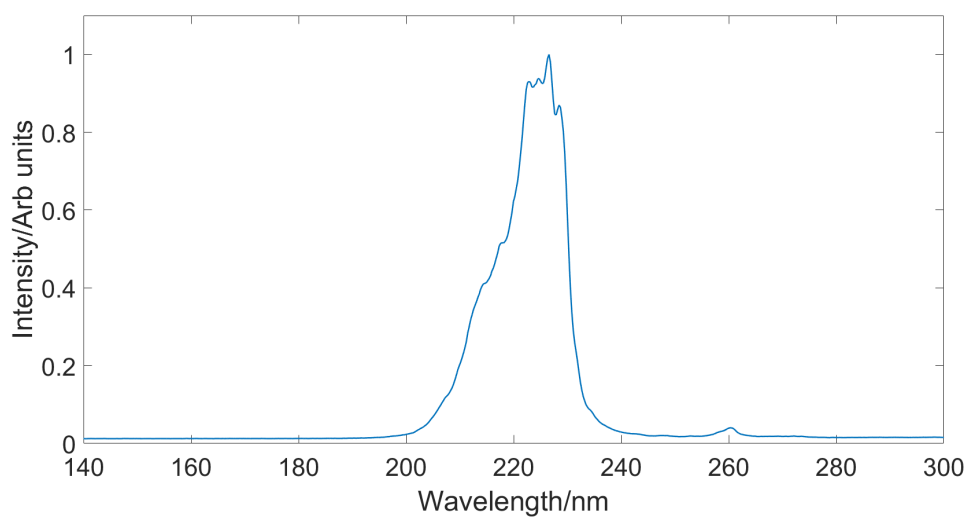


FIGURE 3.5: Spectral throughput of the bespoke band-pass filter from Laser components.

3.4.3 Detector

3.4.3.1 Spectroscopy detectors

Two detectors were used for spectroscopy within this thesis: the Andor iStar DH320T-18U-E3 and the IBH TBX-850C.

The Andor iStar detector is an intensified charge-coupled device (iCCD): a highly sensitive photon detector. A CCD contains a large number of light sensitive pixels that build up a charge by absorbing light, the brighter the light and the longer the interaction the higher the recorded charge. Unlike a traditional CCD detector, the Andor iStar detector has been intensified, meaning that a fibre coupled image intensifier has been added to the detector; this offers a large signal amplification as well as providing optical shuttering capabilities and time resolution within the nano-second regime. The intensifier tube is an evacuated tube which makes up the photocathode; when a photon strikes the photocathode, a photoelectron is emitted which is then drawn towards a micro-channel plate which amplifies the signal. The image intensifier can be operated as an optical switch on very fast timescales. If a positive voltage is applied, the photoelectrons cannot cross the gap between the photocathode and the micro-channel plate and is, therefore, gated off. However, if a negative voltage is applied the electrons can cross the gap and can go on to be amplified it is, therefore, gated on. It is the ability to be able to swap the gate so quickly that allows for the advance optical shuttering properties that the iCCD provides. The Andor iStar detector is a two-dimensional silicon-based matrix of photosensors and is sensitive in the ultra-violet and visible parts of the electromagnetic spectrum. When carrying out luminescence measurements, a pulse generator was used to provide two TTL signals, one to the xenon flash lamp and one to the iCCD. The iCCD signal was delayed by 8 μs with respect to the flash lamp to account for the difference in latency between the two devices. The iCCD was used to record spectra on both a prompt and delayed time frame; when recording prompt spectra, the delay on the iCCD was set to zero in order to record the emission contemporaneously with the lamp pulse, the emission was integrated over a 10 μs gate. When recording delayed luminescence, the delay on the iCCD was set to 100 μs and the emission was integrated over 60 ms.

The IBH TBX-850C is a picosecond photon detection module, commonly referred to as a photomultiplier tube or detector. Photomultiplier detectors are commonly used when dealing with very weak signals, they are sensitive in the ultra-violet, visible and near infra-red regions of the electromagnetic spectrum. Photo multiplier detectors contain a photocathode; when photons are incident on the photocathode, electrons are ejected from the photocathodes surface. The electrons are then directed to an electron multiplier, made up of a series of electrodes called dynodes, the number of electrons present

increases with each dynode the electrons strike. After running through the series of dynodes the electrons will eventually hit the anode, resulting in a sharp current pulse, which is far easier to detect than the original photon emission. In this thesis, the photomultiplier detector is used when carrying out lifetime measurements.

Within this thesis both detectors were used, however, both for different purposes. The Andor iStar DH320T-18U-E3 was used for spectral measurements as the detector can measure the entire dispersion from the grating due to it being imaged on a sensor, as well as its ability to be gated relative to the excitation pulse using the intensifier. The IBH TBX-850C was used for long decay studies, as it measures at single wavelengths and has a higher temporal resolution than the Andor iStar detector.

3.4.3.2 Imaging detectors

Two detectors were also used for imaging within this thesis: the Teledyne Dalsa Genie Nano C2050 and the Basler Ace acA1920-40uc.

The Teledyne Dalsa Genie Nano C2050 is an area scan camera. Area scan cameras contain a matrix of pixels that can capture microsecond time-gated images without the need for moving the camera during the process. The camera and flash lamp were synchronised using the camera's internal timer, with the flash lamp signal offset by 11 μs with respect to the timer to account for the difference in latency between the two devices. If the two devices were triggered electrically simultaneously the flash lamp would fire 11 μs before the camera started recording, adding the 11 μs delay to the flash lamp allows the events to occur simultaneously. For images recording prompt luminescence, images were taken with no delay (despite the offset built in to account for the latency between the two devices). For images recording delayed luminescence, a delay of 100 μs was used and integrated for 30 ms, unless stated otherwise. The majority of the images used within this thesis were an average of 20 individual captures. However, in some cases, fewer or greater numbers of captures were averaged in order to obtain a better image.

The second imaging detector used was the Basler Ace acA1920-40uc. This camera is also an area scan camera and was used in the same way to take luminescence images as described for the Teledyne Dalsa Genie Nano, with the same parameters for prompt and delayed luminescence. However, the camera was synchronised with the lamp in the same way the Andori Star was (using two TTL signals) rather than using an internal timer as was the case with the Teledyne Dasla Genie Nano.

3.5 Cryogenics

The cryostat used in this work is a modified Oxford Instruments Microstat He, with a custom optical housing designed at Cardiff University and an optional ColdEdge Stinger accessory. The system can be used in two ways: using the system as a closed cycle flow cryostat or using the system as a open flow cryostat. Firstly, the closed cycle flow system uses a StingerTM, a closed loop with helium as a refrigerant cools helium in a second loop, that in turn cools the Oxford Instruments cold finger and sample. This configuration allows temperatures as low as 4 K to be reached. The stinger was used a handful of times for the results in this thesis but, primarily, the cryostat was used as a flow cryostat. When used as a flow cryostat, a vacuum pump draws liquid helium or liquid nitrogen into the cryostat to cool the cold finger; using liquid helium allows for temperatures around 4 K to be reached and using liquid nitrogen allows for temperatures around 77 K to be reached. As 77 K was sufficient for most of the experiments presented in this thesis, the cryostat was mainly used as a liquid nitrogen flow cryostat. In both cases, the sample temperature was controlled using an Oxford Instruments iTC mercury temperature controller with a resistor-based heating controller and PID control software. The diamond was mounted in a specially designed cold finger using indium for good thermal contact, large windows were used on the cryostat to allow for excitation and collection to be carried out on the same face of the diamond. Figure 3.2 shows the diamond mounted in the cryostat with the outer cryostat casing removed for ease of viewing the diamond.

3.6 Samples and post processing

All samples used in this thesis were supplied by De Beers Technologies. Three main sample sets were focused on. The first sample set originated from Gemesis and comprised three CVD synthetic gemstones. The second sample set originated from Element 6; these are plated CVD synthetic stones which have been purposely nitrogen doped as well as having a relatively high concentration of silicon although not purposely silicon doped. The final sample set also originated from Element 6 and is comprised plated CVD synthetic stones which have, once again, been doped with nitrogen and contain a very low level of silicon, again not purposely doped. The specifics of each stone within each sample set can be found in Tables 3.1, 3.2 and 3.3.

Sample	Shape and Cutting	Measurements (mm)	Carat Weight	Colour Grade	Clarity Grade
1	Round brilliant	4.40 × 2.70	0.33	F	VVS2
2	Square modified brilliant	3.6 × 3.59 × 2.45	0.28	E	SI2
3	Square modified brilliant	4.09 × 4.05 × 2.81	0.41	F	VVS1

TABLE 3.1: International Gemological Institute grading results for the three synthetic CVD gemstones sourced from Gemesis

Sample	Shape and Cutting	Annealing Conditions (°C/4 h)	x(mm)	y(mm)	z(mm)	Carat Weight
A	Free standing film	1200	5.05	3.73	1.45	0.47
B	Free standing film	1400	3.56	3.58	2.228	0.49
C	Free standing film	1600	4.73	4.16	2.176	0.75
D	Free standing film	1700	4.00	4.21	2.22	0.65
E	Free standing film	1800	3.59	3.48	1.71	0.36
F	Free standing film	1900	5.21	3.99	2.146	0.77
H	Free standing film	2000	3.29	3.44	1.964	0.38
I	Free standing film	2400	3.29	3.35	2.018	0.36

TABLE 3.2: Annealing conditions, physical dimensions and carat weight for each of the samples cut from the original E6 CVD nitrogen-doped diamond plate with high silicon concentration and independently heat treated.

Sample	Shape and Cutting	Annealing Conditions (°C/4 h)	x(mm)	y(mm)	z(mm)	Carat Weight
A	Free standing film	1200	3.32	3.07	2.956	0.57
B	Free standing film	1400	3.18	3.15	0.53	0.07
D	Free standing film	1700	3.38	3.15	3.45	0.64
E	Free standing film	1800	3.32	3.01	2.696	0.46
F	Free standing film	1900	3.22	2.67	0.50	0.07
H	Free standing film	2000	3.25	2.97	3.386	0.53
I	Free standing film	2400	3.45	3.37	0.52	0.10

TABLE 3.3: Annealing conditions, physical dimensions and carat weight for each of the samples cut from the original E6 CVD nitrogen-doped diamond plate with low silicon concentration and independently heat treated.

3.7 Conclusion

Investigations into colour centres present in diamond is the primary focus of this thesis. Colour centres in diamond are of great interest to a wide range of industries, from drill bit manufacturers to jewellers, as well as scientific interest with many centres being investigated for use in quantum technologies. Studies have been carried out on both natural and synthetic diamond with the primary focus on CVD synthetic diamond. The aim of these studies was to interrogate the diamonds in a number of different ways

in order to characterise the defects within the stones and therefore get an insight into the origins of the stones. The experimentation carried out was both time-resolved, to allow the dynamics of the system to be probed on different timescales and temperature dependent in order to learn more about the electronic structure of the stones. The experimentation was carried out both spectroscopically and using imagery, allowing for thorough analysis of the diamond samples.

Chapter 4

Time-Gated Luminescence Imaging of Natural and Synthetic Diamonds

4.1 Background and Motivation

Diamond classification has long been of the upmost importance to jewellery professionals, with the first diamond grading system being established in India over 2000 years ago [76]. Traditionally, classification of diamond relied upon the human eye and usually fell to extremely experienced gemmologists. The value of a diamond depends on a combination of factors therefore it is important that there is a universally accepted systematic way to evaluate and discuss these factors. This came about in the 1950's when the GIA established a grading system which relied upon the four C's: cut, colour, carat and clarity [77].

As time has gone on synthetic diamonds have begun to infiltrate the market and are getting ever more difficult to distinguish from natural diamonds. Many characteristics can be used in order to determine if a diamond is of natural or synthetic origin; however, the properties of natural and synthetic diamond vary inherently, making it a difficult task. There is a requirement for effective discriminatory techniques that give definitive answers without the need for a wealth of experience and expertise to interpret the results. This is especially important as the task of identifying the origin of diamond commonly falls to an appraiser, a grader or a gemmologist, many of whom do not work in gemmological laboratories and instead work in organisations such as independent jewellers, auction houses and pawn brokers [64].

Transmission spectroscopy provides a more sophisticated technique than the human eye alone. Transmission spectroscopy is another passive technique which effectively extends the ability of the human eye, while giving quantifiable results. This has been a very effective technique and has proved very useful to the diamond classification field over time. However, in order to progress further than this when classifying diamond, it is necessary to move from a passive technique to an active technique, meaning to actively excite the diamond in order to gain new information.

4.1.1 UV excitation of diamond

Using ultra-violet (UV) light to excite a diamond is an active surface-level spectroscopy technique. Usually, when energy is supplied to a material the electrons on the surface of the material are excited. This means the electrons absorb the energy of the colliding photons of light and move to higher energy states; when these electrons relax back down photons are produced and this emission is recorded. However, as diamond is an indirect band-gap material, meaning the maximum energy of the valence band and the minimum energy of the conduction band occur at different values of the crystal momentum, band-band recombination cannot happen without the assistance of phonons [78]. A phonon is the vibration of atoms in the crystal lattice: a phonon allows for conservation of momentum in the system. The electron must therefore interact with a photon to gain energy and a phonon to gain or lose momentum. As all three entities, electron, photon and phonon have to intersect, this process is more difficult and therefore takes longer to occur thus causing a time delay. Once this takes place, a photon is emitted with a similar energy to the band gap of the diamond, thus it has weak interaction with the material and so can escape the diamond. This type of band-band recombination is only possible in materials with extremely low defect concentration, for example in intrinsic diamond.

4.1.2 Other relaxation paths

Band-band recombination is not the only way light can be emitted from a diamond, there are other relaxation paths electrons can use in order to relax and produce photons. Diamond is very rarely intrinsic, instead it often contains defects within the lattice. In comparison to the concentration of carbon atoms in the lattice the concentration of defects is usually very low and therefore interaction between defects is negligible. This means that these defects can be classed as isolated systems with sharp defined energy levels; therefore, these are systems with known quantum numbers. The defects therefore provide other routes for electrons to relax and emission to occur.

4.1.3 Fermi's Golden Rule

The length of time it takes for an electron to decay from an excited state and release depends on the probability that this transition will happen. If the probability of the transition happening is small, it may be a long wait to see the photon, and hence the lifetime of the transition would be long. However, if the probability of the transition happening is very high, then the signature photon of the transition may appear very quickly, so the lifetime will be short. Fermi's Golden Rule can be used to calculate the transition rate between two states 1, and 2,

$$W_{1 \rightarrow 2} = \frac{2\pi}{\hbar} |M_{12}|^2 g(\hbar\omega) , \quad (4.1)$$

where $W_{1 \rightarrow 2}$ is the transition rate, M_{12} is the matrix element that describes the overlap of the wavefunctions, and $g(\hbar\omega)$ is the density of final states for the transitions. So, in the event that there are lots of final states that an electron can decay to, $g(\hbar\omega)$ will be large and then the transition rate will consequently be faster.

4.1.4 Atomic Systems

When considering the atomic system the situation is relatively straight-forward. The matrix element is just the overlap integral between the atomic wavefunction, i.e.

$$M_{12} = \int \Phi_2^*(\vec{r}) \hat{\mathcal{H}} \Phi_1(\vec{r}) dV , \quad (4.2)$$

where $\Phi_2^*(\vec{r})$ is the complex conjugate of the final state wavefunction, $\Phi_1(\vec{r})$ is the initial state wavefunction, and $\hat{\mathcal{H}}$ is the Hamiltonian that describes the electromagnetic interaction. If we consider the three $2p$ wavefunctions in the second shell, then there is clearly no spatial overlap between $2p_x$, $2p_y$, and $2p_z$. Therefore, transitions between these states would not be expected. Consequently, such a transition is said to be forbidden. In contrast, parts of the $1s$ wave function $\Phi_{1s}(\vec{r})$ and the $2p$ wave function $\Phi_{2p}(\vec{r})$ overlap in space, so the matrix element will be non-zero. A transition $2p \rightarrow 1s$ would be allowed, and the transition rate could be calculated. For atomic transitions only the spatial wavefunctions need to be taken into consideration when performing this calculation.

4.1.5 Molecular Systems

The situation is more complicated in molecular systems because the spin must also be included in the total wavefunction. The spin component is necessary because the

electrons need to be distinguishable to satisfy the Pauli Exclusion. The simplest case to describe is the hydrogen molecule H_2 . Where a good choice for an approximate solution would be the product of two atomic hydrogen wavefunctions, i.e.

$$\Phi(\vec{r}_1, \vec{r}_2) \propto \Phi_A(\vec{r}_1)\Phi_B(\vec{r}_2) , \quad (4.3)$$

where $\Phi_A(\vec{r})$ and $\Phi_B(\vec{r})$ denote the wavefunctions of the two different hydrogen atoms A and B . The Pauli Exclusion Principle requires that the two electrons are distinguishable, i.e., they cannot both exist in the same place with the same quantum numbers. However, there is a problem with the proposed solution if $r_1 = r_2$ and the two spatial wavefunctions Φ_A and Φ_B are the same. The product $\Phi_A\Phi_B = |\Phi_A|^2 = |\Phi_B|^2$ would not be zero, which would imply that there is a finite probability that two electrons with the same quantum numbers can occupy the same point in space. Considering the wavefunctions below, formed from the superposition of the atomic wavefunctions,

$$\Psi_{\uparrow\downarrow}(\vec{r}_1, \vec{r}_2) \propto \Phi_A(\vec{r}_1)\Phi_B(\vec{r}_2) + \Phi_A(\vec{r}_2)\Phi_B(\vec{r}_1) , \quad (4.4)$$

$$\Psi_{\uparrow\uparrow}(\vec{r}_1, \vec{r}_2) \propto \Phi_A(\vec{r}_1)\Phi_B(\vec{r}_2) - \Phi_A(\vec{r}_2)\Phi_B(\vec{r}_1) . \quad (4.5)$$

The plus term gives a symmetric spatial wavefunction and the negative term gives an asymmetric spatial wavefunction. An asymmetric wavefunction is helpful because $\Psi_{\uparrow\uparrow}(\vec{r}_1, \vec{r}_2) = 0$ when $r_1 = r_2$. However, one symmetric wavefunction is left in this case that does not equal zero when $r_1 = r_2$. The spin component of the wavefunction must be included to ensure that the total wavefunction is always antisymmetric. It is possible to combine 2 spins in 4 different ways. The uncoupled system is described;

$$\begin{aligned} |s, m\rangle &= \left| \frac{1}{2}, +\frac{1}{2} \right\rangle \left| \frac{1}{2}, +\frac{1}{2} \right\rangle \quad (\uparrow\uparrow) \\ &= \left| \frac{1}{2}, +\frac{1}{2} \right\rangle \left| \frac{1}{2}, -\frac{1}{2} \right\rangle \quad (\uparrow\downarrow) \\ &= \left| \frac{1}{2}, -\frac{1}{2} \right\rangle \left| \frac{1}{2}, +\frac{1}{2} \right\rangle \quad (\downarrow\uparrow) \\ &= \left| \frac{1}{2}, -\frac{1}{2} \right\rangle \left| \frac{1}{2}, -\frac{1}{2} \right\rangle \quad (\downarrow\downarrow) \end{aligned}$$

A coupled system can be achieved by changing the basis, re-writing these four states as linear combinations. The first antisymmetric function with $s = 0$ is called the singlet

state, and the three symmetric functions with $s = 1$ are called the triplet states.

$$\left. \begin{aligned} |0,0\rangle &= \frac{1}{\sqrt{2}}(\uparrow\downarrow - \downarrow\uparrow) & s = 0 \\ |1,-1\rangle &= \downarrow\downarrow \\ |1,0\rangle &= \frac{1}{\sqrt{2}}(\uparrow\downarrow + \downarrow\uparrow) \\ |1,1\rangle &= \uparrow\uparrow \end{aligned} \right\} s = 1$$

By combining the asymmetric spin wavefunction with the symmetric spatial part it ensures that the total wavefunction is always asymmetric. As long as one component is symmetric and the other is antisymmetric, then the overall function will be antisymmetric. The plus term gives a symmetric spatial wavefunction. Combining this with an antisymmetric spin component (called the singlet state) satisfies the overall antisymmetric requirement.

$$\Psi_{\uparrow\downarrow-\downarrow\uparrow}(\vec{r}_1, \vec{r}_2) \propto [\Phi_A(\vec{r}_1)\Phi_B(\vec{r}_2) + \Phi_A(\vec{r}_2)\Phi_B(\vec{r}_1)] |0,0\rangle \quad (4.6)$$

$$\Psi_{\downarrow\downarrow}(\vec{r}_1, \vec{r}_2) \propto [\Phi_A(\vec{r}_1)\Phi_B(\vec{r}_2) - \Phi_A(\vec{r}_2)\Phi_B(\vec{r}_1)] |1,-1\rangle \quad (4.7)$$

$$\Psi_{\uparrow\downarrow+\downarrow\uparrow}(\vec{r}_1, \vec{r}_2) \propto [\Phi_A(\vec{r}_1)\Phi_B(\vec{r}_2) - \Phi_A(\vec{r}_2)\Phi_B(\vec{r}_1)] |1,0\rangle \quad (4.8)$$

$$\Psi_{\uparrow\uparrow}(\vec{r}_1, \vec{r}_2) \propto [\Phi_A(\vec{r}_1)\Phi_B(\vec{r}_2) - \Phi_A(\vec{r}_2)\Phi_B(\vec{r}_1)] |1,1\rangle \quad (4.9)$$

The minus term results in an antisymmetric spatial wavefunction needs to be combined with a symmetric spin component (i.e., one of three possible triplet states).

When the full spin wavefunctions are used in Fermi's Golden Rule, an additional set of transition rules applies. In order to go from a triplet state to a singlet state (or vice versa) a spin flip is necessary so that the total spin s goes from $1 \rightarrow 0$. This added complication reduces the transition rate. Luminescent transitions are often fast because they are spin preserving. The lifetime is dictated simply by the spatial overlap of the initial and final states. Phosphorescent transitions are slow because in addition to the spatial overlap, the spin change in the overlap integral must be taken into account. Phosphorescence (or delayed luminescence) is often an indication that there was a change in the electron spin. In this thesis these transitions with long lifetimes are not explicitly referred to as phosphorescence as we cannot be sure there was a spin change, although the timescale suggests this was likely. For this reason the term 'delayed luminescence' has been used to refer to such transitions.

4.1.6 Penetration depth

Penetration depth quantifies how deeply into a material electromagnetic radiation can penetrate; it is defined as the depth at which the intensity of the radiation falls to 1/e of its original value [79].

In order to calculate the penetration depth of the excitation source, the absorption coefficient of the material must be calculated, as shown in equation 4.10, the absorption coefficient is dependent upon the extinction coefficient of the material, this refers to the imaginary part of the complex index of refraction. The inverse of the absorption coefficient gives the penetration depth of the excitation light, as shown in equation 4.11.

$$\alpha = \frac{4\pi\kappa}{\lambda} \quad (4.10)$$

$$\delta_p = \frac{1}{\alpha} \quad (4.11)$$

Where α is the absorption coefficient, κ is the extinction coefficient, λ is the wavelength of the excitation and δ_p is the penetration depth.

Within this thesis the UV excitation source used was of wavelength 190-225 nm. Using recorded values of extinction coefficient from Edwards et al. [80] it was found that the maximum penetration depth of the UV source would be 0.53 mm corresponding to the maximum wavelength of 225nm. However, for most wavelengths within the UV broadband used it was found that the radiation would penetrate around 1 micron in depth. Due to this the technique is referred to as a surface technique.

4.1.7 Diamond types

Diamond Type	Likely defect	Natural diamonds of this type (%)
Type Ia	Nitrogen defects: A centres, B centres and N3	95
Type Ib	Single substitutional nitrogen	0.1
Type IIa	Devoid of impurities	1.8
Type IIb	Boron	0.1

TABLE 4.1: Showing what defects can commonly be found in different diamond types. Further detail: A-centres are comprised of a neutral nearest neighbour pair of nitrogen atoms. B-centres consist of a carbon vacancy surrounded by four nitrogen atoms. The N3 defect consists of three nitrogen atoms surrounding a vacancy.

The purpose of actively exciting the diamond samples is to allow the user to further characterise diamonds using the new information gained by active excitation. Diamonds vary greatly not just between natural and synthetic but also within the natural group and the synthetic group themselves. This means there are lots of different characteristics that can be looked at to assess whether a diamond is natural or synthetic and, indeed, which category of each it would fall into. Natural diamond's defects have been extensively studied and can, therefore, be classified as Type I or Type II diamond; this is then sub categorised as Type Ia, Type Ib, Type IIa and Type IIb as shown in Figure 4.2. Type Ia diamonds are the most common class of diamond and, therefore, can be further categorised into Type IaA and Type IaB depending on the form the nitrogen defects take within the lattice. However, for this thesis we have decided not to subcategorise. As seen in Table 4.2, the main difference between Type I and Type II diamonds is the difference in nitrogen aggregate concentration, with Type I containing nitrogen impurities as their main impurity whereas Type II diamonds have no measurable nitrogen impurities. It is important to note that not all naturals fall easily into one of these categories, often leaving a subset of unusual looking diamonds which may be wrongly categorised as synthetic. It is, therefore, very important that investigations can be carried out easily on these stones in order to find out more about them and make sure they are not wrongly characterised.

4.1.8 Motivation

The motivation behind this chapter was the development of an imaging rig that could be used effectively to help identify diamond samples of both natural and synthetic origin, making the task easier for less experienced users to undertake. The imaging rig produced is a surface technique which uses a shorter wavelength excitation (<225 nm) than most traditional techniques. The light source and the camera have been synchronised allowing the camera exposures to be controlled relative to the lamp pulse with microsecond accuracy. This facilitates the user to assess the stone on both prompt and delayed timescales, allowing for imaging to be undertaken contemporaneously to the pump or any set amount of time after the pump, thus, allowing a greater number of defects to become visible in the stone; as many of them appear on different timescales or have different lifetimes to each other, many of which can be overshadowed when only looking at one timescale. In this chapter, a survey of samples was chosen of natural, CVD synthetic and HPHT synthetic diamonds in order to explore the temporal characteristics of the rig. The survey of samples selected also allows for specific characteristics of many defects to be determined and documented in order to help users to characterise diamonds in the future when using this technique.

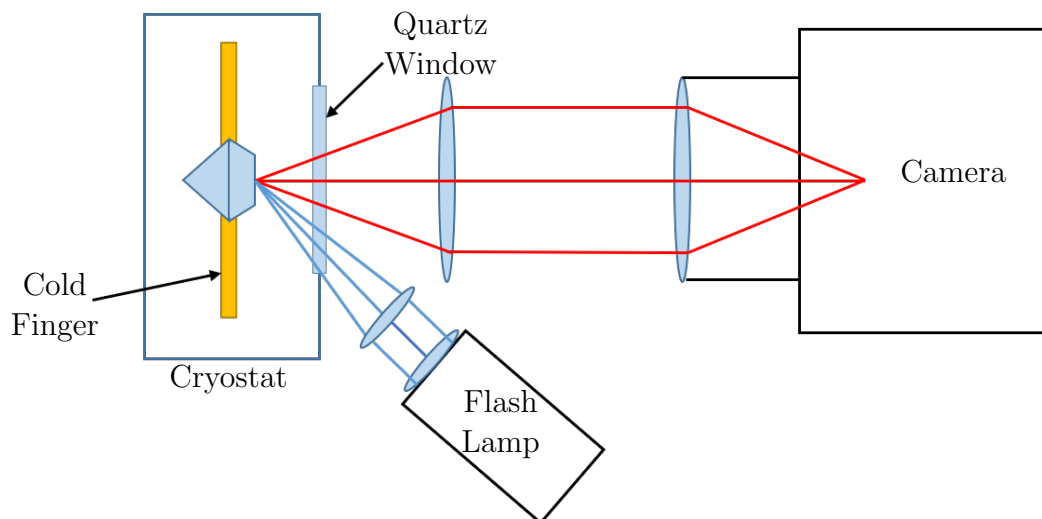


FIGURE 4.1: Schematic diagram showing the experimental imaging rig. The source is a xenon flash lamp spectrally filtered to 190-227 nm, the camera is a Basler Ace aca1920-40uc area scan camera, the two have been synchronised to account for the difference in latency.

4.2 Time-Resolved Imaging Rig

An imaging rig was constructed to carry out time resolved temporal imaging. The rig consists on an excitation source, a sample holder, lens systems and a camera, as shown in Figure 4.1. Above band-gap excitation was provided by a Hamamatsu Photonics L7685 Xenon flash lamp which had been spectrally filtered (using a custom filter) to 190-227 nm output, with a temporal pulse width of $2.9 \mu\text{s}$ at full width half maximum. After excitation the luminescence from the diamond was recorded using a Basler Ace AcA1920-40uc area scan camera. The camera and flash lamp were synchronised using the camera's internal timer, with the flash lamp signal offset by $11 \mu\text{s}$ with respect to the timer to account for the difference in latency between the two devices. Prompt luminescence images were recorded contemporaneously to the excitation flash and delayed luminescence images could be taken at any set delay after the flash with microsecond accuracy. The images shown in this chapter are an average of 20 individual captures.

4.2.1 Sample Selection

A selection of samples was chosen for use with the imaging rig that has been developed; the samples were surveyed and used to explore the wide range of prompt and delayed luminescence characteristics that the imaging rig can record. These samples consisted of a selection of colourless and near colourless polished diamond samples of natural, CVD synthetic and HPHT synthetic origin.

4.3 Natural Diamond Samples

4.3.1 Type IIa

Firstly, a range of natural diamond samples was surveyed using the imaging rig, allowing for an overview of characteristics that different natural diamonds possess on both prompt and delayed timescales.

Figure 4.2 shows the prompt luminescence of a typical Type IIa natural diamond, the prompt luminescence is dominated by blue luminescence. The luminescence is thought to be caused by dislocations in the diamond lattice [81]. The delayed luminescence is shown in Figure 4.2, much like the prompt luminescence the delayed luminescence is also blue in colour. However, it is a much weaker luminescence. Having the ability to observe the luminescence on different timescales allows for luminescence like the weaker blue to be seen which would otherwise be masked by the strong blue prompt dislocation luminescence. While both the prompt and delayed luminescence features share similarities in colour they are not of the same origin. The prompt luminescence is known to be from dislocations in the lattice which can be seen in Figure 4.2 by the dislocation pattern apparent throughout. Spectral data was also taken in order to show how the two luminescence features differ from each other and to help characterise the origin of the delayed luminescence, as shown in Figure 4.3.

It was originally thought that the delayed luminescence may have been due to the N3 defect. However, the spectral data show this is not the case as the N3 defect is known to peak at 415 nm whereas the peak of this luminescence falls at 455 nm; it is still unknown what causes this peak. Although the origin of the peak at 455 nm is unknown it is a very common feature in natural diamonds and is used as a scientific marker to identify natural diamonds in equipment such as the De Beers' SYNTHdetect. The diamond producers' association ASSURE program confirmed that only 1% of natural diamonds do not exhibit this delayed blue luminescence [64].

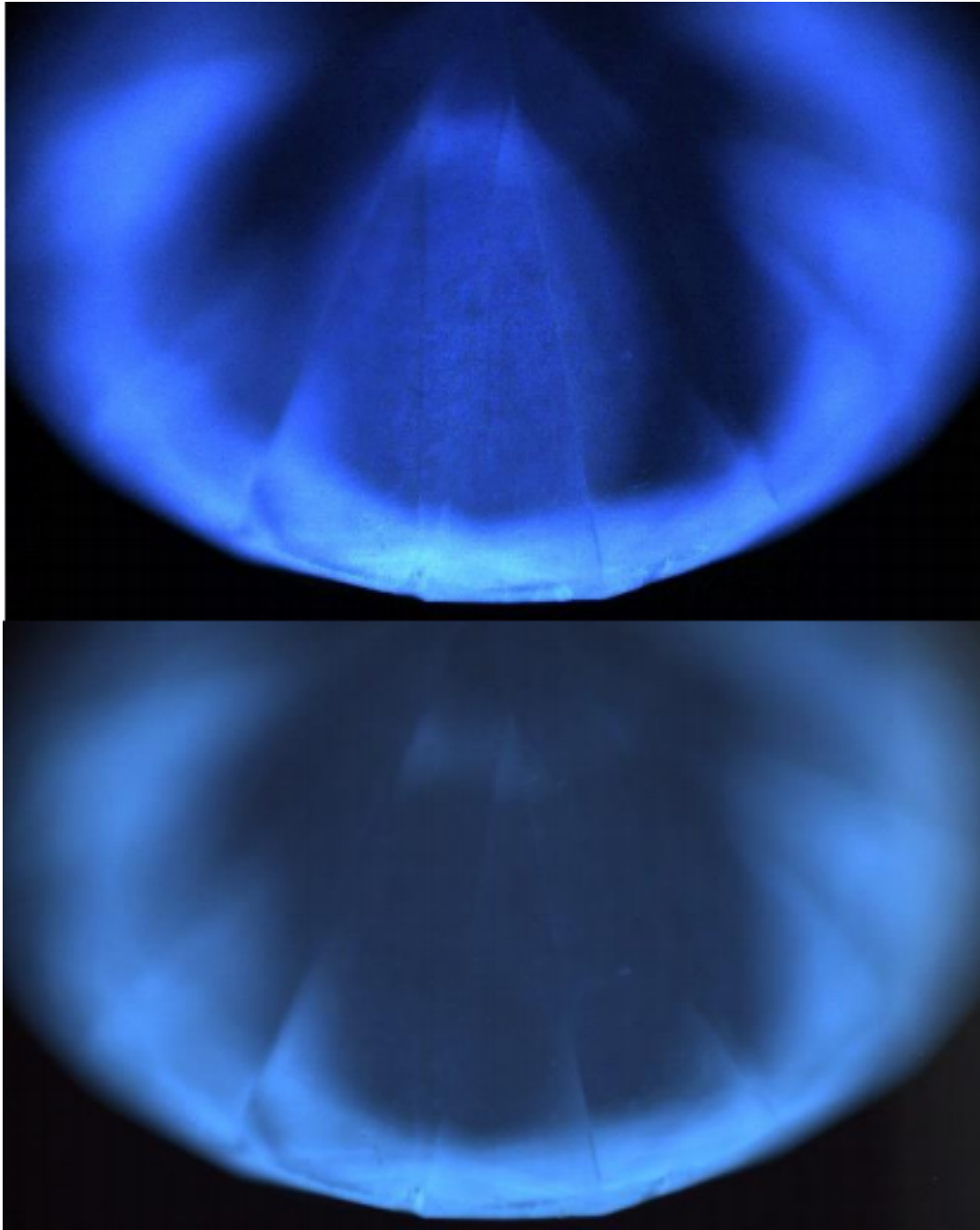


FIGURE 4.2: CMOS image of the prompt (top) and delayed (bottom) luminescence of a typical Type IIa natural diamond. Both the prompt and delayed luminescence are blue in colour. However, the prompt luminescence is a brighter more violet blue whereas the delayed is a duller paler blue. The prompt luminescence also shows a clear dislocation structure in the centre of the image (it is this that causes the bright blue colour) whereas in the delayed luminescence no structure can be seen in this area. The delayed luminescence was recorded with a delay of $100 \mu\text{s}$ after the rising edge of the UV pump pulse and integrated for 30 ms.

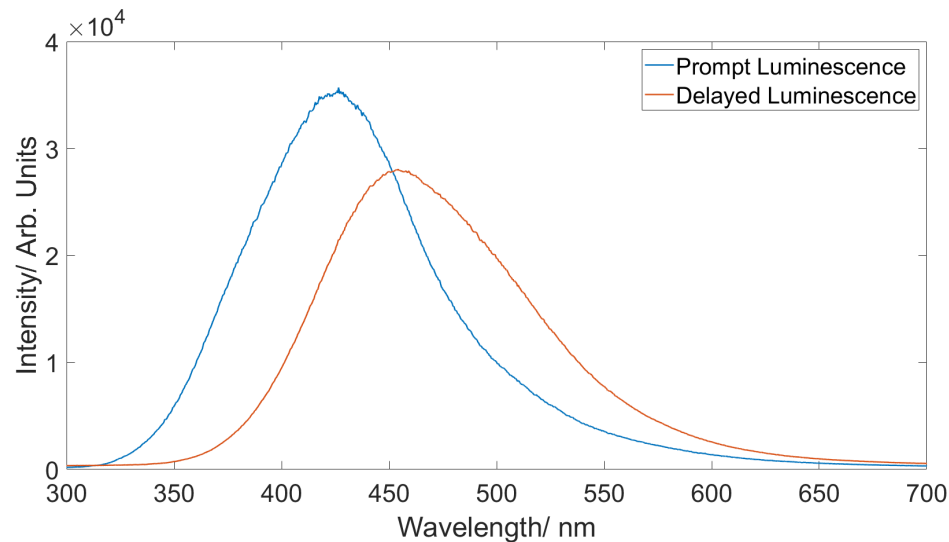


FIGURE 4.3: Spectral data showing both the prompt and delayed luminescence produced by a Type IIa natural diamond. The prompt luminescence is made up of a broadband centred at 435 nm whereas the delayed luminescence is made up of a broadband centred at 455 nm. This explains why the images of both the prompt and delayed luminescence showed different shades of blue.

4.3.2 Type Ia

Figure 4.4 shows the prompt luminescence produced by a natural Type Ia diamond; the luminescence is shown to be green in colour. The predominantly green luminescence is attributed to the H3 defect at 503 nm (consisting of a vacancy neighboured by two nitrogen atoms).

The N3 defect can be seen at 415 nm along with its vibronic sideband as well as the H3 defect at 503 nm and its corresponding vibronic sideband. The prompt blue is associated with the N3 defect, confirmation of this can be seen in Figure 4.5. However, Figure 4.5 also shows that the delayed blue luminescence does not originate from the N3 defect. The delayed blue luminescence does, however, seem to originate from the same region of the stone as the N3 luminescence, as seen in Figure 4.4. This may suggest it is related to the higher aggregated states of nitrogen such as B-centres (which consist of a vacancy with four nearest-neighbours which are nitrogen atoms).

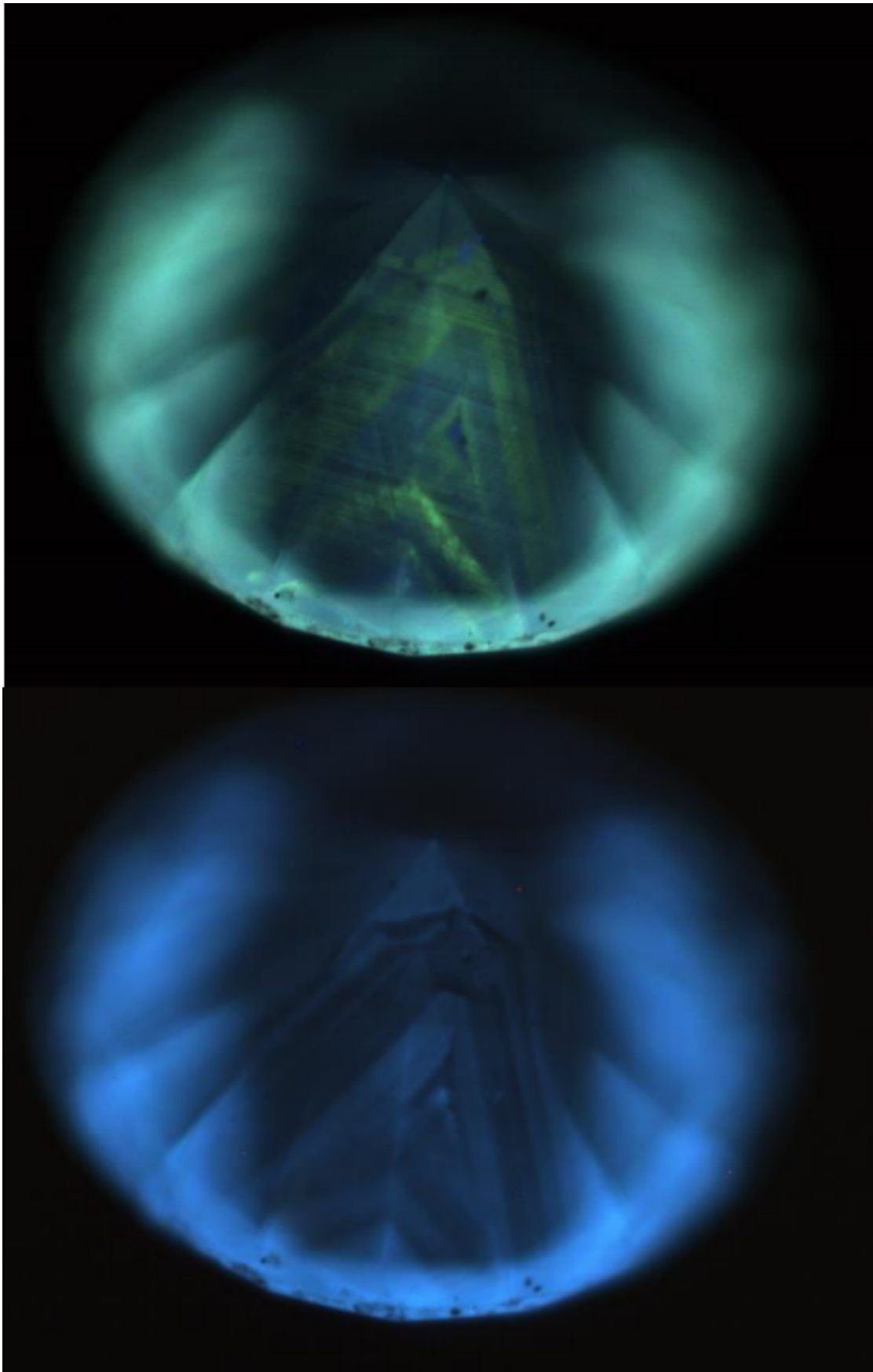


FIGURE 4.4: CMOS image of the prompt (top) and delayed (bottom) luminescence of a Type Ia natural diamond. Overall, the prompt luminescence is turquoise in colour, this is made up of a green component attributed to the H3 defect and a blue component attributed to the N3 defect. The delayed luminescence is blue in colour suggesting the green component of the prompt luminescence decays faster than the blue component which is still visible. The delayed luminescence was recorded with a delay of $100 \mu\text{s}$ after the rising edge of the UV pump pulse and integrated for 30 ms.

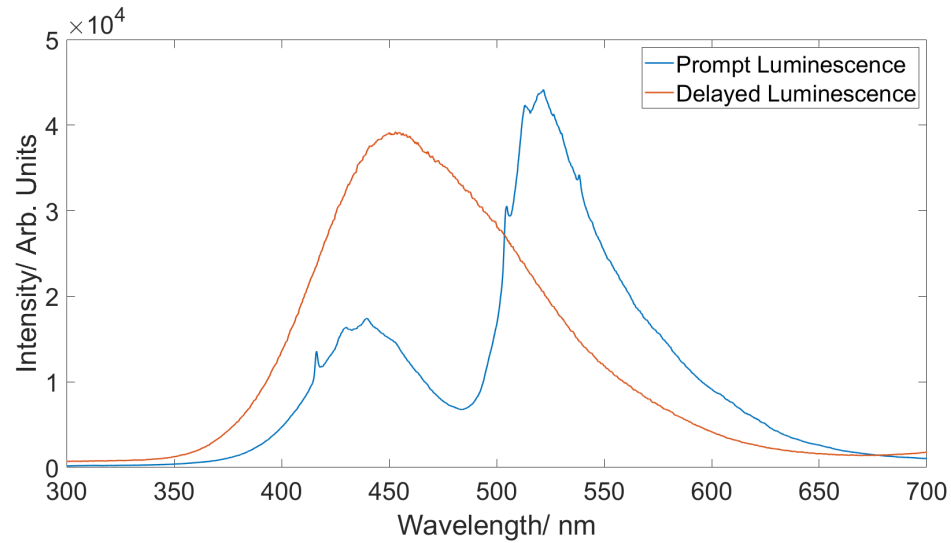


FIGURE 4.5: Spectral data showing both the prompt and delayed luminescence produced by a Type Ia natural diamond. The prompt luminescence shows the N3 defect at 415 nm along with its vibronic sideband and the H3 defect at 503 nm along with its vibronic sideband. The delayed luminescence is made up of a broadband centred at 455 nm, the origin of which is unknown.

4.3.3 Type IIb

The next diamond to be sampled was a typical example of a colourless weak Type IIb natural diamond. Figure 4.6 shows the prompt luminescence is blue in colour, once again due to the dislocations in the stone. The delayed luminescence can be seen to be a turquoise colour as shown in Figure 4.6. Spectral data was also taken for this stone in order to try and identify the long-lived turquoise component shown in Figure 4.7. The prompt luminescence was seen to peak at 425 nm whereas the peak of the delayed luminescence was found to be at 480 nm, this is commonly seen in natural diamonds, but the origin of this feature is unknown. Luminescence that is turquoise in colour such as that exhibited in the delayed luminescence of this sample is often associated with N-B (nitrogen and boron) donor-acceptor pairs.

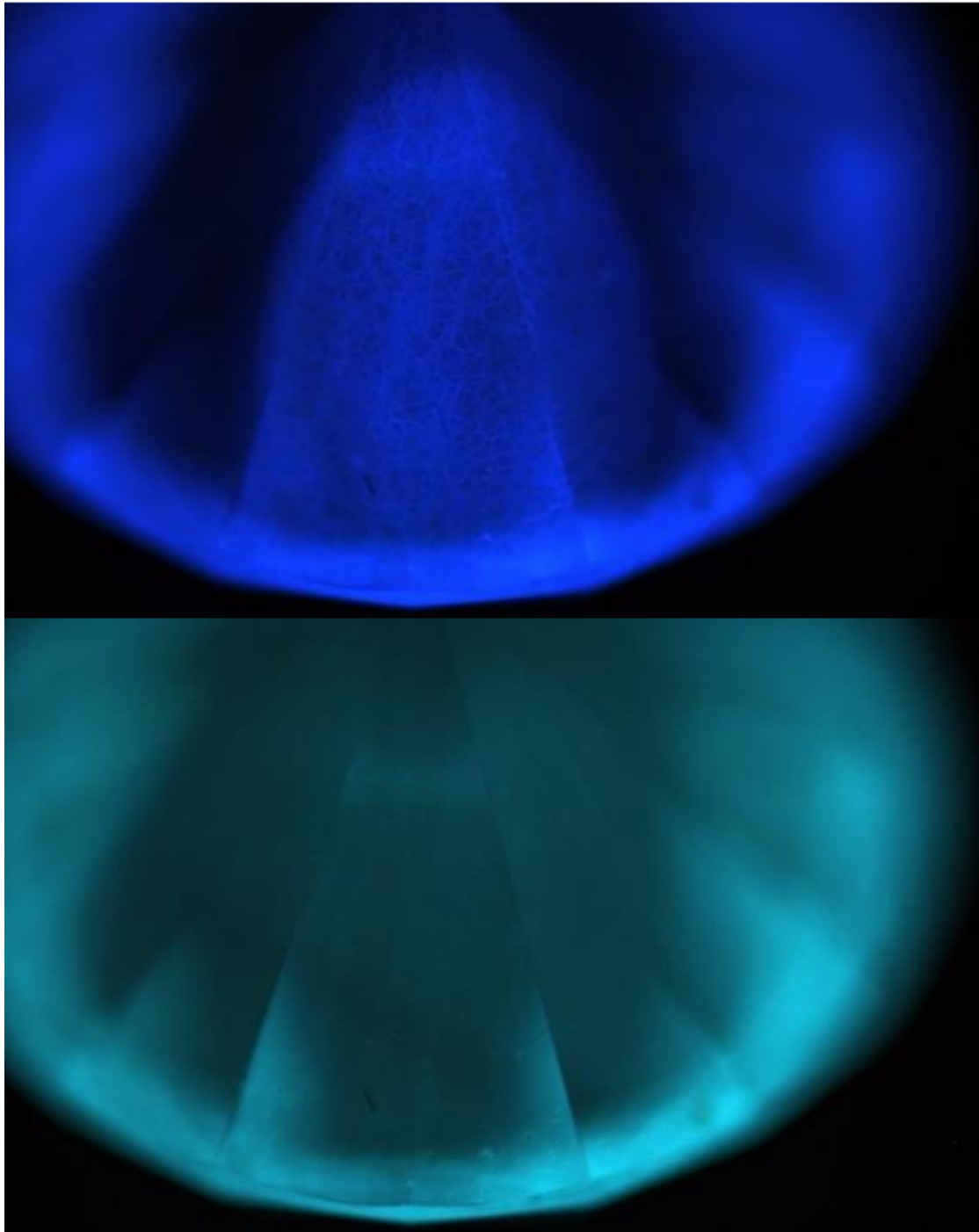


FIGURE 4.6: CMOS image of the prompt (top) and delayed (bottom) luminescence of a Type IIb natural diamond. The prompt luminescence is violet blue in colour and the dislocation pattern can be clearly seen. The delayed luminescence differs as it is turquoise in colour and does not have the visible dislocation structure. The delayed luminescence was recorded with a delay of $100 \mu\text{s}$ after the rising edge of the UV pump pulse and integrated for 30 ms.

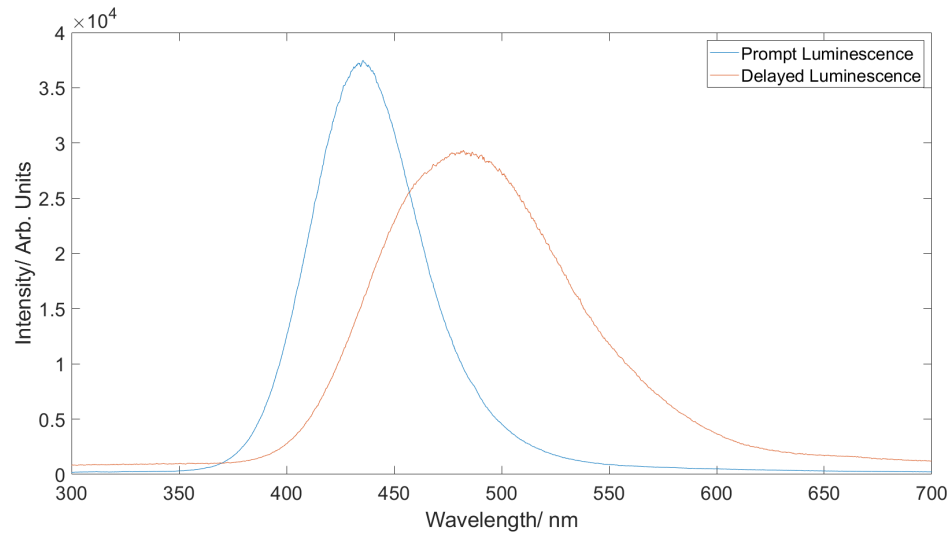


FIGURE 4.7: Spectral data showing both the prompt and delayed luminescence produced by a Type IIb natural diamond. The prompt luminescence is made up of a broadband centred at 425 nm attributed to the dislocation luminescence and the delayed luminescence is made up of a broadband centred at 480 nm, the origin of which is unknown.

4.3.4 Unusual natural diamond

The final natural diamond sampled proved to be quite unusual. The prompt luminescence was much like that seen previously in natural stones with a strong blue luminescence caused by dislocations, as seen in Figure 4.8. The initial delayed luminescence after the standard delay of $100 \mu\text{s}$ was blue/green in colour; this is unusual as most natural diamond's delayed luminescence is blue in colour hence the diamond has been referred to as an 'unusual natural diamond'. Only 1% of natural diamonds do not produce this blue delayed luminescence, therefore it is this blue delayed luminescence that is often used to confirm if a diamond is of natural origin. The lack of the delayed blue luminescence feature could lead to this diamond being incorrectly identified. The green colour shown in the delayed luminescence was attributed to the H3 defect as shown in Figure 4.9, the spectra also shows the H3 defect in the prompt luminescence. The delay placed upon the camera was extended to 2 ms, as shown in Figure 4.8, this showed that the H3 defect causing the delayed green luminescence decayed much faster than the blue delayed luminescence used to identify natural diamonds. This suggests that a technique where the delay placed on the camera can be changed from μs to ms, has significant advantages when identifying diamonds.

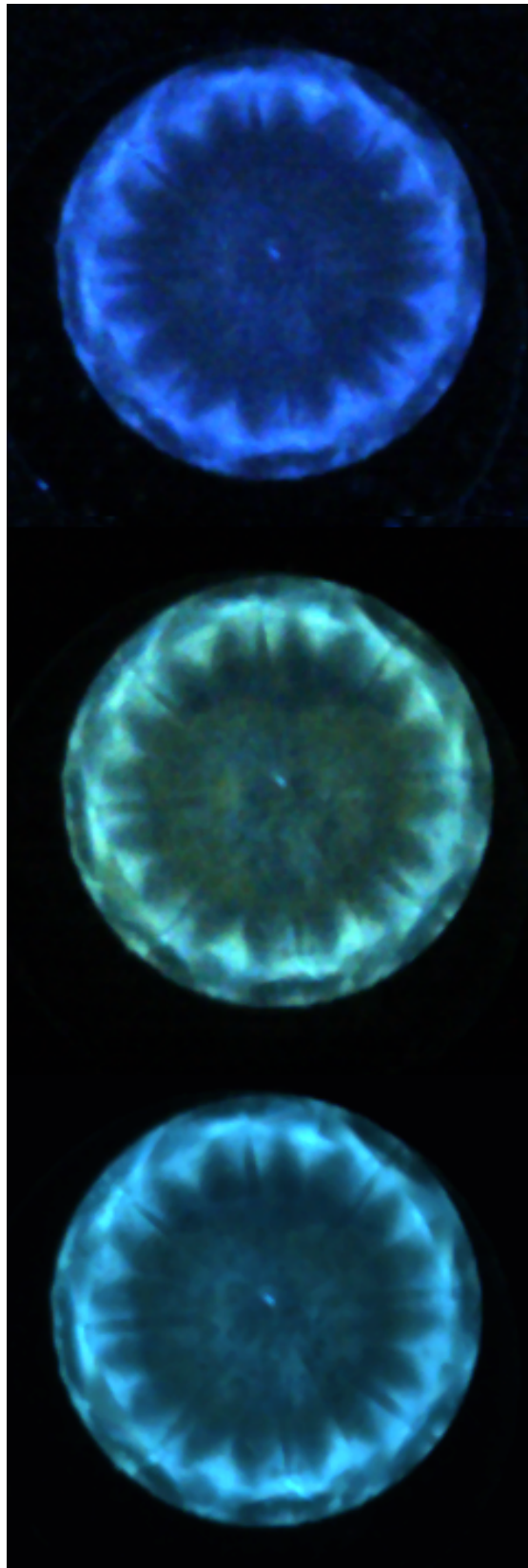


FIGURE 4.8: CMOS image of the prompt (top) and delayed luminescence of an unusual natural diamond, the delayed luminescence was taken at two delays, $100 \mu\text{s}$ (middle) and 2 ms (bottom) after the rising edge of the UV pump pulse and both integrated for 30 ms . The prompt luminescence was the same violet blue as in previous stones caused by the dislocation luminescence. The delayed luminescence with a delay of $100 \mu\text{s}$ was turquoise in colour, this is not a common luminescence colour for the delayed luminescence of a natural diamond and could cause confusion when identifying the diamond. Lengthening the delay to 2 ms showed the duller blue luminescence which is commonly associated with diamond the origin of which remains unknown.

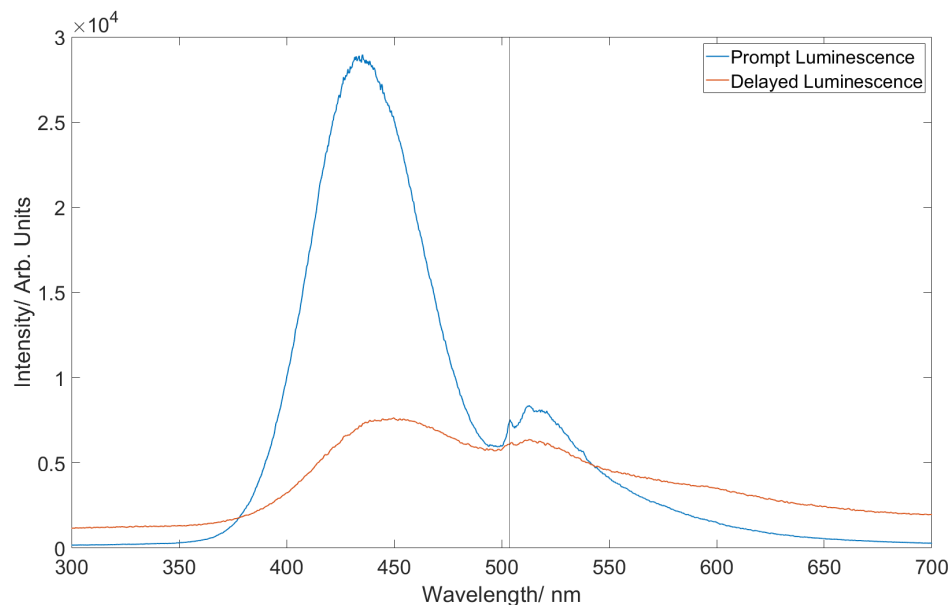


FIGURE 4.9: Spectral data showing both the prompt and delayed ($100 \mu\text{s}$ delay) luminescence produced by an unusual natural diamond. The prompt luminescence consists of a broadband at 435 nm due to the dislocation luminescence. The delayed luminescence produces a turquoise colour due to the broadband centred around 450 nm and the green component at 503 nm due to the H3 defect (shown by line drawn at 503 nm), the H3 defect is also present in the prompt luminescence but overshadowed by the large blue broadband.

4.4 CVD Diamond Samples

4.4.1 As grown CVD

The first CVD sample surveyed was an as-grown CVD synthetic diamond, shown in Figure 4.10, the prompt luminescence is a vibrant orange colour which originates primarily from the neutral nitrogen vacancy centre, NV^0 . Interestingly the delayed luminescence also displays a vibrant orange colour which also originates from the NV^0 centre. Spectral data was taken as shown in Figure 4.11 to confirm the presence of the NV^0 centre, which can be seen at 575 nm in conjunction with its vibronic side band. This leads to the conclusion that the neutral nitrogen vacancy centre can experience a populated triplet state allowing for the longer-lived production of the orange luminescence. However, this has not been further analysed in this thesis. The prompt luminescence also displayed peaks at 503 nm and is attributed to the H3 defect and at 533 nm, the origin of which is unknown, both potentially adding a small green tinge to the prompt luminescence which is overshadowed by the orange luminescence from the NV^0 centre.

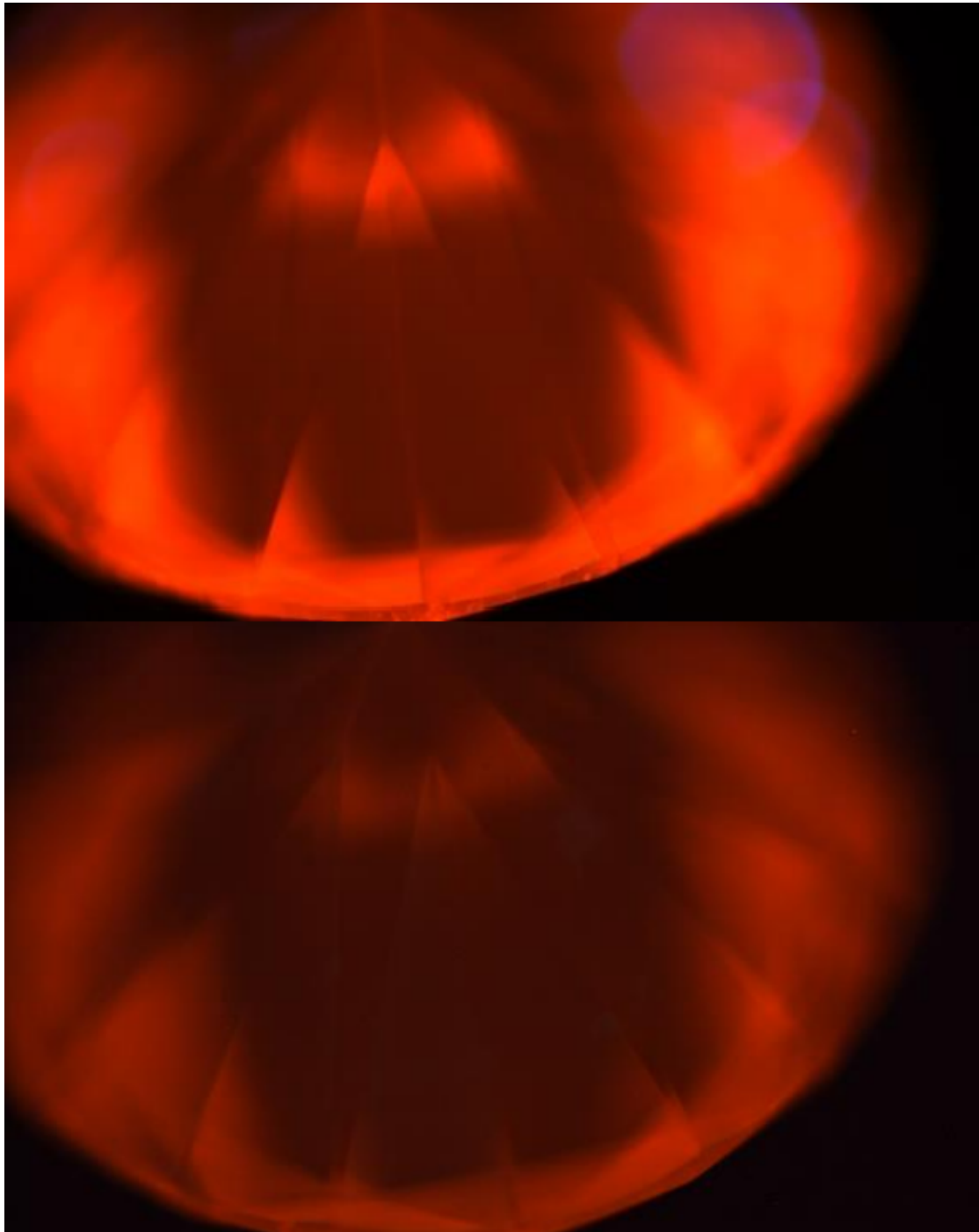


FIGURE 4.10: CMOS image of the prompt (top) and delayed (bottom) luminescence of a typical as grown CVD synthetic diamond. Both the prompt and delayed luminescence are orange in colour, however the prompt luminescence is a much brighter red. The red colour is attributed to the NV^0 defect in both cases. However, as the delay increases the brightness decreases due to being further through the lifetime of the NV^0 centre. The delayed luminescence was recorded with a delay of $100 \mu s$ after the rising edge of the UV pump pulse and integrated for 60 ms.

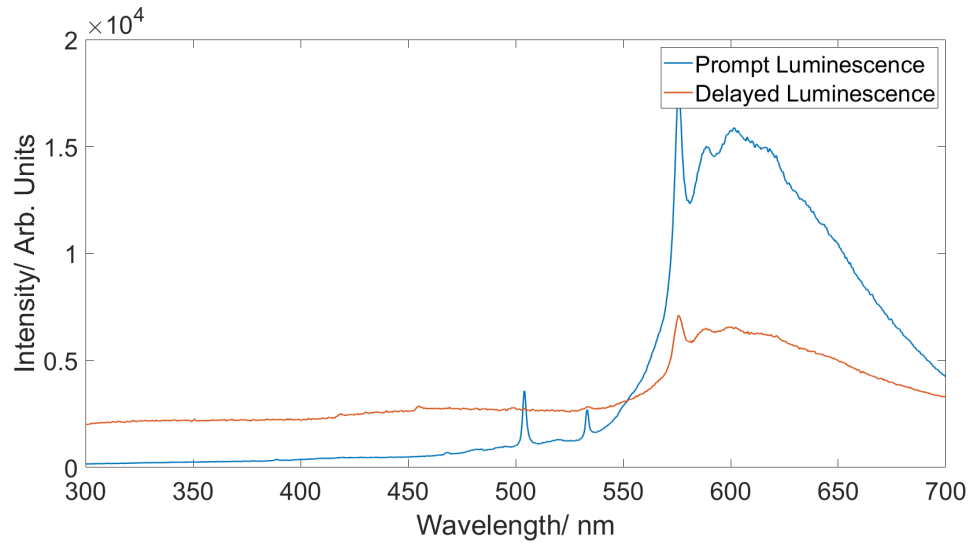


FIGURE 4.11: Spectral data showing both the prompt and delayed luminescence produced by an as grown CVD synthetic diamond. In both cases the NV^0 centre at 575 nm can be seen in conjunction with its vibronic side band. The prompt luminescence also shows two defined peaks at 503 nm (attributed to the H3 defect) and 533 nm (origin unknown).

4.4.2 Commercially sourced LINPO CVD

The next diamond to be sampled was a commercially available CVD synthetic diamond purchased from LINPO Hightech Ltd. Overall, the prompt luminescence shown in Figure 4.12 was predominantly blue in colour with some visible growth structure, much like that seen in a natural stone. There is also a weak red component to the general luminescence that can be seen in addition to discrete narrow bands of red luminescence. The delayed luminescence also shown in Figure 4.12 is green in colour; it was suspected that this was due to the H3 defect at 503 nm. Spectral data was also taken, 4.13, to confirm the origin of the luminescence in both cases, as shown in Figure 4.13, which confirmed that the long-lived green luminescence was, in fact, from the H3 defect at 503 nm and the prompt luminescence was predominantly from the NV^0 defect.

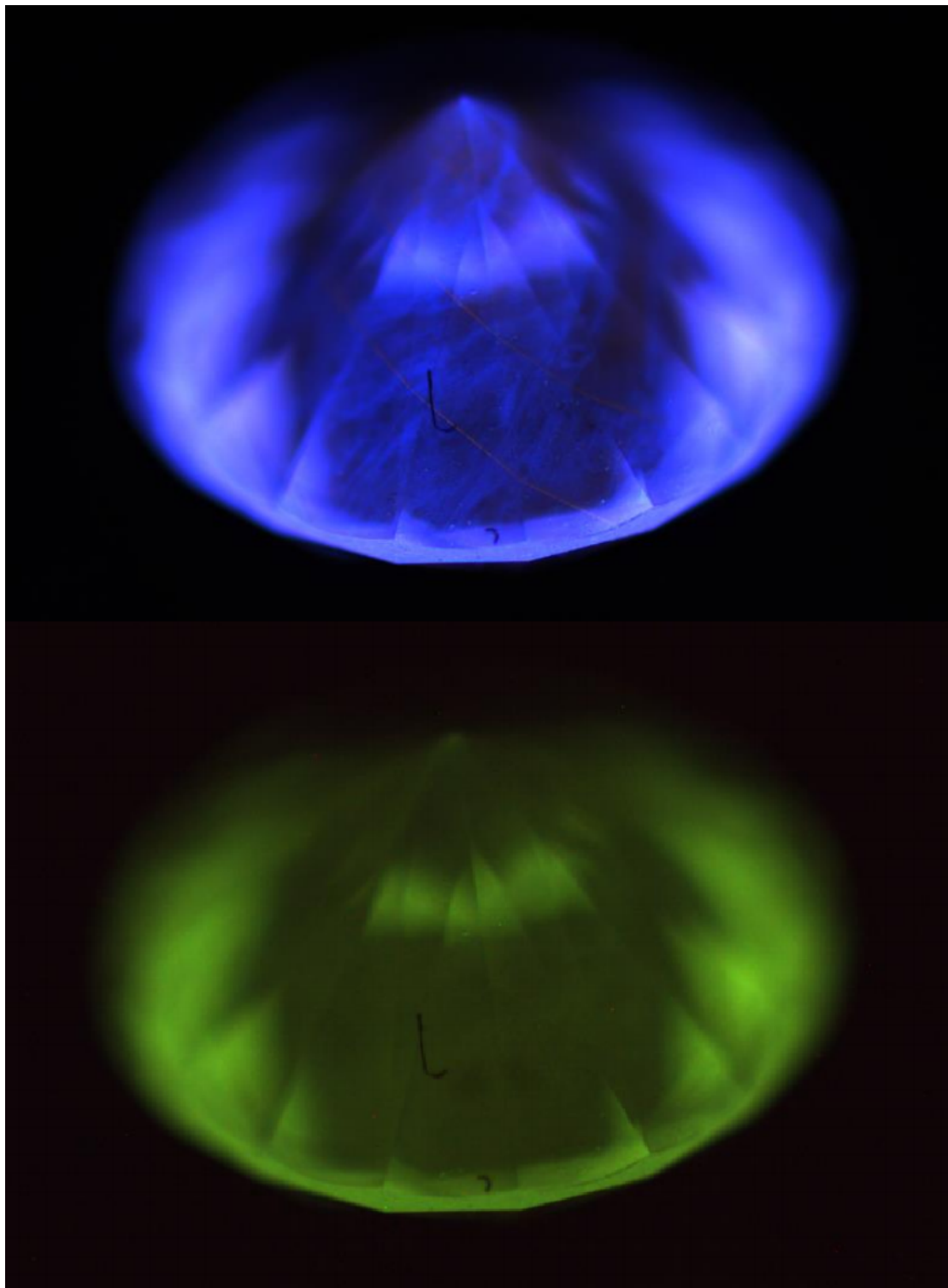


FIGURE 4.12: CMOS image of the prompt (top) and delayed (bottom) luminescence of a commercially available LINPO CVD synthetic diamond. The prompt luminescence was bright blue in colour with some growth structure patterning, quite similar to that seen in natural diamonds. The prompt luminescence also has a vague red component running through it as well as some discrete red narrow bands of luminescence due to the NV^0 defect. The delayed luminescence was, however, not like that seen in natural diamond as it was green in colour, due to the H3 defect. The delayed luminescence was recorded with a delay of $100 \mu s$ after the rising edge of the UV pump pulse and integrated for 30 ms.

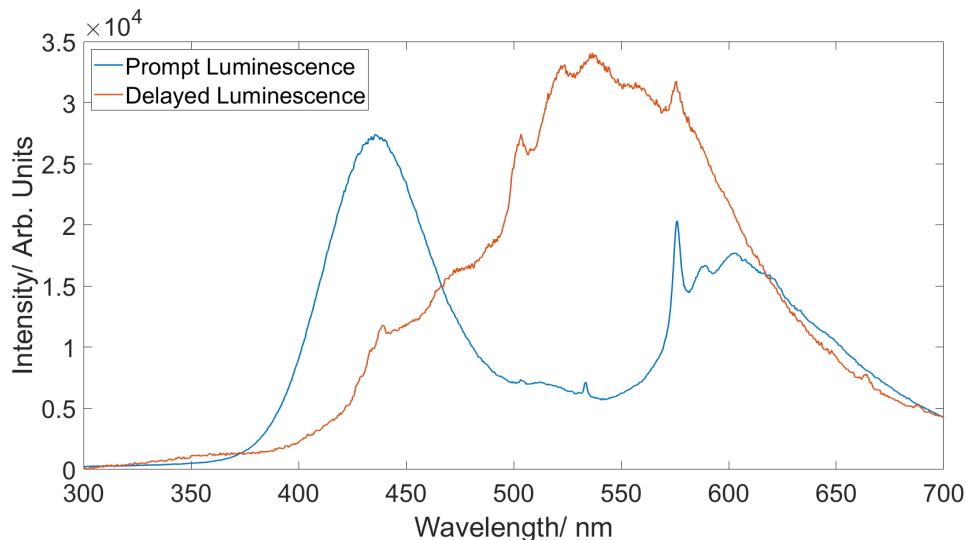


FIGURE 4.13: Spectral data showing both the prompt and delayed luminescence produced by a commercially sourced LINPO CVD synthetic diamond. The prompt luminescence consists of a broadband centred around 440 nm. The delayed luminescence shows a broadband centred around 540 nm, the H3 centre can be seen at 503 nm, a peak of unknown origin is seen at 533 nm, as well as the NV^0 defect at 575 nm in conjunction with its vibronic side band.

4.4.3 Commercially sourced Gemesis CVD

The next CVD sample to be surveyed was a commercially available CVD synthetic diamond purchased from Gemesis. The prompt luminescence of this diamond can be seen in Figure 4.14, it produces a prompt blue luminescence which comes from localised dislocation patterns which give it characteristics very similar to that of a natural Type IIa diamond, making it very interesting for diamond verification projects. The delayed luminescence shown in Figure 4.14 on initial inspection looks much like that in Figure 4.12, thus leading to the assumption that it could originate from the H3 defect. However, further spectral analysis of the feature, Figure 4.15, showed that it originates from an entirely different feature with a zero-phonon line at 499.6 nm (from now on referred to as the 499 nm feature). This defect has never been reported in natural diamonds and, therefore, could potentially be used as a characteristic to identify CVD synthetic diamonds. As very little has been reported about this defect, further investigations have been carried out in the following chapter.

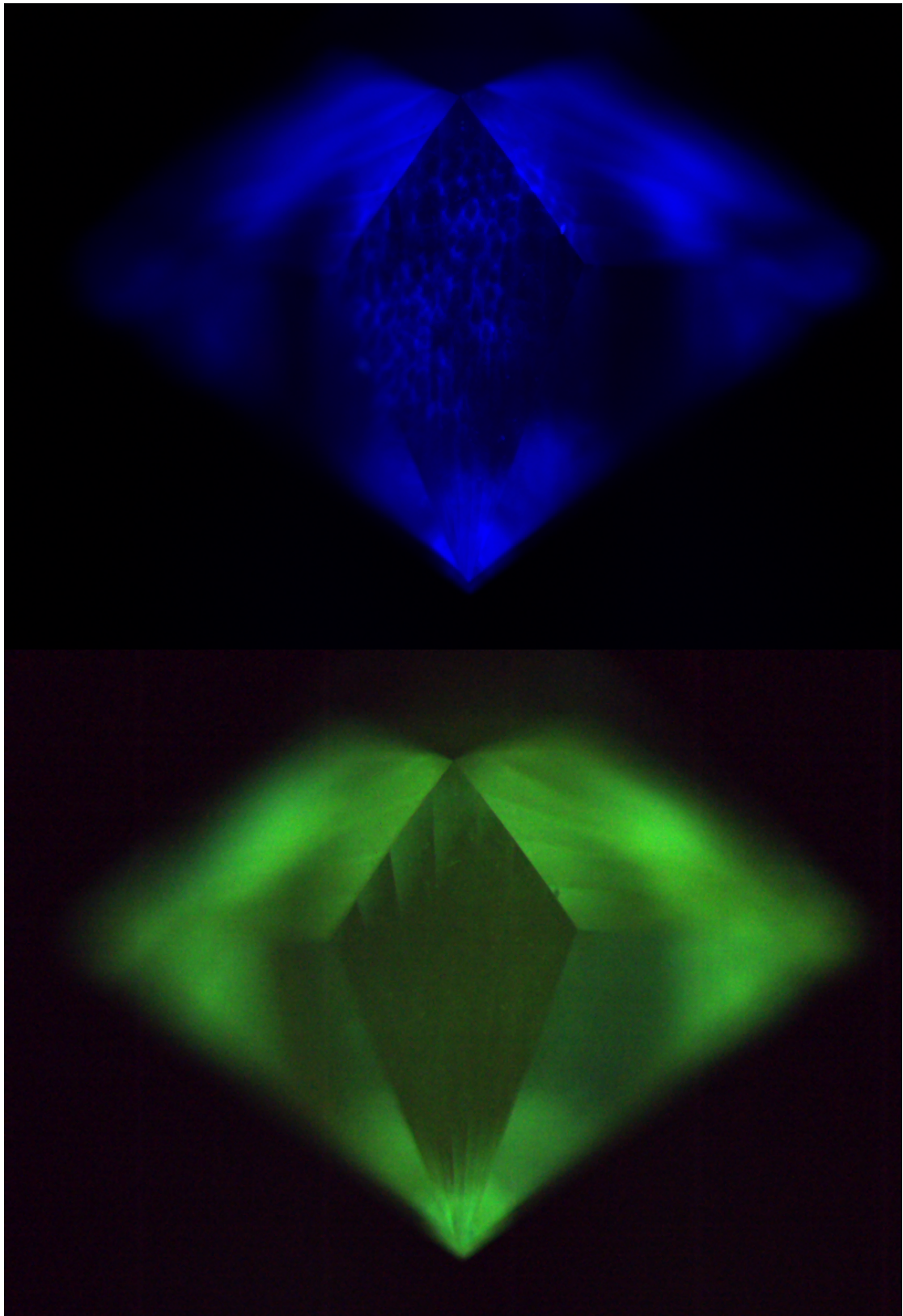


FIGURE 4.14: CMOS image of the prompt (top) and delayed (bottom) luminescence of a commercially available Gemesis CVD synthetic diamond. Much like the LINPO stone, the prompt luminescence is bright blue in colour with a growth pattern structure that could potentially be mistaken as natural diamond. The delayed luminescence once again is green in colour. However, this time the luminescence is not due to the H3 defect and is instead caused by a defect found at 499 nm. The delayed luminescence was recorded with a delay of 100 μ s after the rising edge of the UV pump pulse and integrated for 30 ms.

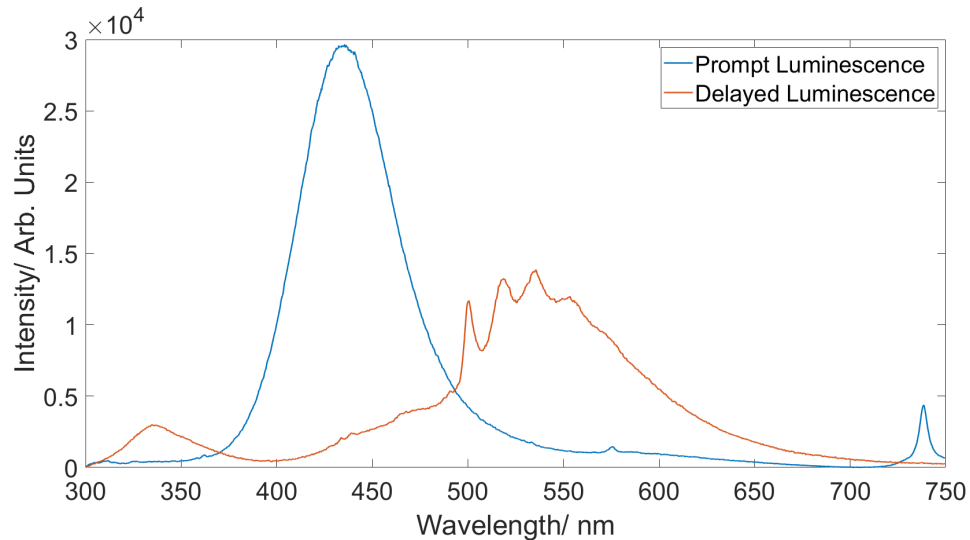


FIGURE 4.15: Spectral data showing both the prompt and delayed luminescence produced by a commercially sourced Gemesis CVD synthetic diamond. The prompt luminescence consists of a broadband at 435 nm, there is also a peak at 575 nm due to the NV^0 centre, as well as a peak at 737 nm attributed to the SiV^- centre. The delayed luminescence is comprised of the 499 nm peak in conjunction with its vibronic side band. In addition, there is a broadband at 340 nm, the NV^0 centre is also present in the delayed luminescence but it is harder to see as it sits on top of the 499 nm feature's vibronic side band.

4.4.4 Commercially available Diamond Foundry CVD

The following CVD sample to be surveyed was a commercially sourced sample from the Diamond Foundry, both the prompt and delayed luminescence were green in colour, as shown in Figure 4.16. As previously stated, green luminescence is most widely attributed to the H3 centre. In this case, however, spectral analysis showed that the luminescence was in fact due to the 499 nm feature as shown in Figure 4.17. This is the same feature observed in the previous Gemesis stone. However, the way in which the 499 nm feature appears in this stone differs from the Gemesis stone as it can be seen in both the prompt and delayed luminescence rather than just the delayed. The prompt and delayed spectra observed are very similar; however, the delayed luminescence also shows a broadband at around 360 nm.

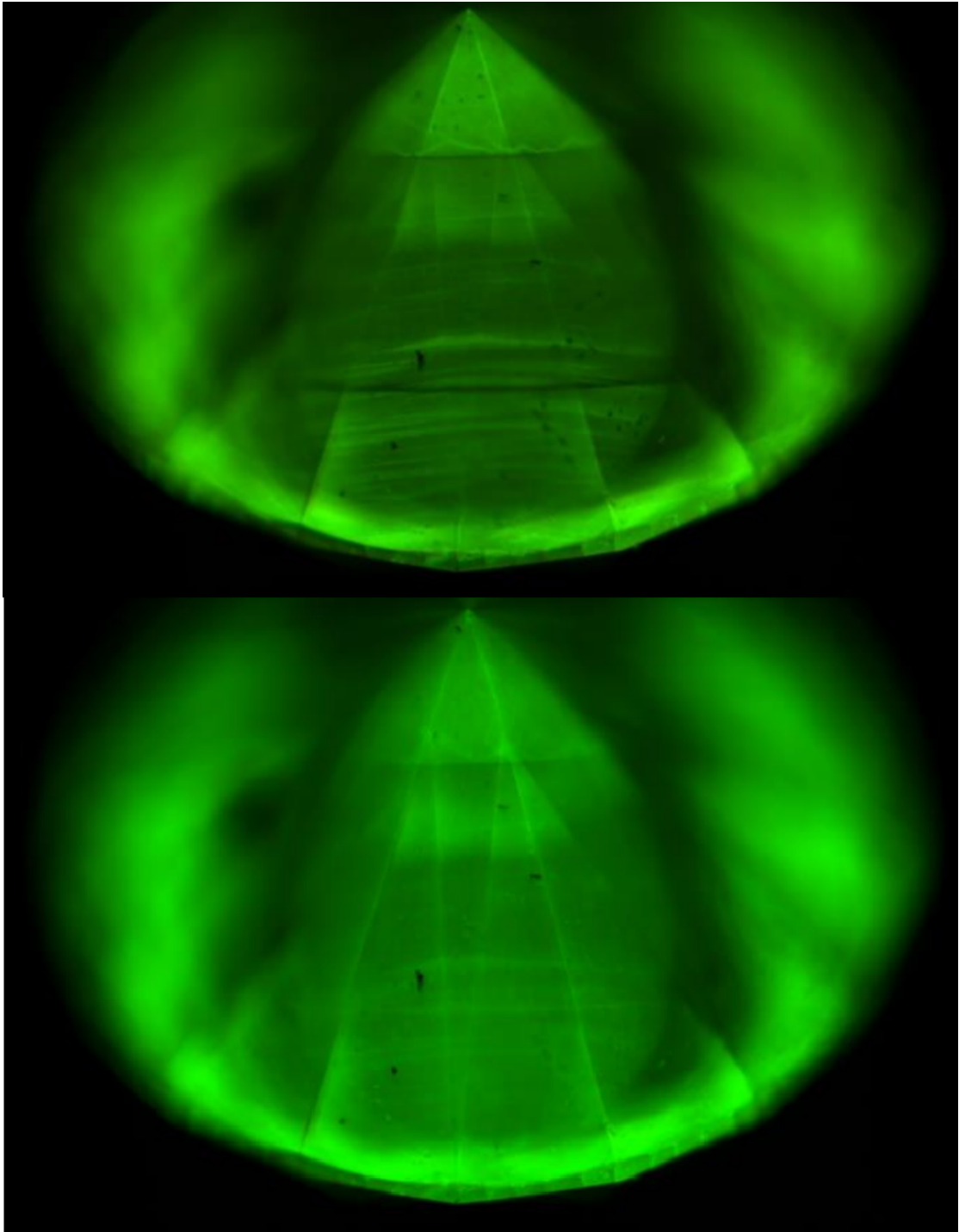


FIGURE 4.16: CMOS image of the prompt (top) and delayed (bottom) luminescence of a commercially available Diamond Foundry CVD synthetic diamond. Both the prompt and delayed luminescence are a similar green in colour. The delayed luminescence was recorded with a delay of $100 \mu\text{s}$ after the rising edge of the UV pump pulse and integrated for 30 ms.

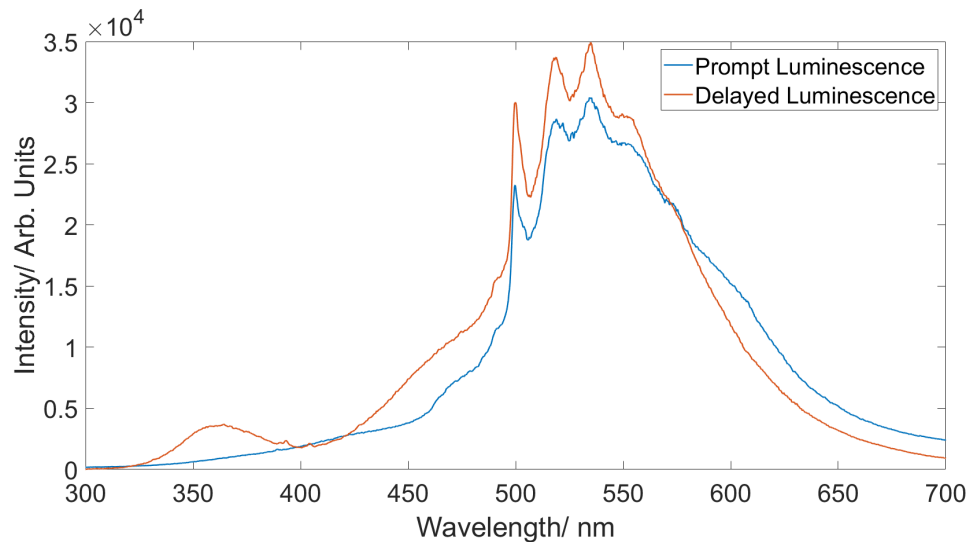


FIGURE 4.17: Spectral data showing both the prompt and delayed luminescence produced by a commercially sourced Diamond Foundry CVD synthetic diamond. The 499.6 nm line can be seen in both the prompt and delayed luminescence in conjunction with its vibronic side band. The delayed luminescence also has a small broadband centred at 360 nm.

4.4.5 Commercially available CVD of unknown origin

The final CVD stone to be surveyed was a commercially available CVD synthetic diamond of unknown origin. The prompt luminescence recorded from this sample was once again green in colour, with growth bands perpendicular to the growth direction consistent with CVD growth as shown in Figure 4.18. Spectral data was recorded in order to confirm the origin of the green luminescence, which once again originated from the 499 nm feature, as shown in Figure 4.19. The spectral data also confirmed the presence of the NV^0 defect at 575 nm and the N3 defect at 415 nm, neither of which could be identified while imaging. The delayed luminescence is dominated by a turquoise luminescence, Figure 4.18; however, a very small amount of the 499 nm feature is visible as shown in 4.19. Interestingly, the growth pattern that could be seen in the prompt luminescence is not visible in the delayed luminescence, suggesting that the delayed turquoise luminescence does not form these patterns in the same way; it is not known why.

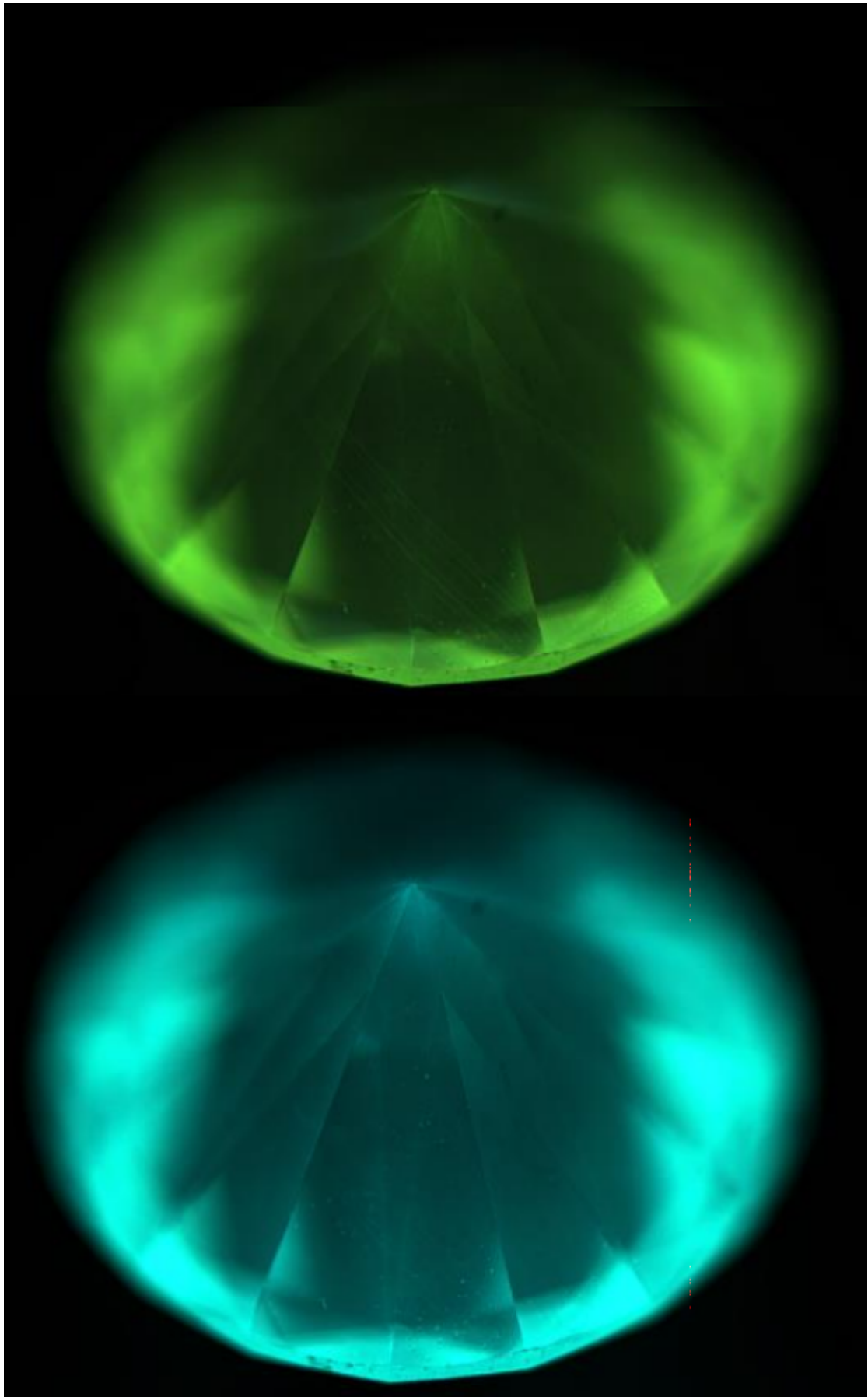


FIGURE 4.18: CMOS image of the prompt (top) and delayed (bottom) luminescence of a commercially available CVD synthetic diamond of unknown origin. The prompt luminescence was green in colour, in contrast the delayed luminescence was bright turquoise. The delayed luminescence was recorded with a delay of $100 \mu\text{s}$ after the rising edge of the UV pump pulse and integrated for 60 ms.

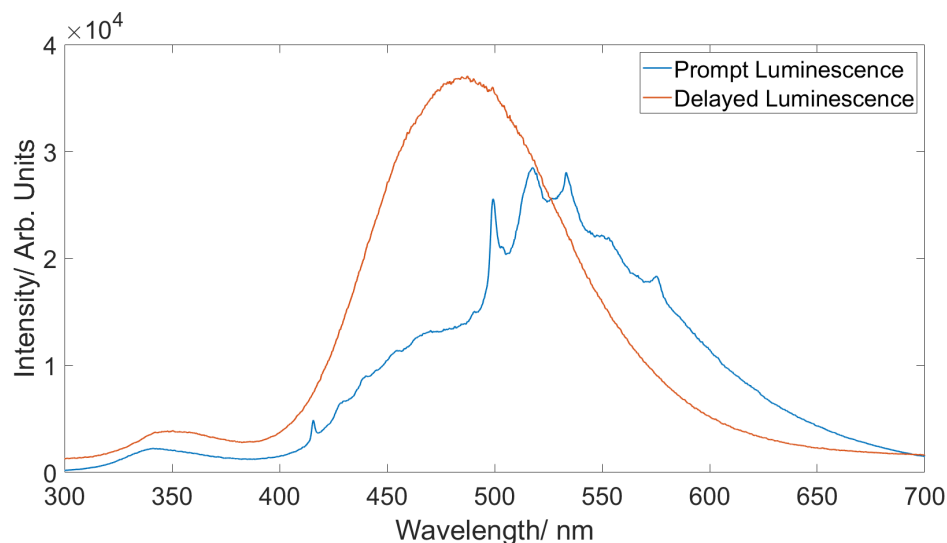


FIGURE 4.19: Spectral data showing both the prompt and delayed luminescence produced by a commercially sourced diamond of unknown origin. The prompt luminescence is dominated by a broadband centred around 535 nm upon which sits the 499nm feature in conjunction with its vibronic band. The delayed luminescence consists of a broadband at around 480 nm; as well as a small broadband centred around 340 nm, a similar small broadband is seen in the prompt luminescence centred at 350 nm.

4.5 HPHT Diamond Samples

4.5.1 Colourless HPHT

The only HPHT diamond to be sampled was a colourless HPHT synthetic diamond which was commercially sourced. The prompt luminescence seen in Figure 4.20 is a weak green/red colour of unknown origin. Spectral data shows that the feature is broad and featureless at room temperature giving little in the way of information. It has been speculated that the luminescence could be present due to metal ions in the solvent catalyst used during growth; however, the spectral data was not able to confirm this. The delayed luminescence in this case is a bright blue and is known to be caused by phosphorescence from donor-pair recombination [82].

It is very common for HPHT synthetics to have a green prompt luminescence and a strong turquoise phosphorescence and therefore it can be used as an identifying feature in verification, as this combination has never been seen in natural diamond.

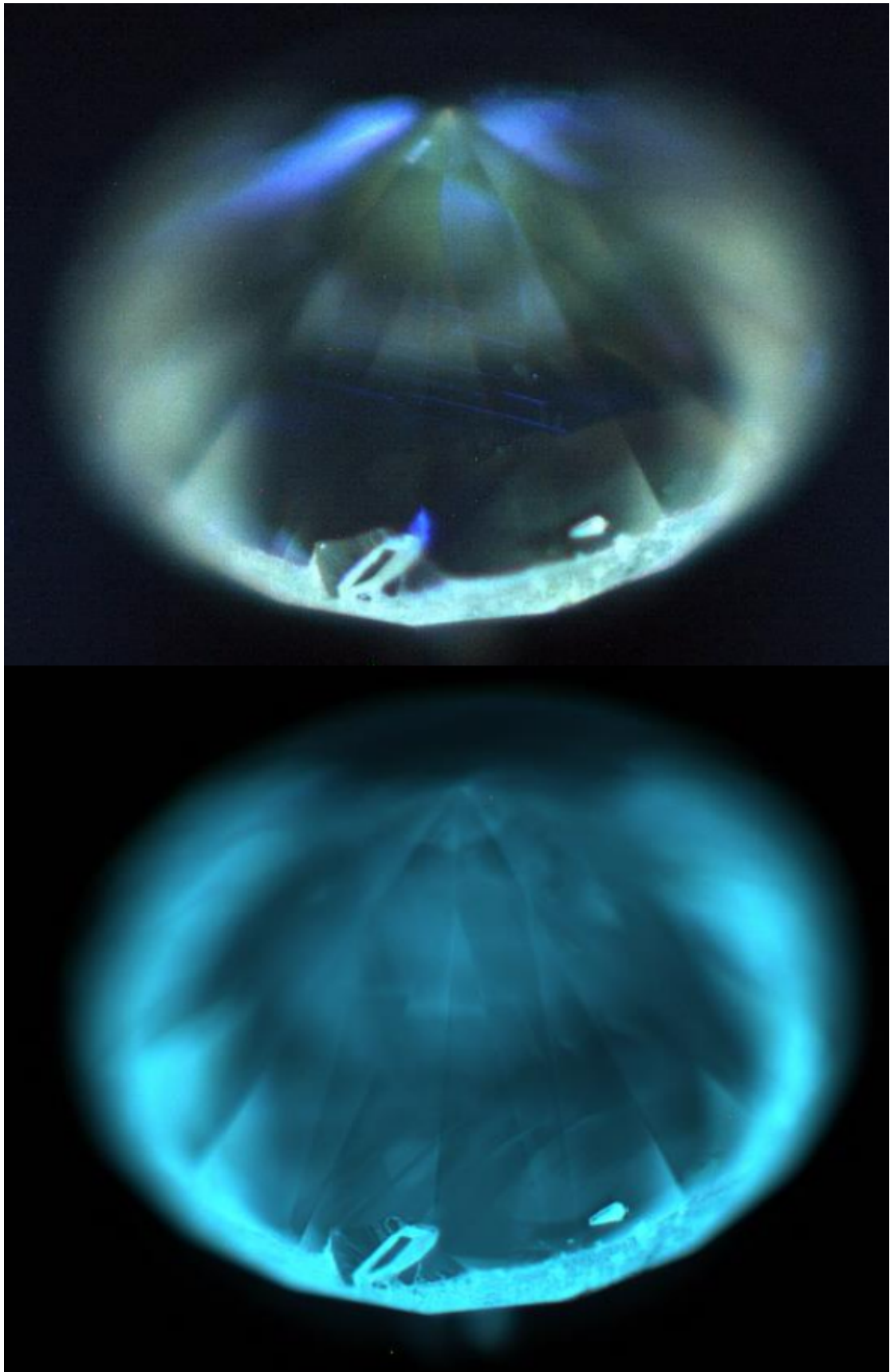


FIGURE 4.20: CMOS image of the prompt (top) and delayed (bottom) luminescence of a colourless HPHT synthetic diamond. The prompt luminescence is quite hard to distinguish as a colour but is made up of a green/red colour the origin of which is unknown, the delayed luminescence is bright blue in colour. The delayed luminescence was recorded with a delay of $100 \mu\text{s}$ after the rising edge of the UV pump pulse and integrated for 10 ms.

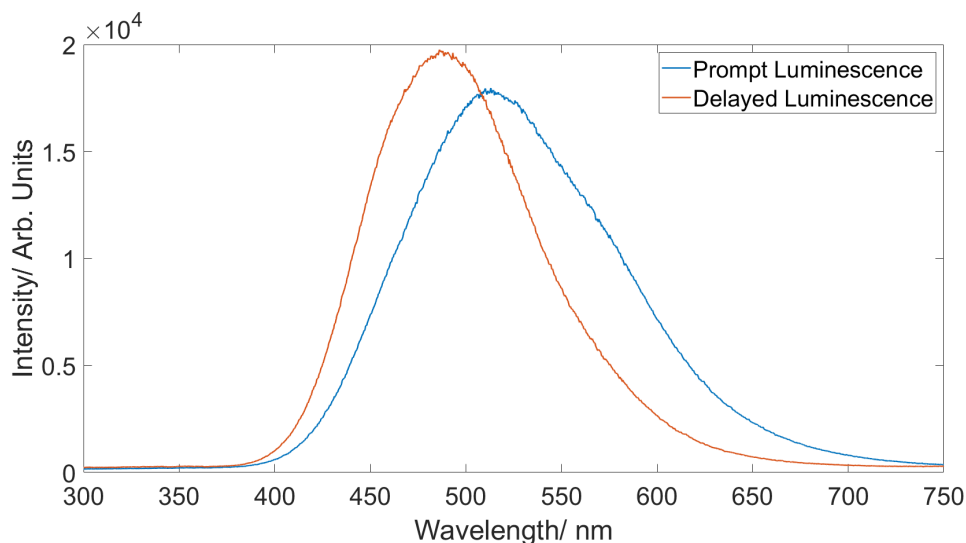


FIGURE 4.21: Spectral data showing both the prompt and delayed luminescence recorded for a typical HPHT synthetic. The prompt luminescence consists of a broadband centred at around 510 nm and the delayed luminescence consists of a broadband centred around 480 nm. As both spectra are broad and featureless not much information can be gained as to the origin of both the prompt and delayed luminescence.

4.6 Discussion

Diamond Type	Likely defect	Natural diamonds of this type (%)	Most common luminescence
Type Ia	Nitrogen defects: A centres, B centres and N3	95	Predominantly prompt blue, delayed blue
Type Ib	Single substitutional nitrogen	0.1	Not sampled
Type IIa	Devoid of impurities	1.8	Prompt blue luminescence, delayed blue luminescence
Type IIb	Boron	0.1	Prompt blue, delayed turquoise

TABLE 4.2: Table as in Figure 4.2 describing natural diamond types, the most likely defect to be found in each type, the percentage of natural diamonds of each type with the addition of the luminescence observed for each type surveyed in this chapter. It is important to note that the luminescence recorded is not the only luminescence that can be observed for each diamond type: rather it is the most commonly seen.

As synthetic diamond gemstones' quality is ever increasing, the task of diamond screening is becoming much more challenging. Given that it is becoming common practice for less experienced diamond appraisers to carry out this task, it is important there are less complex and time-consuming techniques that can be used to identify the origin of diamonds. The diamond rig produced and discussed in this chapter provides an easy-to-use technique, which can be used in conjunction with a survey of imaged samples

for comparison in order to identify the origin of diamond samples. Such a selection of diamonds made up of natural and synthetic colourless diamonds was surveyed in this chapter. Ultra-violet excitation was used to study the luminescence produced by the diamond; the excitation pulse was synchronised with the recording of the luminescence to allow for time-gated measurements. Time-gated measurements allowed for the differentiation between prompt and delayed luminescence, allowing defects in the diamond to emerge that could otherwise (at shorter timescales) have been overshadowed by another defect. Table 4.2 summarises the luminescence most commonly observed for each natural diamond type. However, some samples that were surveyed in this chapter, such as the sample referred to as Type Ia showed green prompt luminescence rather than the blue prompt luminescence most commonly seen. Of the natural diamonds sampled only the Type IIb diamond did not show delayed blue luminescence, it is known that only 1% of natural diamonds do not exhibit delayed blue luminescence [64]. The CVD samples surveyed showed that in some cases, such as the commercially sourced Gemesis CVD synthetic, looking at the delayed luminescence helped to identify this stone as a CVD synthetic when it could easily have been confused as a natural diamond when looking at its prompt luminescence alone. It is for this reason that the Gemesis CVD synthetic will be extensively studied in this thesis in order to further characterise what occurs within the stone. The HPHT sample surveyed had a green component to its prompt luminescence and had turquoise delayed luminescence; very common traits to HPHT diamond and therefore useful characteristics to look out for when identifying a HPHT diamond [64].

4.7 Conclusion

It is important to develop new techniques to help with the growing task of diamond identification. As larger numbers of synthetic diamond are reaching the market consumers must be confident that synthetic diamonds can be distinguished from natural diamonds. As this job is more commonly falling to less experienced diamond appraisers, it is important that new techniques are simple to carry out and that the results can be interpreted easily. In this chapter an imaging rig was discussed and used to survey a selection of natural, CVD and HPHT stones in order to test the capabilities of the rig. The imaging rig was able to record images on both prompt and delayed lifetimes, allowing luminescence from many defects in the stone to be observed which could otherwise have been masked by other defects on different time frames. It is proposed that this type of imaging in conjunction with a comprehensive sample survey could be used for diamond identification purposes.

Chapter 5

Anomalous Green Luminescent Properties in CVD Synthetic Diamond

5.1 Background and Motivation

The unique combination of diamonds optical and mechanical properties has made it arguably the world's most sought-after gemstone. Both its beauty and rarity have contributed to the significant intrinsic value placed on diamond. Synthetic diamond can now be grown to gemstone quality creating a whole new market for synthetic diamond jewellery. As both natural and untreated diamonds have a value higher than synthetic diamond it is imperative that undisclosed synthetics are able to be detected with a high degree of confidence. More information can be found on this in Chapter 1. Gemologists use numerous interrogation methods to verify the origin of a gemstone, a detailed analysis of some of these methods can be found in Chapter 2. One such method which we will focus on in this chapter is deep ultra-violet (UV) excited luminescence. When excited with UV light natural diamonds most commonly produce a blue luminescence signature: this signature is attributed to dislocations within the diamond lattice [81]. However, we have recently observed a similar blue luminescence feature in a synthetic gemstone; this is cause for concern as this stone and other stones alike may be mistaken for natural gemstones. As such we felt it was cause for further investigation.

We have the ability to record both the luminescence produced by the diamond contemporaneous with the pulse of the UV light but also to change the timescale upon recording the luminescence to a set delay after the pulse of UV light. Thus, we can record both

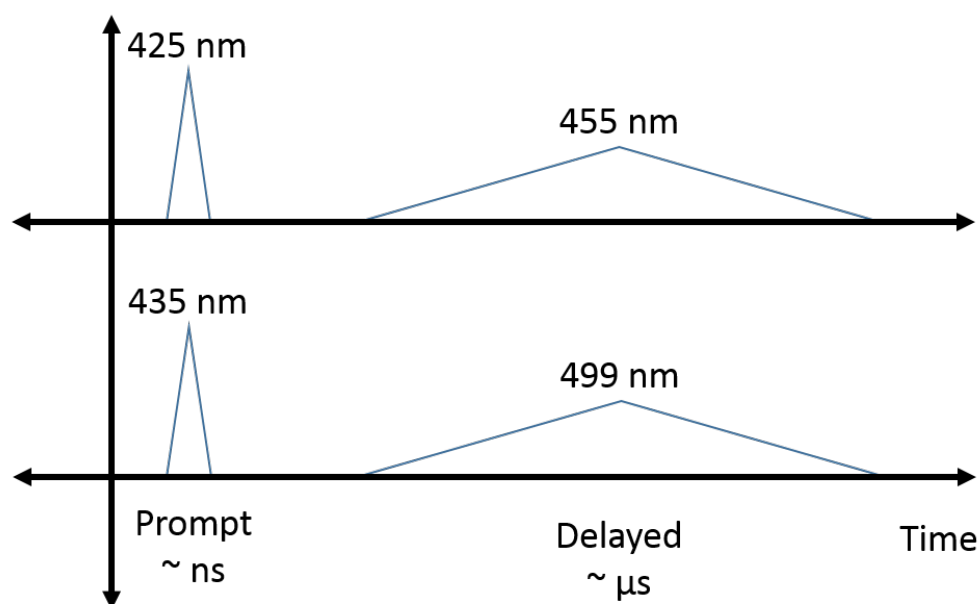


FIGURE 5.1: Schematic diagram showing the difference in prompt and delayed luminescence of a natural diamond sample (top) and a CVD synthetic diamond sample (bottom). The natural diamond displays a prompt luminescence signal at 425 nm and a delayed luminescence signal at 455 nm whereas the prompt luminescence for the CVD sample is seen at 435 nm and the delayed luminescence at 499 nm.

a prompt luminescence signal (contemporaneous with the pulse) or a delayed luminescence signal (any given delay after the pulse). Figure 5.1 provides a schematic diagram of the prompt and delayed measurements of both a natural diamond gemstone and the CVD diamond gemstone under investigation. It can be seen that both the natural gemstone and the CVD gemstone produce a prompt and delayed luminescence. However, the wavelength at which this occurs is different. The natural stone has a prompt luminescence signature at 425 nm whereas the CVD stone's prompt luminescence signature is seen at 435 nm. Although these appear the same, as they are both blue in colour, they are of two differing wavelengths. The delayed luminescence for the natural stone is seen at 455 nm which is blue in colour; in contrast the delayed luminescence for the CVD stone is seen near 499 nm which is green in colour. Green delayed luminescence is not a feature commonly observed in natural diamond gemstones; on the occasions green delayed luminescence is observed it is attributed to the H3 defect found at 503 nm. In this case, the green luminescence signature was attributed to the 499.6 nm spectral line; to date, there is very little about this feature mentioned in literature. Possibly the most helpful hypothesis stems from a comment made by Khong and Collins who inferred the feature may be associated with synthetic growth. This is discussed in more detail later in this chapter [83].

As very little was known about the 499 nm feature, I decided to make this the focus of the investigations. Investigations were carried out on the sample in order to determine

which elements were incorporated into the diamond lattice during growth. The main features identified in the stone using photoluminescence were the negatively charged silicon vacancy centre (SiV^-) found at 737 nm and the neutral nitrogen vacancy centre (NV^0) found at 575 nm. With this knowledge a library of stones with similar defects was searched for, leading to the acquisition of an annealing sequence which also contained the NV^0 centre and the SiV^- centre. The sample set acquired showed similar luminescence features to the original samples; the origin and subsequent treatments of which are well documented. This sample set originally comprised a single wafer slice which was then split into 8 separate pieces, each of which underwent annealing at a series of different temperatures. A second sample series was also obtained with similar characteristics and annealing history to the first, but from a different wafer and consequently different concentrations of dopants, thus allowing comparisons to be made between the two sets. In this chapter we use the comparison between the two annealing sequences along with the information we have about the original stone in order to provide a hypothesis regarding the origin of this new luminescence feature.

5.2 Experimental Details

Three different sample sets were used to produce the results in this chapter. The first sample set consists of three CVD gemstones purchased from Gemesis and supplied to us by De Beers Technologies. The second set consists of an annealing sequence produced by Element Six and supplied by De Beers Technologies: the samples were grown without silicon doping and have a negligible silicon concentration. The third sample set consists of an annealing sequence produced by Element Six and supplied by De Beers Technologies: the samples were silicon-doped when grown. Detailed analysis of each stone can be found in Chapter 3.

5.3 Prompt Luminescence

The synthetic diamond gemstone set found in Table 3.1 provided the basis for the investigation. Sample 3 from this sample set was used as part of the diamond survey performed in Chapter 4. The gemstone produced a prompt blue luminescence signature which was recorded with a low noise high efficiency CMOS camera with a global shutter during UV illumination: shown in Chapter 4 and repeated in Figure 5.2 to aid the reader.

This prompt blue luminescence feature is much like a fluorescence feature shown in many natural diamonds, as shown in Figure 5.3. The spatial pattern/distribution of

the luminescence in both the natural diamond sample and the CVD sample have distinct similarities, with both producing a deep blue luminescence. The blue fluorescence pattern recorded is typical for Type IIa natural diamond, the luminescence is thought to originate from dislocations within the diamond lattice [63]. It is this blue luminescence pattern, demarking dislocation networks in Type II diamonds and growth zones in Type I diamonds that is often used as evidence for a gemstone's natural origin. However, given the similarity observed between the natural and synthetic gemstone it is not possible to conclude from this feature alone that a diamond has natural origin.

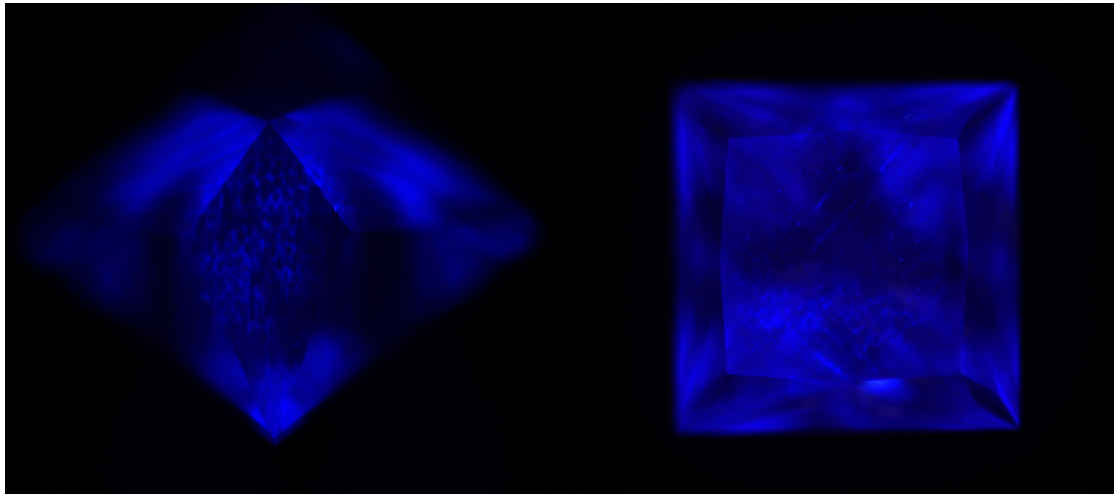


FIGURE 5.2: CMOS image of the prompt blue luminescence signal recorded for Sample 3 of the Genesis synthetic CVD diamond gemstones. The left-hand image shows the side of the gemstone, the right-hand side shows the table (top) of the gemstone.

Due to the similarities in the images of both the natural and CVD synthetic diamonds a photoluminescence study was performed. The optical pump used was a spectrally filtered xenon flash lamp with UV emission confined to 190-227 nm using a bespoke band pass filter (further experimental details can be found in Chapter 3). The CVD diamond showed a prompt photoluminescence signal centred at 435 nm whereas the natural diamond had a broadband centred at 425 nm as shown in Figure 5.4. The recorded photoluminescence signals from the CVD synthetic stone also showed some well-known features often seen in diamond, both the nitrogen vacancy centre NV^0 at 575 nm and the silicon vacancy centre SiV^- at 737 nm were observed.

5.4 Delayed Luminescence

A CMOS image was also taken of the spatial pattern/distribution of the delayed luminescence produced by the CVD sample; this was done in the same way as with the prompt luminescence. However, a delay of 90 μs was placed on the camera before the

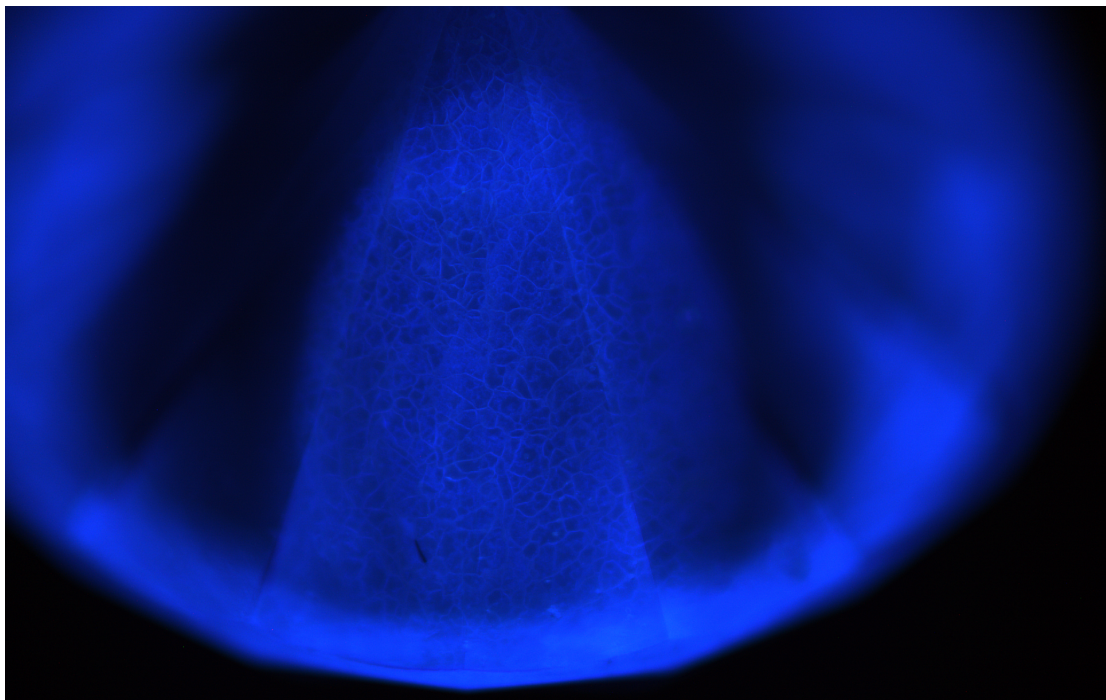


FIGURE 5.3: CMOS image of the prompt blue luminescence signal, recorded from a natural diamond gemstone. The dislocation structure in the stone can be clearly seen, and is attributed most commonly to the blue luminescence.

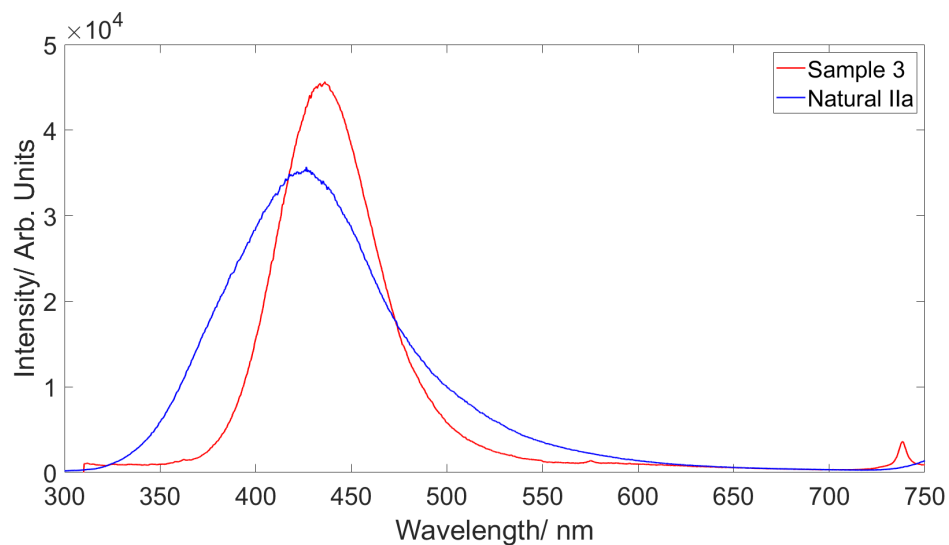


FIGURE 5.4: Comparing prompt blue luminescence spectra under UV illumination of the synthetic Genesis diamond gemstone (Sample 3) and the natural Type IIa diamond gemstone. The natural Type IIa stone is dominated by a broadband at 425 nm, Sample 3 of the Genesis CVD sample set is also dominated by a broadband found at 435 nm, the NV^0 centre is also present at 575 nm along with the SiV^- centre at 737 nm.

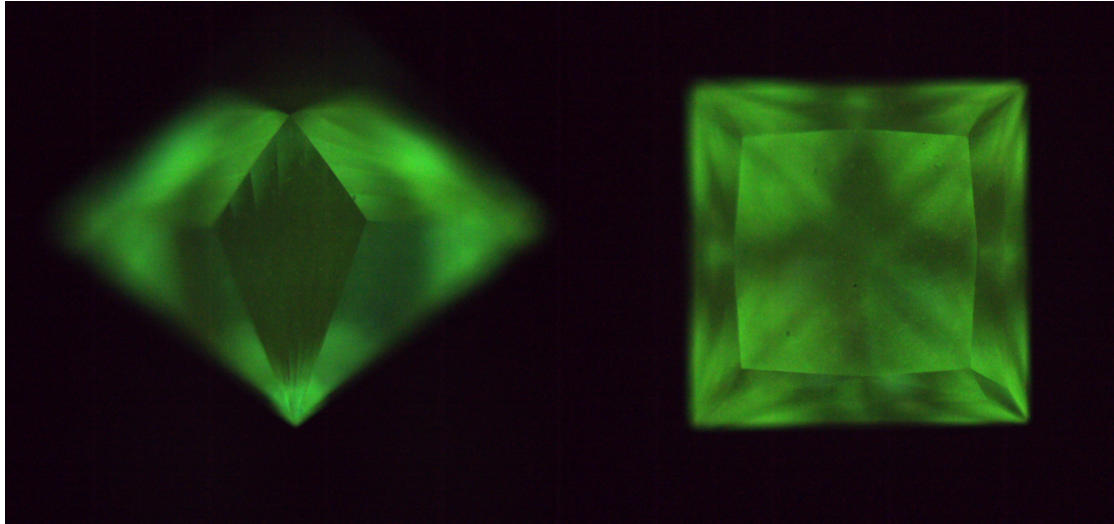


FIGURE 5.5: CMOS image of the delayed 499 nm luminescence signal, recorded for Sample 3 of the Gemesis synthetic CVD diamond gemstone. The left-hand image shows the side of the gemstone, the right-hand side shows the table (top) of the gemstone.

image was recorded. The image showed a long-lived green luminescence feature as shown in Figure 5.5, as previously mentioned in Chapter 4.

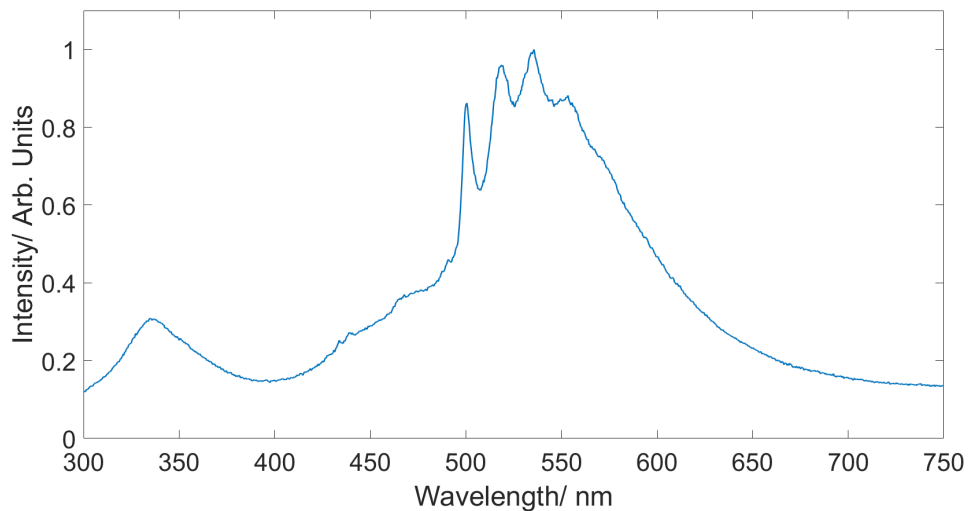


FIGURE 5.6: Delayed luminescence signal, recorded after $100 \mu\text{s}$ delay after the rising edge of the UV pump pulse, for the synthetic Gemesis diamond gemstone (Sample 3). The spectra is dominated by a broadband feature centred at 550 nm with an additional broad peak centred at 340 nm. A sharp green luminescence feature can also be seen at 499.6 nm which is not normally seen in gemstones.

A photoluminescence study was also performed; with a $90 \mu\text{s}$ delay before the spectra were recorded. It was noted that once the prompt blue luminescence feature centred at 435 nm decayed, a much weaker long-lived green luminescence signal centred at 540 nm dominated the spectrum, as seen in Figure 5.6. There is also a sharp spectral feature

at 499.6 nm, with a corresponding vibronic side band. It is this particular line that becomes the focus of the rest of this chapter.

There is very little information about this spectral line in existing literature. Khong and Collins first reported a spectral line matching this wavelength after observing a feature centred at 2.48 eV (approximately 499 nm) in the cathodoluminescence spectrum [83]. Three samples were studied: two of which were grown by the CVD technique and the third by combustion flame technique and all were produced by different institutes. The authors did not report whether any post processing was performed on the samples after growth. All three samples show four cathodoluminescence peaks at 2.33, 2.42, 2.48 and 2.57 eV. However, in the two samples produced by CVD synthesis the peaks were significantly broader than in the sample produced by flame combustion. The relative intensities of the peaks between each sample differed significantly but a correlation was identified between the integrated intensities of the 2.42 eV and the 2.57 eV features. The energy spacing between these two peaks is around 158 meV leading the authors to speculate that the 2.42 eV peak is a phonon replica of the 2.75 eV peak. There is a weak inference in Kong and Collins' paper that the origin of the 2.48 eV (499 nm) spectral line is due to a defect incorporated during growth. In a second paper by the same authors there is further mention of a spectral line matching this wavelength, as well as in a paper by Kawarada et al., published the following year [84]. The samples from the Kawarada paper were also grown by microwave assisted CVD, and the 2.48 eV (499 nm) feature was observed in the cathodoluminescence spectrum. The only other reference to a spectral line matching this wavelength that could be found was a short communication by Kitawaki et al. from the central gem laboratory, Tokyo, concerning measurements made on undisclosed CVD diamond samples [85]. The authors report that under 325 nm excitation, 462 nm and 499 nm peaks with unknown origins were detected, although no spectra were included to aid comparison. Kitawaki et al. also speculated that the samples may have undergone post-growth HPHT treatment. No literature has been found regarding the 499 nm spectral line pertaining to natural diamond, supporting Khong and Collins' original speculation that the origin of this line is from an impurity incorporated during growth.

As previously mentioned, this stone was taken from a sample set of 3 stones all grown and treated under the same conditions; Samples 1 and 2 were subsequently acquired due to the initial interest in Sample 3 after use in the Chapter 4 sample survey. Samples 1 and 2 were also imaged in order to determine if all three samples contained the 499 nm feature.

Both stones showed a strong blue prompt luminescence and a green delayed luminescence, as shown in Figure 5.7. The long-lived green component did not appear quite as

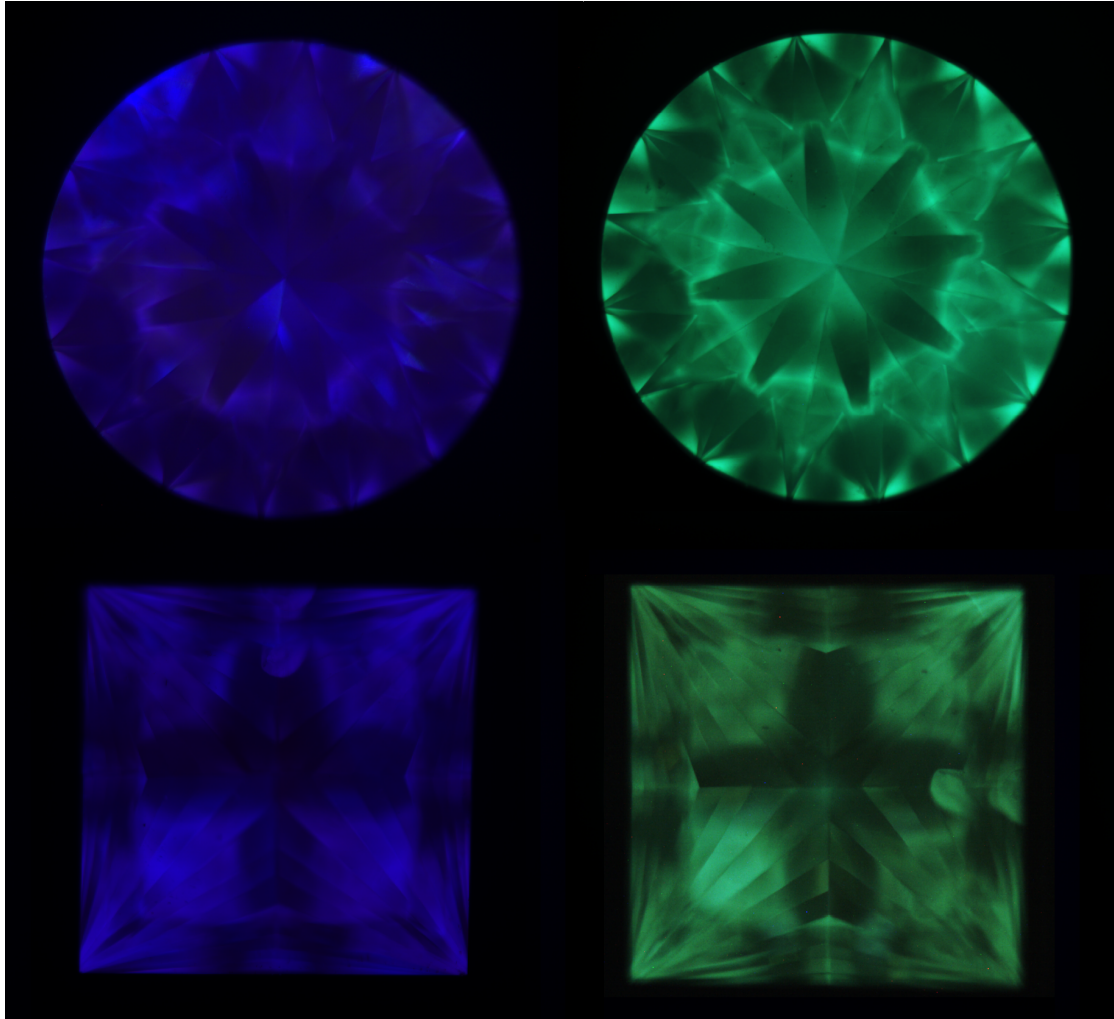


FIGURE 5.7: CMOS images of the prompt and delayed luminescence of both Sample 1 and Sample 2 from the Genesis CVD samples. The top left image shows the blue prompt luminescence of Sample 1; the top right image shows the delayed green luminescence of Sample 1; the bottom left image shows the prompt blue luminescence of Sample 2; the bottom right image shows the delayed green luminescence of Sample 2.

strong as that seen in Sample 3.

A spectroscopic study of all three stones from the Genesis sample set was carried out, the prompt luminescence from each stone can be seen in figure 5.8 and the delayed luminescence can be seen in figure 5.9. The prompt luminescence showed that each stone had the same broadband at 435 nm, as well as the NV^0 centre at 575 nm. The SiV^- centre was very prominent in sample 3 and the SiV^- peak was also seen in the other two stones but cannot be clearly identified in figure 5.8. A peak was also recorded in all three stones at 533 nm, however, the origin of this peak is unknown. The delayed luminescence showed that all three samples did in fact all contain the 499 nm feature, it was most prominent in sample 3 and due to this sample 3 became the primary sample for all following investigations into the 499 nm feature.

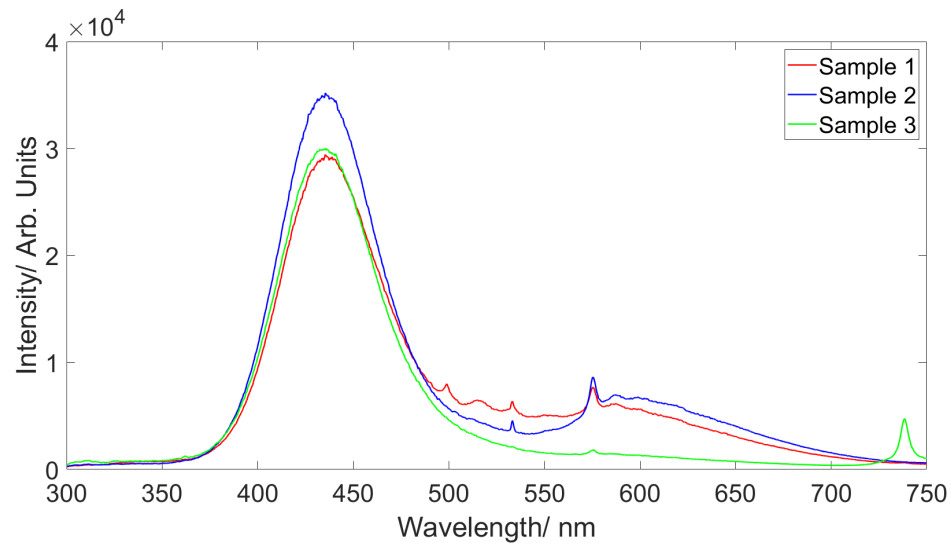


FIGURE 5.8: Spectra showing the prompt luminescence of all of the Gemesis sample set. All three samples show a broadband centred at 435 nm. All three samples also contain the NV^0 centre at 575 nm. However, it is in far greater concentration in Samples 1 and 2. Whereas Sample 3 also shows the SiV^- centre at 737 nm, the other two stones also contain the SiV^- centre but in a much smaller concentration which is not visible in this graph. There is also a peak at 533 nm in all 3 samples but most apparent in Samples 1 and 2; the origin of the 533 nm spectral line is unknown.

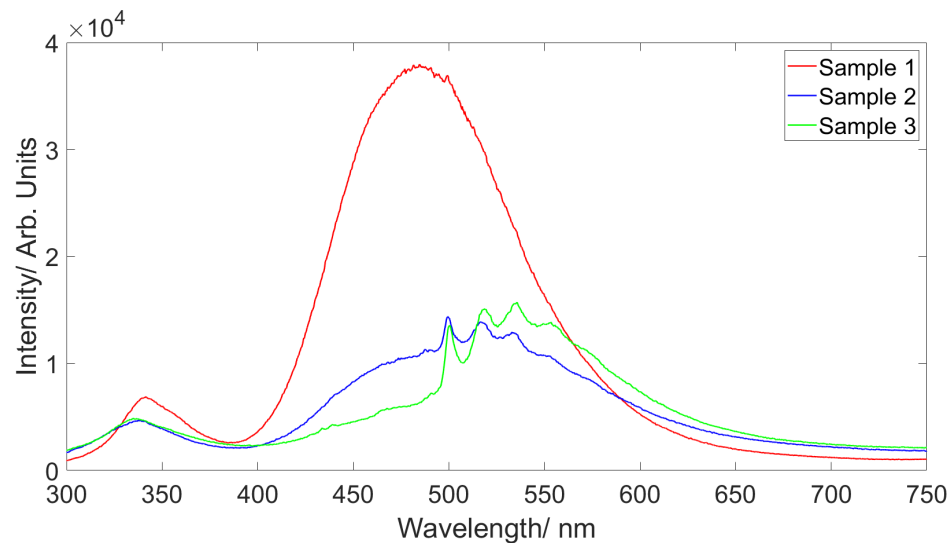


FIGURE 5.9: Spectra showing the delayed luminescence of the Gemesis sample set. Sample 1 has a broadband around 490 nm, whereas Samples 2 and 3 have a broadband centred around 520 nm. All 3 samples display a second broadband. In sample 1 this is centred around 345 nm, in Samples 2 and 3 this is centred at 340 nm. All 3 samples contain the 499.6 nm feature, although it is much harder to distinguish in Sample 1 due to the large broadband surrounding it.

5.5 Annealing Sequence

Proceeding on the assumption that the 499 nm spectral line originates from an impurity incorporated during growth, two further sample series were obtained from De Beers Technologies which exhibited the 499 nm spectral line.

The first series was originally produced by Element Six and provided by De Beers Technologies. It consisted of CVD synthetic diamond plates with a high nitrogen concentration that had been unintentionally doped with silicon and subsequently undergone annealing. The samples also contained nitrogen which had been intentionally introduced into the plasma at a level of 1.85 ppm during growth. The original sample was grown on a polycrystalline substrate that was subsequently removed by laser cutting and polishing. The evidence for silicon incorporation in the CVD diamond came from the photoluminescence spectrum taken with a 633 nm pump wavelength as shown in Figure 5.10 which exhibited the characteristic sharp peak at 737 nm attributed to the SiV^- defect centre. It is very rare for silicon to be found in natural diamond and is most commonly associated with CVD growth; it is thought that the silicon originates from the quartz windows commonly found on the CVD plasma chamber and consequently is incorporated into the diamond crystal lattice during the growth process [86]. Spectral evidence of a complex involving silicon therefore provides strong evidence that the diamonds have synthetic CVD origin. The original sample was divided into 8 similar sized pieces, with each piece annealed at a different temperature, details of which can be found in Figure 3.2. Luminescence spectra were recorded at a delay of 100 μs after the rising edge of the UV pump pulse, as shown in Figure 5.11.

The spatial distribution of the luminescence was recorded using a low noise CMOS camera which can be seen in Figure 5.12. For the lower annealing temperatures (1200 °C - 1400 °C), the long-lived luminescence appears red, primarily due to the presence of NV^0 at 575 nm. At higher annealing temperatures the nitrogen vacancies become mobile and aggregate with other defects, resulting in the reddish colour beginning to fade. Consequently, the sharp NV^0 peak at 575 nm disappears from the luminescence spectrum. Above 1600 °C, the emission is predominantly green due to the formation of the 499 nm feature and its associated vibronic side bands. At the highest annealing temperatures above 2000 °C when the complex responsible for the 499 nm peak disassociates the emission appears turquoise caused by a large broadband dominating the spectrum centred at 490 - 500 nm. The turquoise colour is most commonly associated with nitrogen-boron donor-acceptor pairs. However, no evidence of boron has been found in these stones.

The spectroscopic features associated with the changes in emission colour were investigated further. Prior to the annealing process there was no evidence of a 499 nm spectral

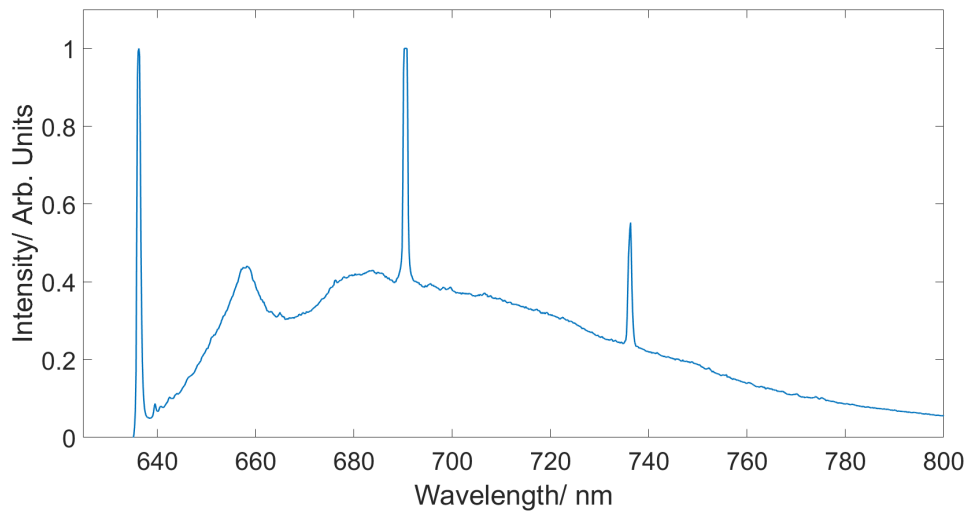


FIGURE 5.10: Photoluminescence spectrum for a pump wavelength of 633 nm recorded at 77 K. The spectrum shows a sharp peak at 737 nm attributed to the SiV^- centre, it also shows a peak at 637 nm attributed to the NV^- centre, as well as a peak at 690 nm which is often attributed to radiative recombination between donor-acceptor pairs in CVD diamond.

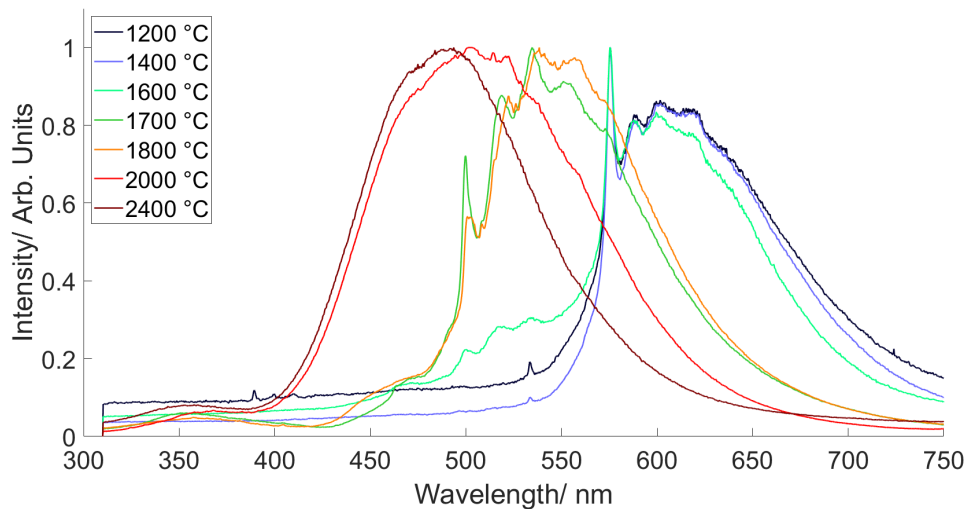


FIGURE 5.11: Room temperature delayed luminescence spectra for the series of annealed E6 CVD diamond samples with comparatively higher silicon and nitrogen concentrations annealed at different temperatures. The 499 nm spectral line can only be observed in the temperature range 1600 - 2000 °C. The NV^0 centre at 575 nm is only observed in the delayed luminescence sample annealed up to 1600 °C, the temperature at which NV^0 centres are known to become mobile.

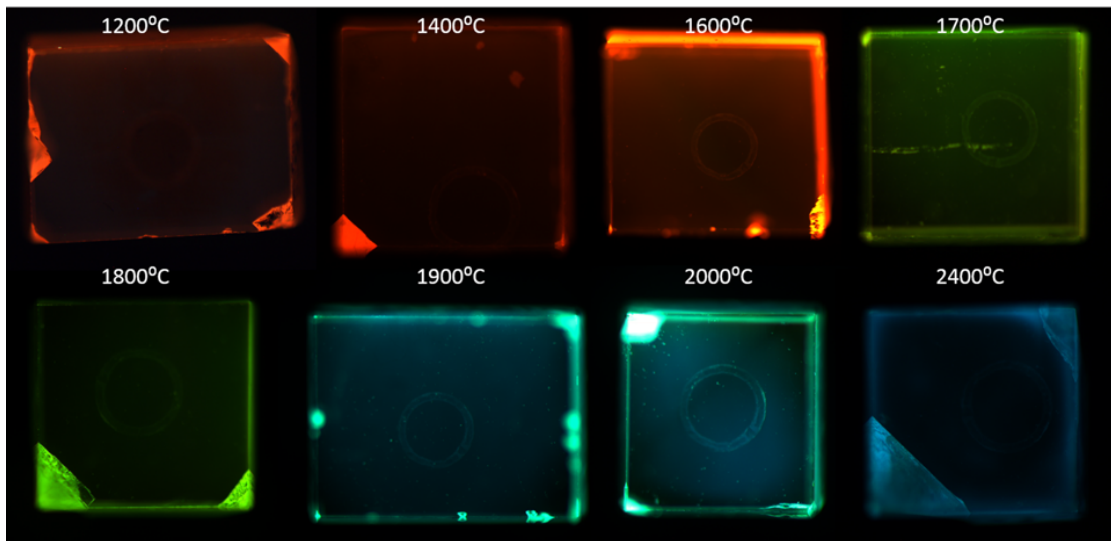


FIGURE 5.12: Composite CMOS image recording the luminescence from the 8 high concentration silicon-doped samples under UV illumination. This figure highlights a progressive colour change from red through green and then turquoise with increasing annealing temperature.

line in the sample. However, a small subset of the annealed series showed the presence of the 499 nm spectral line in the delayed luminescence spectrum. The 499 nm spectral line was only observed in samples that had been annealed between 1600 °C and 2000 °C, with the peak intensity observed in the stone that was annealed at 1800 °C. Overall, this suggests that a defect that becomes mobile or breaks down at around 1600 °C is involved in the defect responsible for the 499 nm emission. Nitrogen vacancies are known to become mobile at 1600 °C leading to speculation that either nitrogen, vacancies, or both could be involved in the complex [87].

It has been speculated that silicon may also have some involvement in the complex as it was incorporated in the samples during the CVD growth as previously stated. To investigate the involvement of silicon in the 499 nm defect, a further set of measurements on a second sample series (which had similar nitrogen concentrations) was taken; additional care was taken during the growth of the sample to ensure negligible silicon was introduced. This reference sample was treated similarly, dividing it into a series of 7 similar sized pieces and annealing the series under similar conditions. The low-silicon samples exhibit similar luminescence behaviour with comparable progressive colour changes from red through green followed by turquoise as the annealing temperature increases. However, the spectroscopic measurements revealed no evidence of the 499 nm spectral line for any of the annealed samples, on any timescale. Figure 5.14 shows the luminescence spectra for the sample annealed at 1800°C, the temperature at which the peak intensity of 499 nm was seen in the last sample series. However, in this sample series there was no spectral line observed at 499 nm. The nearest sharp observable spectral feature was

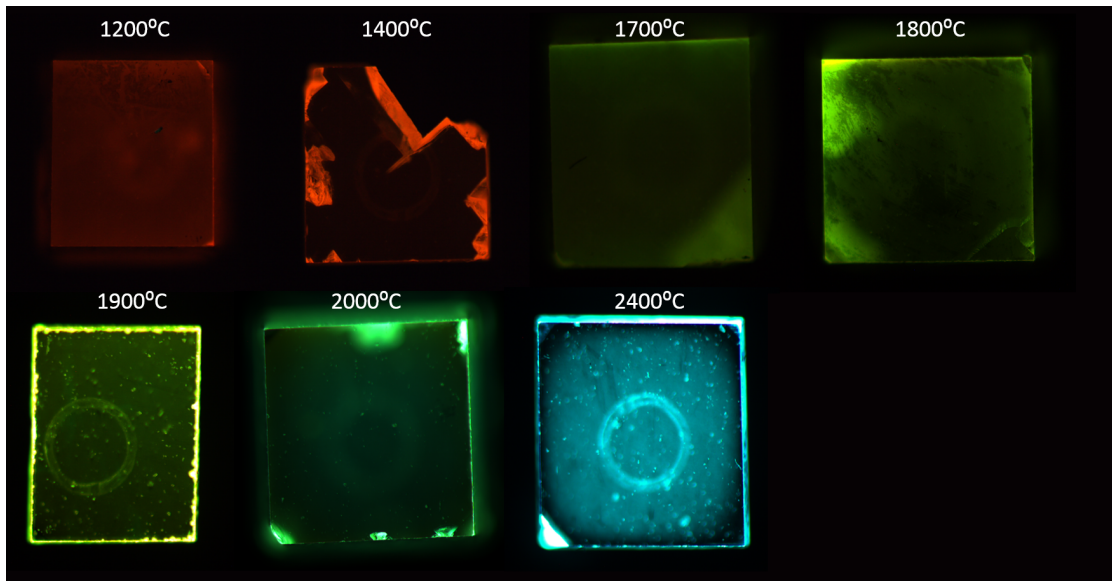


FIGURE 5.13: Composite CMOS image recording the luminescence from the 7 low concentration silicon-doped samples under UV illumination. This figure highlights a progressive colour change from red through green and then turquoise with increasing annealing temperature much like that seen in Figure 5.12.

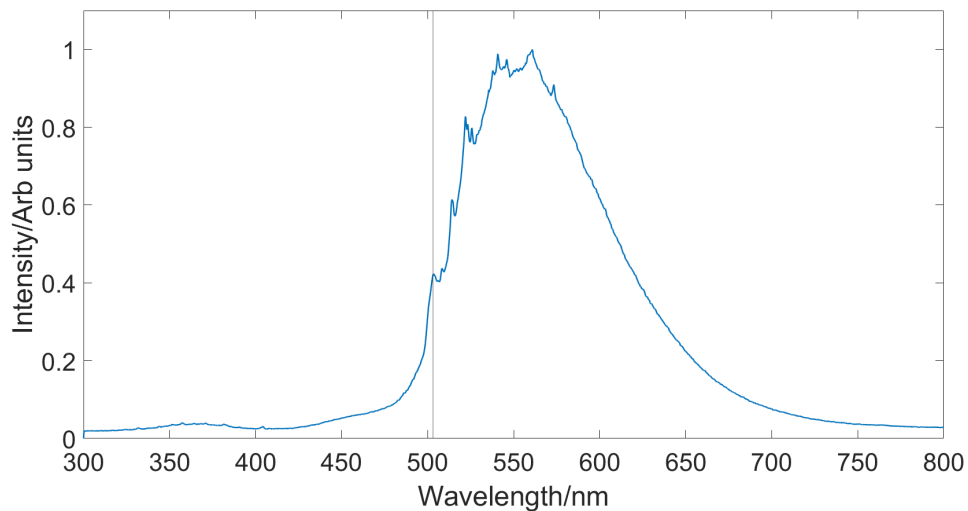


FIGURE 5.14: Delayed luminescence spectrum for the Element 6 CVD diamond sample annealed at 1800°C with negligible silicon concentration. The H3 defect can be seen at 503 nm, shown by the vertical line on the graph.

seen at 503 nm, which is known to be due to the H3 defect, a neutral complex containing two nitrogen atoms and a vacancy [22]. The H3 defect was not observed in the samples containing both nitrogen and silicon; it is therefore speculated that the 499 nm forms preferentially over H3. This result also indicates that nitrogen and vacancies alone are insufficient to produce this defect. Combining all information from the results so far leads to the belief that nitrogen, silicon and vacancies are most likely involved in the complex that produces the 499 nm spectral line.

Subsequent to these investigations a paper was published by Breeze et al. investigating Si-N complexes in diamond doped with both silicon and nitrogen which was then annealed at a series of temperatures. During their investigations Breeze et al. identified the neutrally charged silicon vacancy nitrogen complex SiVN^0 as well as concluding that this defect could not be a $\text{Si}_x\text{N}_y\text{V}$ defect as we had originally predicted. This was due to the fact that no 499 nm feature was found in their investigations along with the annealing behaviour of SiVN differing from the annealing behaviour of the 499 nm feature [88]. Due to this and preliminary theoretical simulations carried out by Claire Meara suggesting defects such as SiV_2N are theoretically possible we believe that this defect is more likely to be a $\text{Si}_x\text{N}_y\text{V}_z$. We would suggest further investigation in the form of Electron Paramagnetic Resonance studies (EPR) could assist in the characterisation of the 499 nm defect.

5.6 Discussion

The observation of a luminescence line at 499 nm, here attributed to a $\text{Si}_x\text{N}_y\text{V}_z$ colour centre provides a further identifying feature of synthetic diamonds. High concentrations of silicon in diamond are normally associated with CVD growth. It is generally accepted that silicon can be unintentionally introduced during the CVD process by plasma related etching of the quartz walls or windows of the reactor chamber, or from the substrate during heteroepitaxial growth on silicon. An important signature of silicon incorporation is the silicon vacancy centre SiV^- line at 737 nm [89]. Diamond can also be doped with silicon intentionally by introducing silane into the plasma; careful studies have revealed many other silicon related spectral lines [89, 90]. Natural growth conditions do not favour the incorporation of larger atoms such as silicon into the compact diamond lattice [91] However, the presence of silicon alone is not sufficient to rule out the possibility that the diamond is not of natural origin. A very small number of natural diamonds containing the SiV^- centre have previously been reported by Breeding and Wang [89]. Using FTIR analysis they revealed that the diamonds included both Type IIa diamonds and Type Ia diamonds with nitrogen concentrations ranging from 0 to 4.7 ppm, predominantly in the form of A-aggregates. Breeding and Wang did not report a 499 nm line in their comprehensive spectral study of these natural samples. All the evidence in the literature to date suggests that the 499 nm line has only ever been observed in synthetic diamond and therefore it is believed that the feature has the potential to be used to detect such synthetic diamonds. The 499 nm line has only been observed in samples that have been annealed in a narrow temperature window between 1600 °C and 2000 °C, which means it could be used to detect whether a diamond has undergone heat treatment in this temperature range. It has been reported by Wang et al. that spectroscopic

evidence indicates the likelihood that the CVD synthetics can undergo post-growth HPHT processing in order to enhance their colour and possibly their clarity. These investigations were carried out on CVD stones sourced from Gemesis [17].

5.7 Conclusion

Investigations into the properties of a sharp spectral feature centred at 499.6 nm in CVD synthetic diamond gemstones were carried out. The gemstone investigated also exhibited a blue luminescence usually indicative of a Type IIa natural diamond. However, spectral characterisation showed that there were subtle differences between those exhibited by natural IIa stone and that recorded for the CVD stone. The luminescence peak recorded for the synthetic CVD diamond samples was centred at 435 nm whereas the Type IIa natural diamond was centred at 425 nm. This is the first time the 499 nm has been reported in a CVD synthetic gemstone; 499 nm had been previously reported a small number of times, but these were not in gemstone form. The 499 nm centre was also found in a set of well documented CVD diamond with a high concentration of both nitrogen and silicon which had undergone different annealing treatments. The 499 nm feature was only observed in samples which had been annealed in the temperature range of 1600 °C and 2000 °C. It is well documented that the nitrogen vacancy centres become mobile around 1600 °C, indicating the involvement of nitrogen, vacancies, or both in the defect's structure. Heat treatment above 2000 °C removed the 499 nm colour centre completely. A comparison was carried out with a second set of well documented CVD diamond samples with a high concentration of nitrogen but a negligible concentration of silicon; these had also undergone treatment at various annealing temperatures. The 499 nm feature was absent in this sample set, leading to the conclusion that silicon is also involved in the defect's structure. The overall conclusion is that the defect would be some kind of $\text{Si}_x\text{N}_y\text{V}_z$ complex. The results also suggest that the presence of this spectral line could be used as an additional test for detecting specific synthetic diamonds which might be mistaken for Type IIa natural diamond.

Chapter 6

Temperature Dependent Studies of three CVD synthetic diamond samples

6.1 Background and Motivation

Temperature dependence studies allow for further interrogation into a material's electronic structure. Optical spectroscopy allows for the optical characteristics of a gemstone to be recorded in a way that is quantifiable and reproducible. Looking at the temperature dependence of these optical characteristics allows for further interrogation into how the feature changes with temperature. There are certain characteristics expected such as spectral lines becoming more defined when the temperature is decreased due to vibrations in the lattice being reduced when the thermal energy is reduced. However, some characteristics can show more individual changes. For example, if a new spectral line appears when the temperature is increased, this could be a sign of a thermally activated mechanism being turned on allowing for a previously unseen emission. Temperature dependence studies of two spectral peaks with a very similar wavelength can often prove beneficial, as the two features may be affected differently with temperature, meaning the spectral lines can go from indistinguishable to distinguishable. Gaining a greater understanding of the electronic structure of colour centres in diamond can allow them to become more useful within the scientific community whether this is characterising the defects as natural or of synthetic origin or finding scientific applications for the specific defects. With a full understanding of a defect, it becomes possible to synthesise diamond samples containing the defects of interest for use in identified applications. For example, the nitrogen vacancy centre and silicon vacancy centre have both been extensively

studied and are now frequently grown into diamond gemstones most commonly for use in quantum technologies.

In the rest of this thesis, the narrative has focused on exploiting spectroscopic techniques to reveal the provenance of gemstones. However, much still remains unknown about the physical origins of many luminescent features in diamond. For example, while the blue luminescence that some diamonds exhibit on excitation with UV light; has been visually associated with dislocations in the lattice, it is unclear whether the optical transition is due to impurity atoms or defects in the crystal structure. The work described in this chapter was aimed at identifying common features, as well as differentiating features, in diamond material that was exclusively synthetic in origin. Specifically, spectroscopic properties of a sample containing the 499 nm feature have been compared and contrasted with an intentionally nitrogen-doped CVD synthetic and a high-purity CVD synthetic diamond, which were used for reference.

6.2 Experimental Techniques and Sample Selection

A temperature dependence study was carried out on three different CVD gemstones. The first was the previously referenced Sample 3 sourced from Gemesis, widely explored in Chapter 5, specific details of the sample can be found in the experimental theory section 3.1. The second sample was sourced from Element Six, it is a CVD sample containing high concentrations of nitrogen vacancy centres. The stone was intentionally doped during growth with nitrogen at a concentration of 0.668 ppm. The third sample was a high purity CVD sample, also sourced from Element Six. This sample was not intentionally doped with any defects in order to produce a high purity stone with negligible defects; this stone was chosen to provide a comparison in the following chapter.

The Horiba Fluorolog was used to carry out the spectroscopy both for luminescence measurements and lifetime decays with the use of the two different detectors discussed in Chapter 3. The use of cryogenics allowed for both the luminescence and time decays to be recorded within a temperature range of 77 and 370 K. The Andor iStar iCCD detector was used for luminescence measurements and the IBH TBX-850C photon detection detector was used to record lifetime measurements. Details of all equipment can be found in Chapter 3.

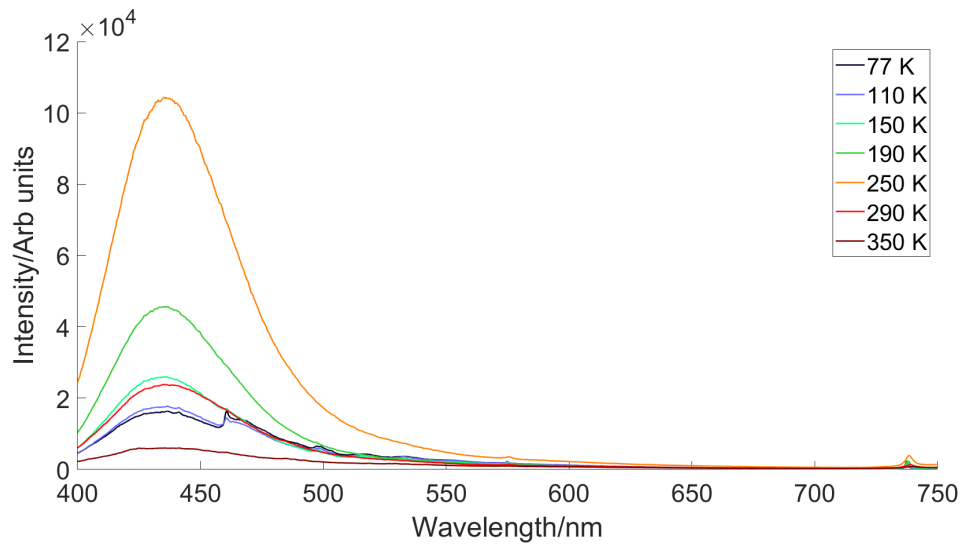


FIGURE 6.1: Spectral data showing the prompt blue luminescence of Sample 3 over a range of different temperatures. A broadband can be seen at all temperatures centred around 435 nm. In the lower temperature spectra, a peak can be seen at around 460 nm, 499 nm, 575 nm (attributed to the NV^0 centre) and 737 nm (attributed to the SiV^- centre).

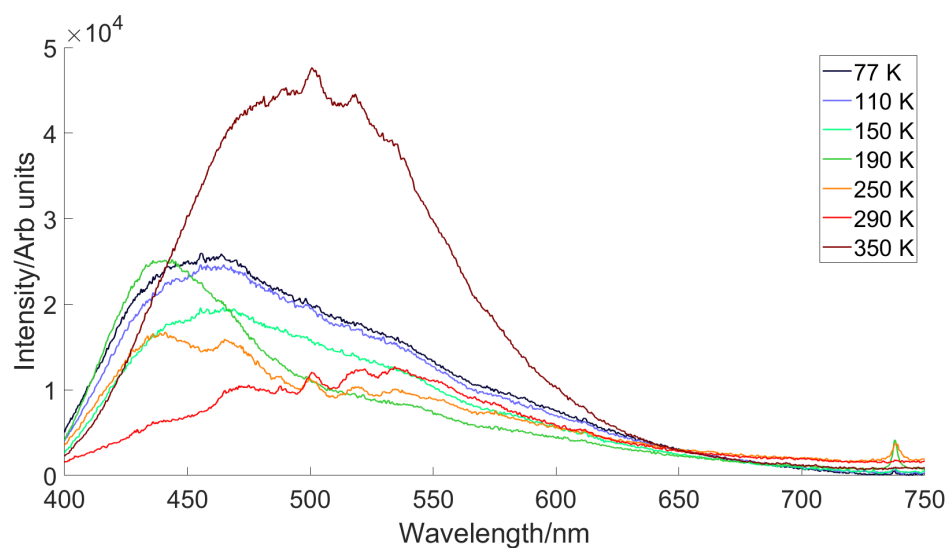


FIGURE 6.2: Spectral data showing the delayed luminescence of Sample 3 over a range of different temperatures. At lower temperatures a broadband is seen around 465 nm; as temperatures increase, this shifts to a broadband around 440 nm, followed by a split broadband at 440 nm and 465 nm, before finally at very hot temperatures a broadband centred at around 480 nm. A peak at 737 nm attributed to the SiV^- centre can be seen at all temperatures. The 499 nm feature can be seen in temperatures above 250 K.

6.3 Sample 3: 499 nm containing CVD synthetic sample

Spectral data was recorded on both prompt and delayed timescales to record the luminescence emitted after excitation with a deep UV light source. This luminescence was measured at a range of temperatures, in order to observe how certain features emitted by the diamond varied at different temperatures. The prompt luminescence can be seen in Figure 6.1. The broadband is centred around 435 nm for all temperatures and at high temperatures this broadband is very shallow, becoming more prominent as temperatures increase until it peaks at 250 K. Above 250 K the broadband begins to diminish in height. At 110 K a small peak and what looks to be its vibronic sideband become apparent at 460 nm; this effect is also seen in 77 K and, despite the 435 nm broadband being smaller, the size of the 460 nm peak and vibronic sideband increases. At temperatures lower than 110 K, the 499 nm feature and vibronic side band are visible; the feature is not apparent in prompt timescales at higher temperatures. It was originally thought that the 499 nm feature was only seen on delayed timescales when carrying out work at room temperature. However, this has shown that the 499 nm feature can, in fact, be seen in prompt luminescence when the temperature is sufficiently low. The NV^0 centre is also present in the prompt luminescence, this feature can be seen in all temperatures but is most prominent in the lower temperatures. The SiV^- centre can also be seen at all temperatures at 737 nm, however, it is much sharper at temperatures below 250K.

The delayed luminescence can be seen in Figure 6.2, this data was recorded with a delay of 30 ms. At low temperatures, an asymmetric broadband can be seen peaking around 465 nm and as temperature increases this broadband shifts to approximately 440 nm before splitting into two broadbands at 250 K, with peaks at both 440 nm and 465 nm. The peak at 465 nm can still be seen at 290 K but disappears at higher temperatures. The 499 nm feature and vibronic sideband can be seen in temperatures above 190 K, this agrees with the previous room temperature data in Chapter 5 which only showed the 499 nm feature on delayed timescales. The broadband seen at around 480 nm at 350 K dominates the overall spectra, this is thought to be a long-lived feature originating from boron in the sample. Boron follows traditional phosphorescence mechanisms, the boron acts as an acceptor within the diamond lattice allowing donor - acceptor recombination to occur and luminescence to be emitted; this only happens at high temperatures as the mechanism is thermally activated. The SiV^- centre at 737 nm is also present at all temperatures below 250 K. The peak at 250 K is of particular interest as it suggests a connection between the broadband seen at 440 nm at 190 K and the broadband at 460 nm seen at 77-150 K, at 250 K both broadbands can be seen splitting apart from one another.

The prompt and delayed luminescence vary greatly in overall appearance; however, they do share some similarities. Firstly, the SiV^- centre can be seen in all temperatures on prompt timescales and is most prominent at mid-low temperatures, on delayed timescales it can be seen at mid to low temperatures. The 499 nm feature was thought to be observable only on delayed timescales. However, these studies have shown that it can be seen in prompt luminescence at cold temperatures (it was observed at both 77 K and 110 K) and, as expected, it is also seen at delayed timescales but only at temperatures above 250K. Overall, the delayed luminescence has a lot more observable features than the prompt luminescence with different features appearing at different temperatures unlike the prompt, which for the majority of temperatures, is dominated by a singular broadband.

Imaging was also carried out at 77 K, 150 K and 296 K as shown in Figure 6.3. At 77 K, both the prompt and delayed luminescence were blue in colour; this was the same at both a 90 μs delay and a 70 ms delay, showing that even though the 499 nm feature appeared at 77 K in the prompt spectra, Figure 6.1, the overall blue broadband was large enough to overshadow it. At 150 K, the prompt and delayed luminescence was again blue in colour, with no obvious sign of the 499 nm feature it is thought it was again overshadowed by the blue broadband. At 296 K, the prompt luminescence remained blue in colour as expected from the spectra; however, the delayed luminescence at both 90 μs delay and a 70 ms was green in colour which is thought to be due to the 499 nm feature.

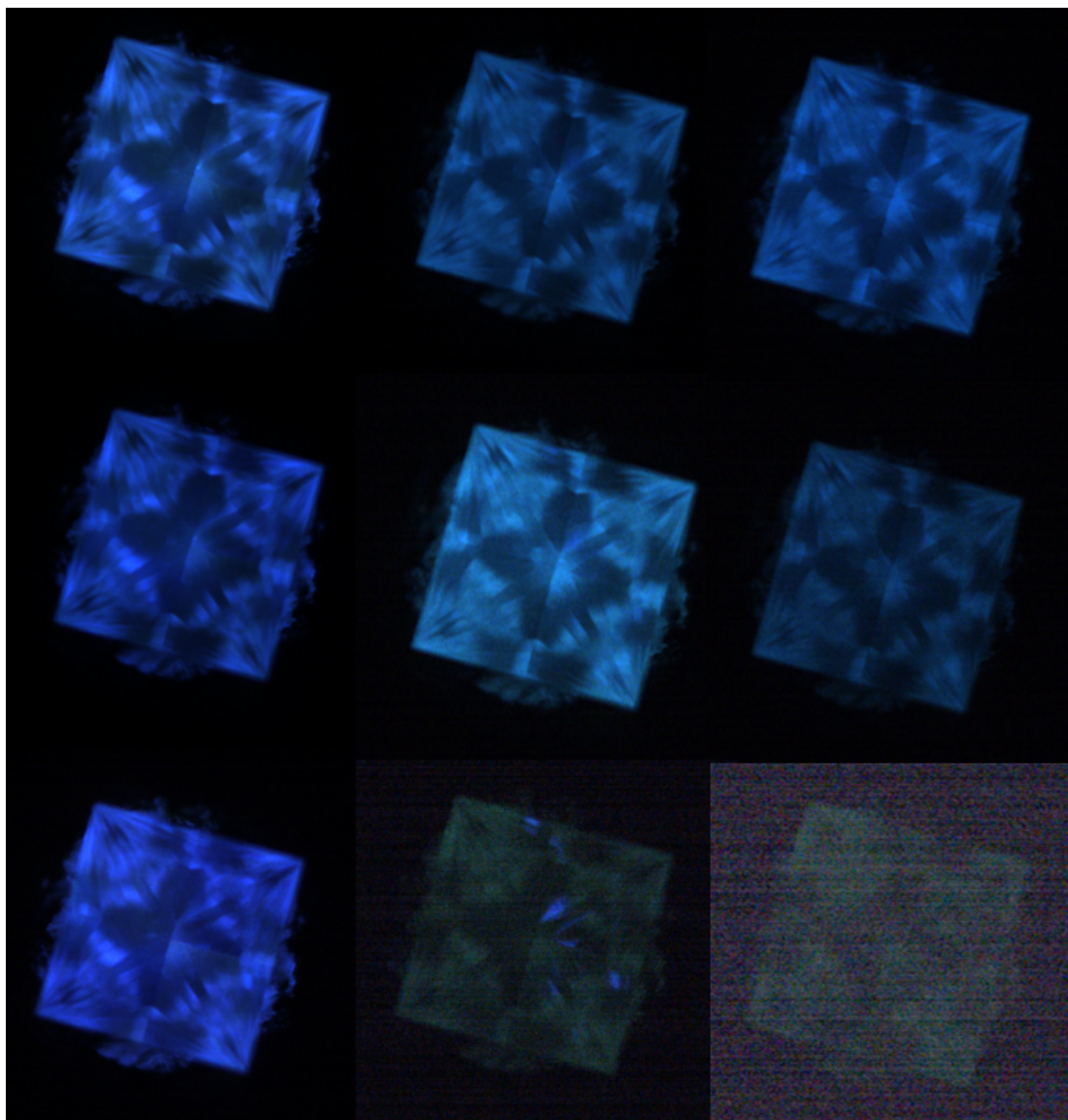


FIGURE 6.3: Imaging of Sample 3 taken at 77 K (top row), 150 K (middle row) and 296 K (bottom row). The images were taken at 0 delay after excitation (1st column), $90 \mu\text{s}$ after excitation and $70000 \mu\text{s}$ after excitation. At 77 K and 150 K the luminescence at both prompt and delayed timescales was blue, at 296 K the prompt luminescence was also blue in colour but the delayed luminescence at both delays was green in colour; this is thought to be due to the 499 nm feature.

6.4 Intentionally nitrogen doped CVD synthetic

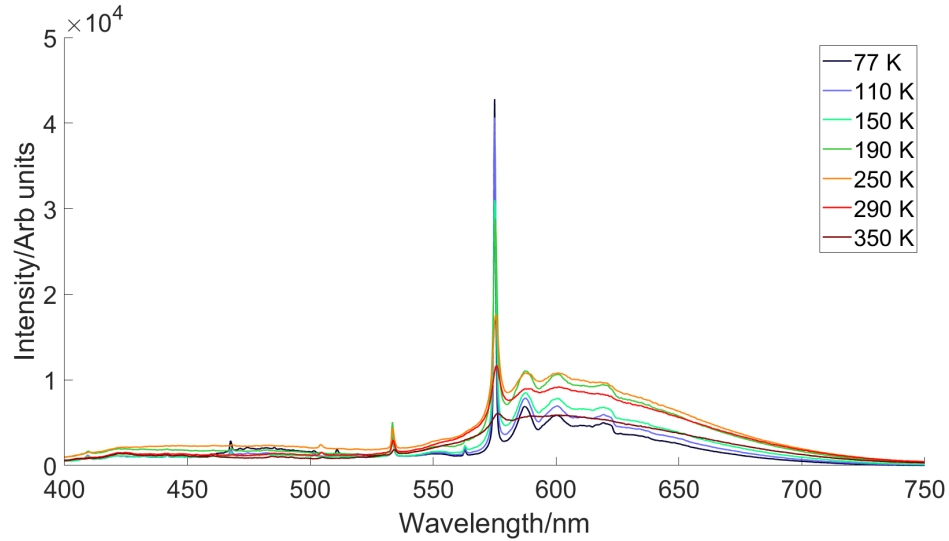


FIGURE 6.4: Spectral data showing the prompt luminescence of the nitrogen doped sample over a range of different temperatures. A sharp peak at 575 nm in conjunction with its vibronic side band is seen at all temperatures, this is due to the NV^0 centre. A sharp peak at 533 nm can also be seen at all temperatures the origin of which is unknown.

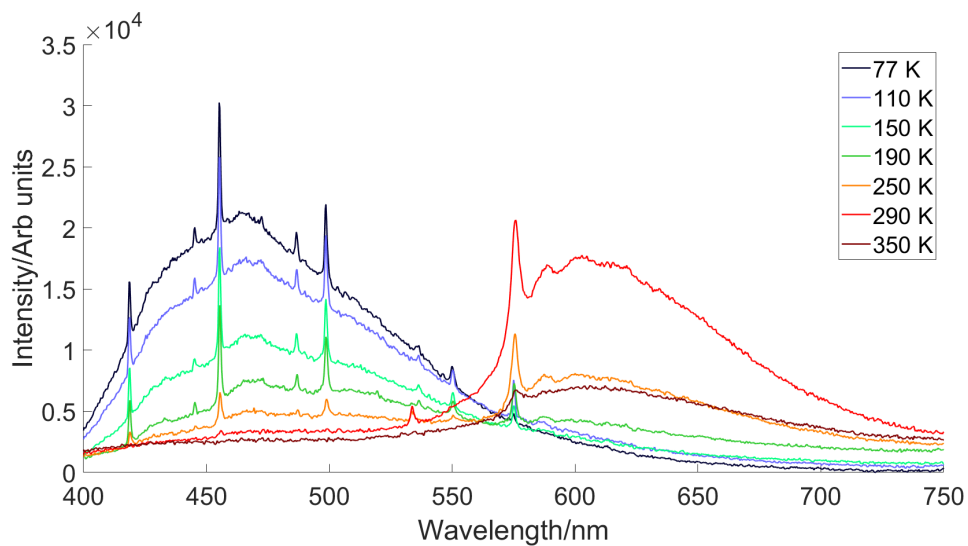


FIGURE 6.5: Spectral data showing the delayed luminescence of the nitrogen doped sample over a range of different temperatures. A peak at 575 nm is seen at all temperatures, at low temperatures a range of other sharp peaks emerged with the most prominent being at 419 nm, 455 nm and 498 nm, these sat on top of a broadband centred at around 460 nm.

The prompt luminescence is shown in Figure 6.4, the NV^0 centre is present at 575 nm along with its vibronic side band and can be seen at all temperatures, the lower the temperature the sharper the peak and side band are. This peak and sideband are characteristic of the emission seen from the NV^0 centre which is reported as comprising

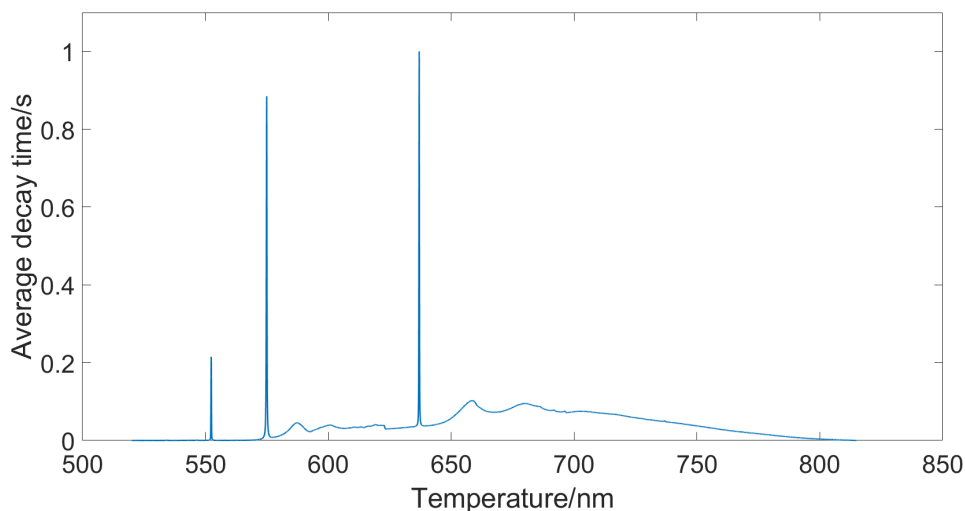


FIGURE 6.6: Spectral data showing the photoluminescence recorded at 77 K with an excitation of 514 nm. Both the NV^0 centre at 575 nm and NV^- centre at 637 nm.

a sharp zero-phonon line with increasingly broad phonon replicas. Despite the fact that the stone was doped with 0.668 ppm of nitrogen when grown, the NV^- centre is not seen in the luminescence recorded for this sample, this may be due to the use of above band-gap excitation causing the NV^0 centre to be the preferential route for decay. Further photoluminescence studies carried out at 77 K with a 514 nm excitation source (below band-gap) did, however, show the presence of the NV^- centre which can be seen in Figure 6.6. A peak can also be seen at 533 nm at all temperatures; once again the peak is sharper at lower temperatures, the origin of the peak is unknown. At temperatures below 250 K peaks can also be seen at 409 nm, 442 nm, 468 nm, the origins of which are also unknown, as well as a peak at 563 nm which has been previously documented in literature using cathodoluminescence. This defect is thought to appear in Type IIa diamonds which have been irradiated with light ions, the nitrogen containing stone had not been irradiated. However, the defect has also been tentatively attributed to an interstitial-type intrinsic defect [22, 92].

The delayed luminescence spectra can be seen in Figure 6.5. The NV^0 centre can be seen at all temperatures along with its vibronic sideband, the centre becomes less prominent at lower temperatures with the vibronic sideband becoming harder to distinguish below 190 K, with the exception of 350 K where the peak and broadband are still visible but less sharp. At lower temperatures the broadband shifts to around 465 nm, this broadband remains up to 250 K progressively diminishing in height. There are a number of peaks sitting on top of the broadband at 465 nm, these peaks vary greatly in size and are seen at 419 nm, 445 nm, 455 nm, 472 nm, 487 nm, 498 nm, 533 nm and 550 nm. These peaks appear at temperatures above and including 250 K, the origin of these peaks is unknown.

However, the sharpness of the peaks indicates that the transitions are between discrete levels rather than bands.

Overall, the delayed luminescence is very similar to the prompt luminescence at higher temperatures; however, at low temperatures they differ. With the delayed spectra there is a shift towards lower wavelength emission. The prompt and delayed luminescence at both 290 K and 350 K follow the same pattern as each other; both contain the NV⁰ centre at 575 nm in conjunction with its vibronic side band as well as a peak of unknown origin at 533 nm. At 250 K the delayed luminescence begins to differ in shape from the prompt luminescence with the 575 nm peak and vibronic side band looking much like the prompt luminescence. But a broadband begins to appear centred around 460 nm as well as various small peaks sitting on top of the broadband. The broadband centred around 460 nm gets steadily larger as temperature decreases, at temperatures below 190 K this broadband dominates the spectrum.

Imaging was once again carried out at 77 K, 150 K and 296 K, as shown in Figure 6.7. At 77 K the prompt luminescence was overall orange in colour but with a blue hue, this luminescence is due to the nitrogen vacancy centre. However, on delayed timescales the luminescence is blue in colour, this can be seen in Figure 6.5 as the blue broadband overshadows the NV⁰ peak. At 150 K both the prompt and delayed luminescence look much the same as at 77 K, this fits with what was seen in the spectral data as around 150 K; the amount of NV seen in comparison to the blue broadband was still very small. At 296 K both the prompt and the 90 μ s delayed luminescence were orange in colour, as Figure 6.5 shows. At higher temperatures the NV centre is the most prominent peak in the delayed luminescence and it would, therefore, dominate the luminescence image hence the orange appearance. By 70 ms the delayed luminescence had disappeared due to the lifetime of the feature.

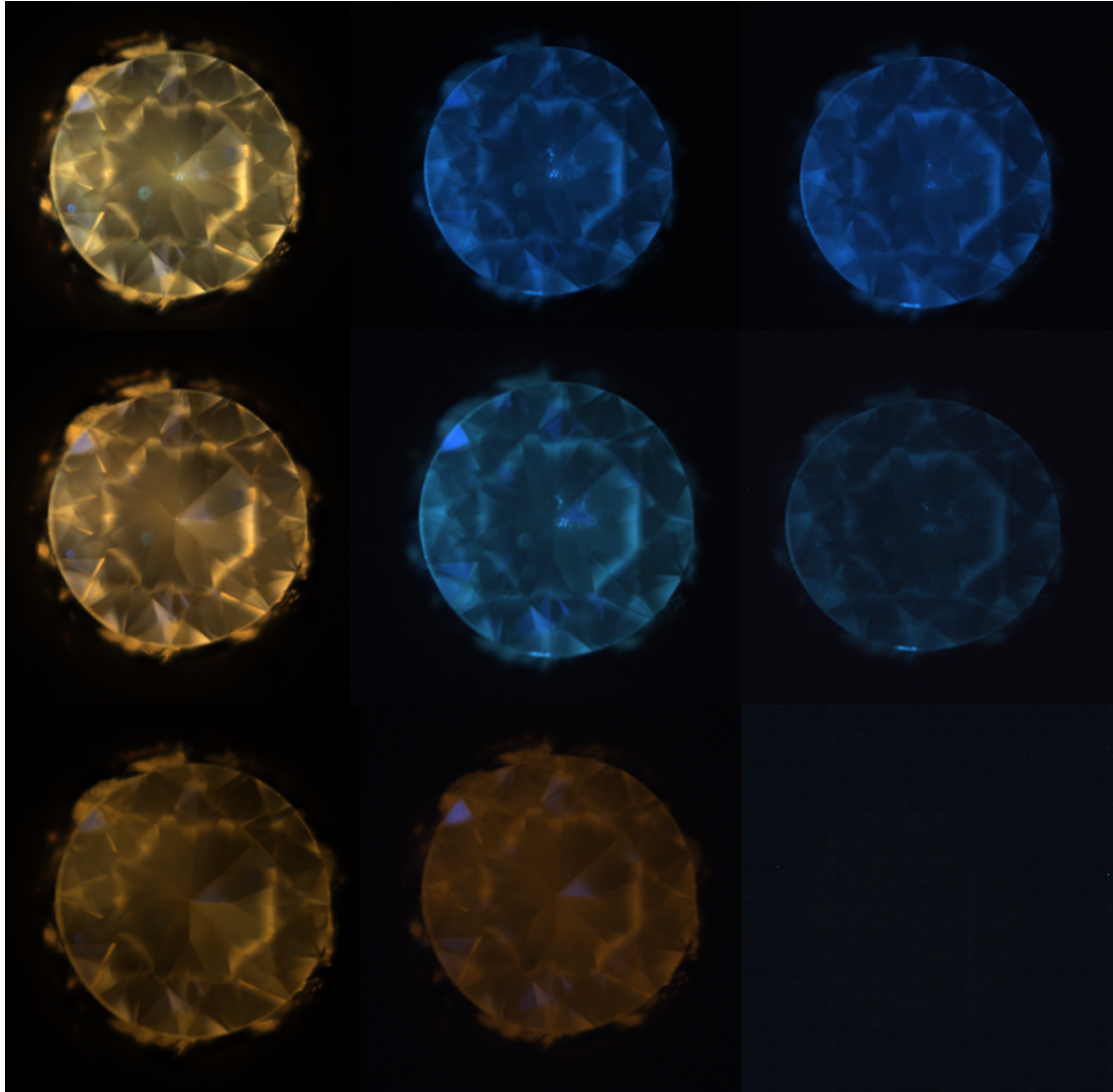


FIGURE 6.7: Imaging of the nitrogen containing sample taken at 77 K (top row), 150 K (middle row) and 296 K (bottom row). The images were taken at 0 delay after excitation (1st column), 90 μs after excitation and 70000 μs after excitation. At 77 K and 150 K the prompt luminescence was orange in colour and the delayed luminescence was blue in colour, at 296K the prompt and 90 μs delayed luminescence was orange in colour and the 70000 μs delayed showed no luminescence. The orange colour is associated with the NV^0 centre.

6.5 High purity CVD synthetic sample

The last stone to be sampled was the high purity stone. Once again, the prompt and delayed luminescence was recorded for this stone; the prompt luminescence can be seen in Figure 6.8. All temperatures show a broadband centred around 435 nm, this feature increases in size as the temperature decreases becoming most prominent at 250 K; the feature then begins to decrease in size with temperature until 130 K, where the size of the peak then increases again slightly at 77 K. A further small peak and vibronic side band can be seen at 485 nm at all temperatures as a shoulder on the 435 nm peak.

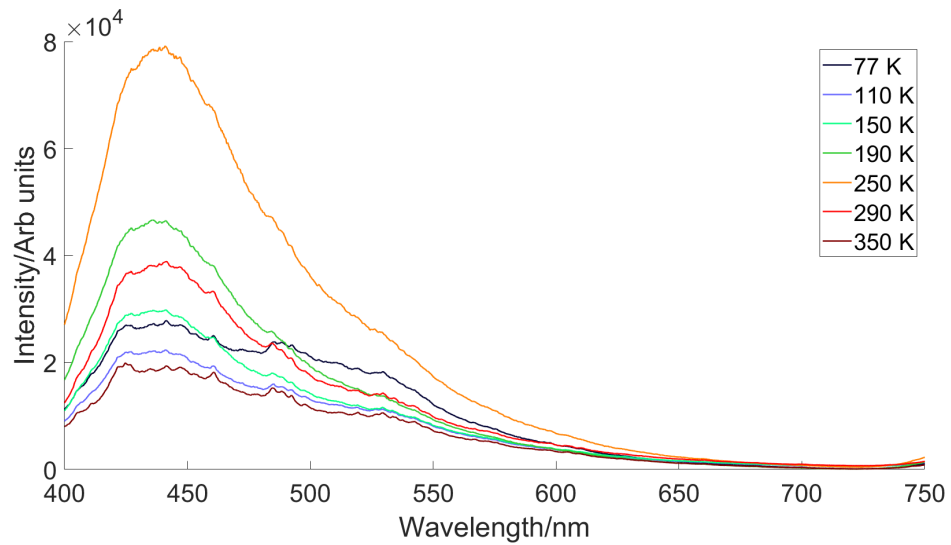


FIGURE 6.8: Spectral data showing the prompt luminescence of the high purity sample over a range of different temperatures. All temperatures show a broadband centred around 435 nm as well as two peaks with vibronic side bands at 485 nm and 530 nm; the origin of both is unknown.

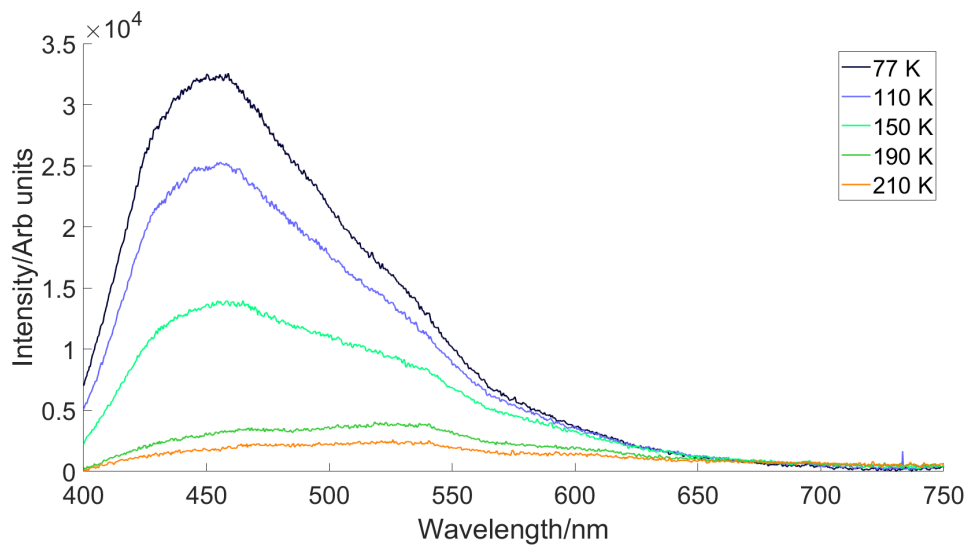


FIGURE 6.9: Spectral data showing the delayed luminescence of the high purity sample over a range of different temperatures. A broadband is seen in all temperatures centred at 450 nm, a small peak is seen at 733 nm at 110 K; this is of unknown origin.

What looks to be a peak with a vibronic side band can also be seen at 530 nm in all temperatures; however, it is less visible at 190 K and 250 K as it is overshadowed by the 435 nm broadband.

The delayed luminescence can be seen in Figure 6.9. For this stone, the delayed luminescence was recorded at a temperature range of 77-210 K as at higher temperatures no delayed luminescence was emitted by the sample. All temperatures have a broadband peaking around 450 nm, the broadband for each temperature has a shoulder around 540 nm which is more prominent at high temperatures. There is also a small sharp peak seen at 733 nm at 110 K the origin of which is unknown.

Although both the prompt and delayed luminescence look similar in appearance the broadbands in each are not the same with the broadband in the prompt luminescence being centred at 435 nm and the delayed luminescence being centred at 450 nm. The most apparent difference between the prompt and delayed luminescence is the two extra peaks seen in the prompt luminescence at 485 nm and 530 nm. In the prompt luminescence, emission was recorded at all temperatures up to 350 K. However, no delayed luminescence was present over 210 K.

Figure 6.10 shows the prompt luminescence of the high purity stone at room temperature (~ 296 K). As expected from the spectra, the luminescence is blue in appearance with some growth patterning present. No delayed luminescence was seen at this temperature for this sample. Unfortunately, for this stone, imaging was unable to be carried out at 77 K and 150 K as with the other stones due to a problem with the equipment.

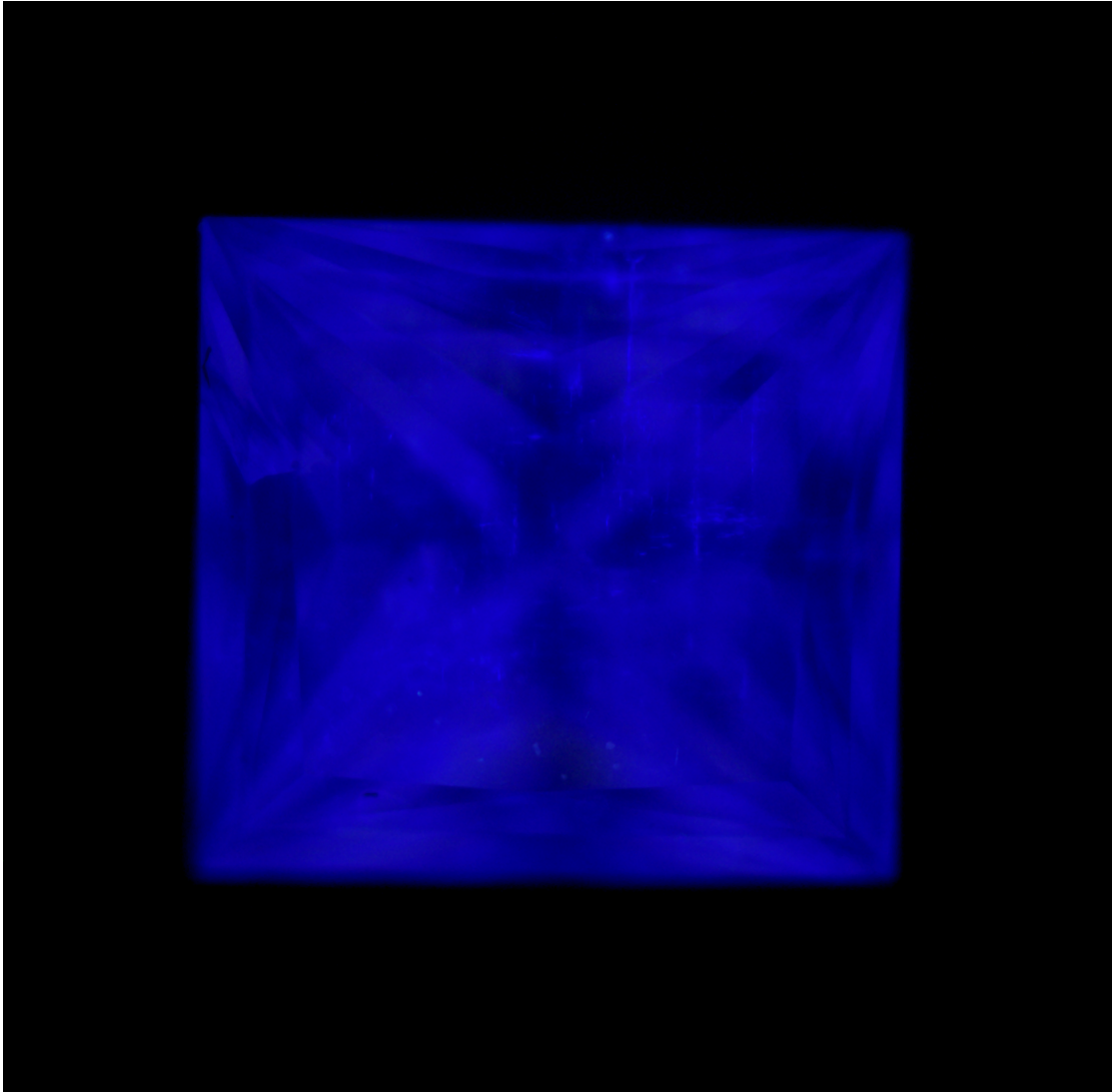


FIGURE 6.10: Image of the prompt luminescence of the high purity sample taken at room temperature, the sample does not exhibit delayed luminescence at room temperature. Unfortunately, at this time it was not possible to record an image of the prompt and delayed luminescence at any other temperature.

6.6 Comparison of Prompt Luminescence

The appearance of the prompt luminescence seen in Sample 3 and that seen in the high purity diamond is somewhat similar with both being dominated by a large broadband. The broadbands are centred at a similar wavelength, with Sample 3 being centred at 435 nm and the high purity sample centred at 440 nm. The effect of the temperature on the size of the broadband peak also shows similarities between the two stones with the most prominent peak being at 250 K in both stones and 350 K the least prominent. The broadbands seen in these stones also share the same trend with temperature with the highest broadband intensity being in the mid-range temperatures and the lower

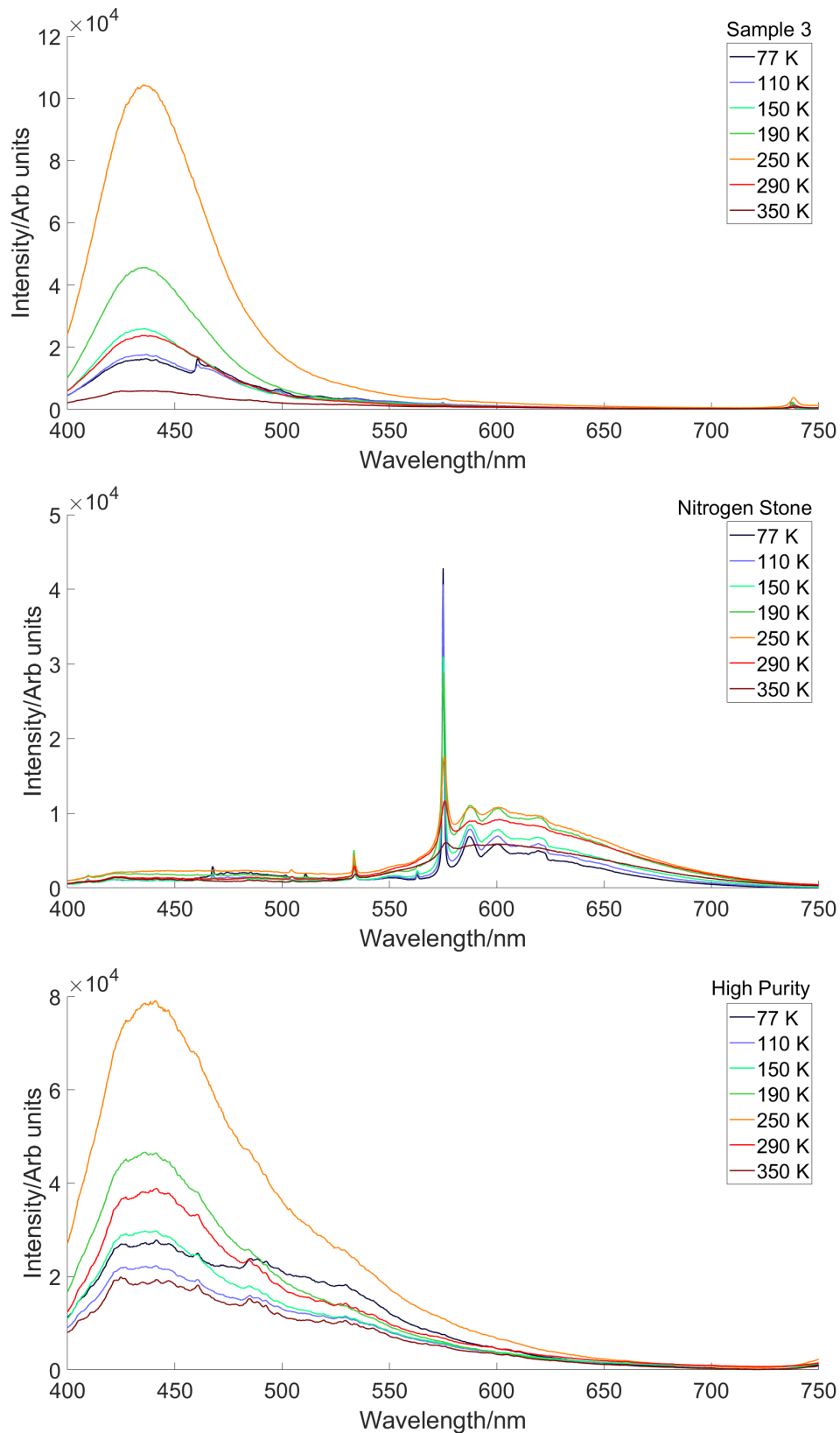


FIGURE 6.11: Spectral data for comparison of prompt luminescence between each stone, this is repeat spectra of Sample 3: Figure 6.1 (top), nitrogen containing sample: Figure 6.4 (middle) and the high purity sample: Figure 6.8 (bottom) shown together for ease of comparison. All three samples are overall quite different in shape; however, NV^0 can be seen in both Sample 3 and the nitrogen containing stone, a peak at 460 nm can be seen in both Sample 3 and the high purity stone.

and higher temperature emissions being less intense. Unlike the other two stones, the nitrogen containing stone does not have a broadband feature.

There is a peak at 460 nm in both Sample 3 and the high purity stone, this can be seen at all temperatures in the high purity stone but only at cold temperatures in Sample 3 although the feature is much more defined in Sample 3. This peak is not apparent in the nitrogen containing stone.

Sample 3 and the nitrogen containing stone both contain the NV^0 centre at 575 nm. This is visible in all temperatures in both stones, the feature is far more prominent at all temperatures in the nitrogen containing stone. There is no NV^0 present in the high purity sample.

6.7 Comparison of Delayed Luminescence

All three stones share a similar blue broadband luminescence feature from 77 - 150 K, the overall broadbands are not centred at the same wavelength to each other, however, the intensity of the broadbands and the way in which the broadband falls off around 460-500 nm is very similar in each. At high temperatures the stone's luminescence differs greatly from each other. With the nitrogen containing stone being dominated by red luminescence, from the NV^0 zero phonon line and its vibronic sideband. Sample 3 is dominated by a large broadband at 350 K due to boron, however, at intermediate-high temperatures other peaks appear. Specifically at 250 K a split broadband can be seen made up of two broadbands, one centred at 440 nm and the other at 465 nm, both of these broadbands can be seen independently at other temperatures. There is no high temperature data for the high purity stone as the stone did not exhibit delayed luminescence at temperatures above 210 K. There was a similarity observed between which temperatures have the most prominent features with the cold temperatures being more prominent in every stone, moving down sequentially to the warmer temperatures, the only exception being 350 K in Sample 3 which dominates the spectrum and is thought to be due to boron within the stone.

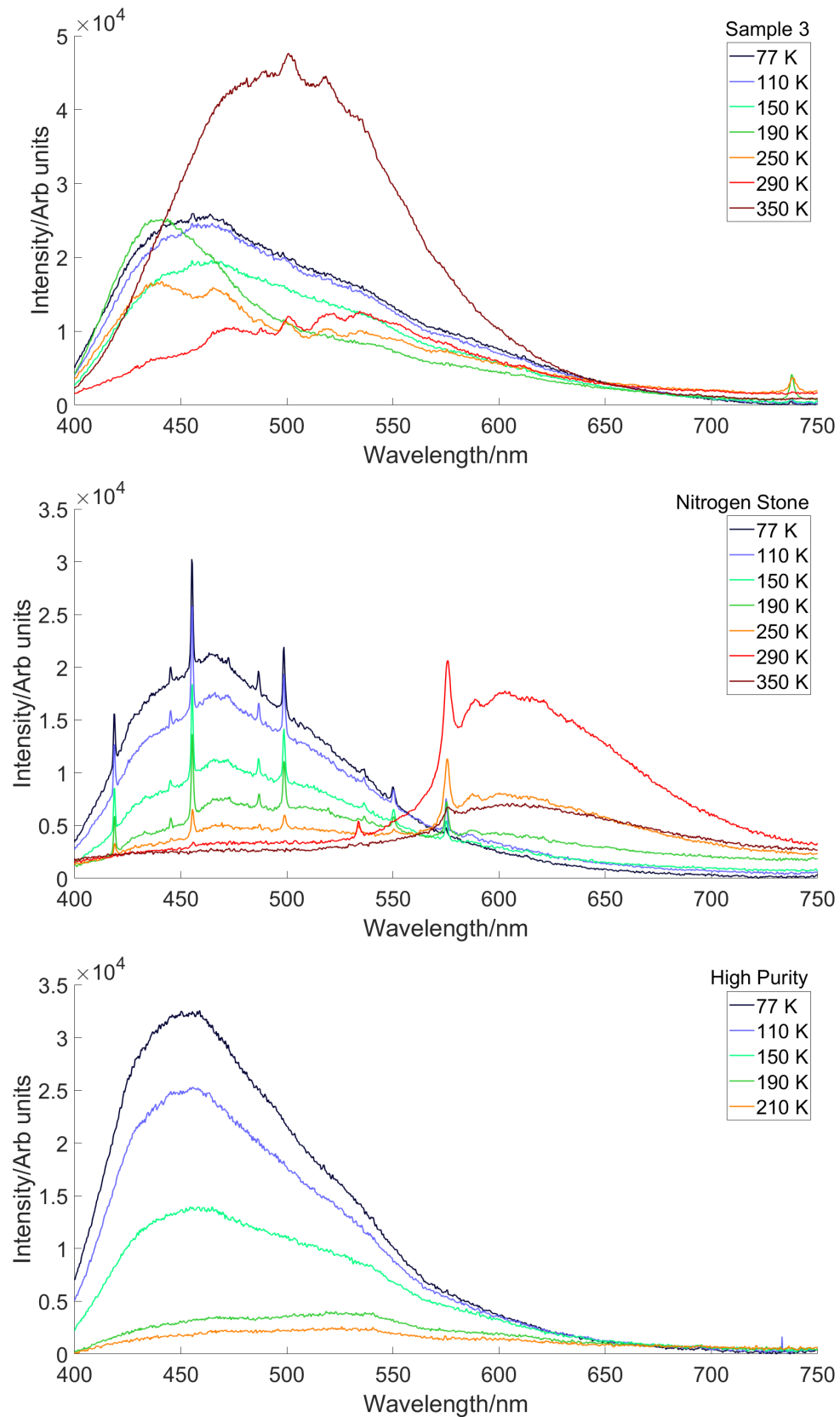


FIGURE 6.12: Spectral data for comparison of delayed luminescence between each stone, this is repeat spectra of Sample 3: Figure 6.2 (top), nitrogen containing sample: Figure 6.5 (middle) and the high purity sample: Figure 6.9 (bottom) shown together for ease of comparison. All three stones have a similar blue broadband feature from 77-150 K. The graphs differed a lot from each other at mid-high temperatures. No high temperature data was recorded for the high purity stone as it did not exhibit delayed luminescence at high temperatures.

6.8 Sample 3: Intensity vs Temperature

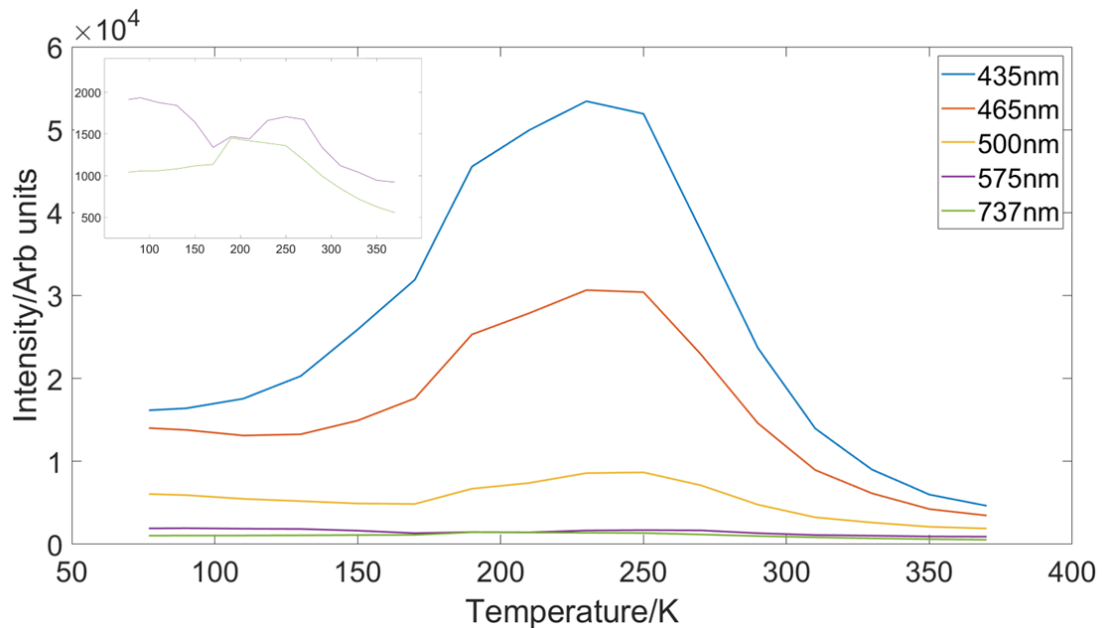


FIGURE 6.13: Spectra showing the prompt luminescence intensity vs temperature for a number of different wavelengths for Sample 3. The 435 nm, 465 nm, 500 nm and 737 nm wavelengths all share a similar profile, while 575 nm does not. Both the 575 nm and 737 nm profile can be seen more closely in the top left hand corner of the graph.

A range of wavelengths were chosen for further study based on peaks of interest seen in the previous luminescence results. These wavelengths were 435 nm, 465 nm, 500 nm, 575 nm and 737 nm. The wavelengths were chosen as areas of interest primarily from Sample 3 in order to learn more about the 499 nm feature, all five of these peaks are seen within the prompt, delayed or both luminescence spectra. The same regions in the other two stones were explored as comparisons, the nitrogen containing stone was chosen in order to look for similarities as nitrogen is thought to be involved in the characterisation of the 499 nm feature and the high purity stone was chosen to try and isolate the differences seen from as close to intrinsic diamond as possible.

The luminescence was recorded for each stone (the luminescence data already discussed in this chapter) at 20 °C temperature steps on both prompt and delayed timescales, the wavelengths of interest were then isolated in order to compare the intensity of the wavelength at each temperature. The intensity plotted was the average intensity at the wavelength of interest +/- 2 nm.

The results collected from the prompt luminescence can be seen in Figure 6.13. As the temperature was increased from 77 K, the 435 nm feature became more prominent reaching peak amplitude at 230 K at which point the amplitudes began to diminish with temperature and at a faster rate than was seen in the initial increase. The lowest

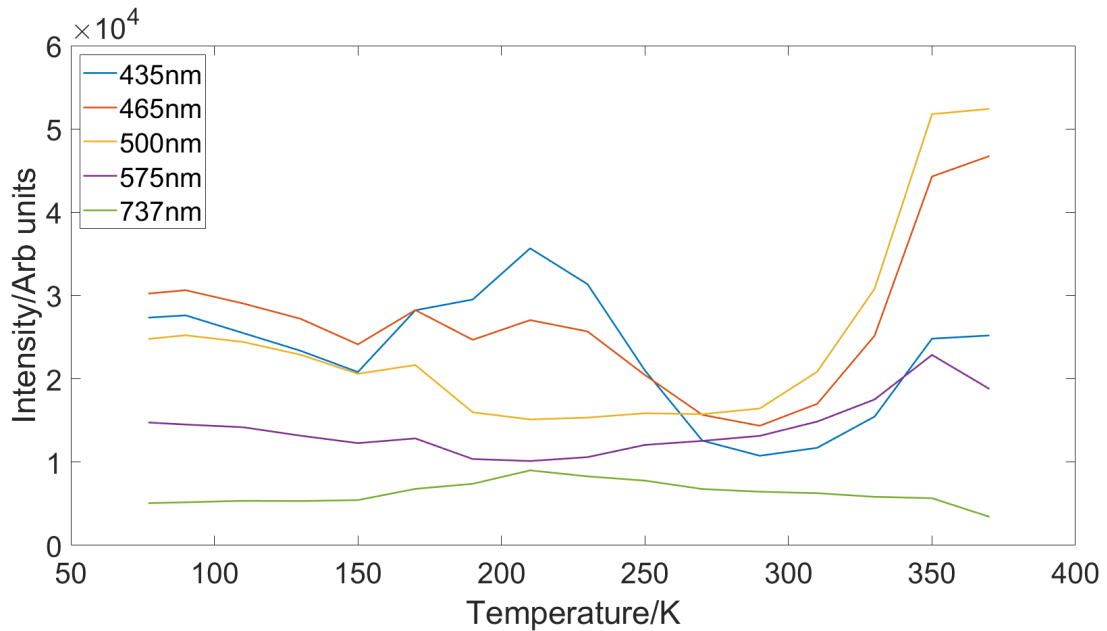


FIGURE 6.14: Spectra showing the delayed luminescence intensity vs temperature for a number of different wavelengths for Sample 3. The 435 nm and 465 nm followed a similar profile to each other, the 500 nm and 575 nm wavelengths followed a similar profile to each other and the 737 nm wavelength did not follow a similar profile to any of the other wavelengths.

intensity was measured at 370 K. The intensities observed at the highest temperatures were lower than those observed at lowest temperatures. The 465 nm feature followed a similar trend with the exception of a small drop in wavelength at 110 K, before going on to peak at 230 K and falling to its lowest point at 370 K in line with the 435 nm feature. Once again, the 500 nm feature followed a similar trend to the previous features. However, initially the intensity of the feature dropped very steadily from 77 K to 190 K before rising to its highest intensity at 250 K and then once again dropping off to its lowest intensity at 370K. The intensity of both the 575 nm feature (NV^0) and the 737 nm feature (SiV^-) are significantly lower overall than the lower wavelengths studied. The highest observed intensity of the NV^0 is at 77 K, it decreases until 170 K before rising and falling with a maxima at 250 K: this profile differs the most but still has similarities with the others. However, the intensity of the maxima does not exceed those seen at lower temperatures. Finally, the SiV^- centre once again follows a similar trend to that seen at lower wavelengths, with the intensity initially rising from 77 k to its peak at 190 K, before decreasing in intensity and reaching its lowest point at 370 K.

The results collected from the delayed luminescence can be seen in Figure 6.14. The 435 nm results consist of two troughs either side of a peak. As the temperature was increased from 77 K, the intensity of the 435 nm feature decreased until 150 K before increasing to a peak at 210 K, then falling rapidly to 290 K and once again rising until 350 K. Overall, the feature is most prominent at 210 K and least prominent at 290 K.

The 465 nm feature has the same overall profile as the 435 nm feature. However, the relative intensities of the peak and troughs differ. The intensity falls from 77 K to 150 K before rising to a maxima at 170 K. However, unlike with the 435 nm feature, the maxima is lower in intensity than the initial intensity at 77 K. The intensity then drops once again until 290 K followed by an increase in intensity to 370 K, which unlike the 435 nm feature, is the highest observed intensity. The 500 nm feature has a different profile from the lower wavelength features until 290 K. The overall intensity gradually falls from 77 K to 290 K before rising sharply to its highest intensity at 370 K in the same way as the 465 nm feature and to some degree the 435 nm did. The NV^0 centre at 575 nm followed a similar profile to that seen in the 500 nm feature, with a fall in intensity from 77 K to 190 K before steadily rising to its peak at 350 K. The intensity observed at high temperatures was much lower for the NV^0 centre than for the 500 nm featured. The SiV^- centre at 737 nm follows a different trend to the other wavelengths, gradually rising in intensity from 77 K to 210 K before steadily dropping in intensity to its lowest point at 370 K.

The data taken from the prompt luminescence and the delayed luminescence for each wavelength look quite different on first appearance. However, there is a number of similarities between them with the 435 nm feature and 465 nm feature sharing a similar profile on both timescales, but with the profile being shifted to lower temperatures in the delayed luminescence. A similar overall profile is seen from 77 K to 370 K in the prompt luminescence and from 77 K to 300 K in the delayed luminescence, after which a sharp rise in intensity is seen in the delayed luminescence; it is unknown whether a similar increase would be observed in prompt luminescence if the temperature could have been increased further. It was not possible for the temperature to be increased further at this time due to the melting point of the indium used to mount the sample in the experimental set up. The SiV^0 centre at 737 nm shares a very similar trend in both the prompt and delayed luminescence.

6.9 NV sample: Intensity vs Temperature

The results collected from the prompt luminescence can be seen in Figure 6.15, as well as a zoomed in version shown in Figure 6.16. It is clear that the 575 nm wavelength dominates this stone at all temperatures; this is expected as the stone was doped with nitrogen during growth hence the formation of NV^0 centres. The centre is most prominent at 190 K and least prominent at 350 K. The 435 nm, 465 nm and 500 nm features all have very similar profiles and amplitudes as each other. At all three wavelengths, a decrease in intensity occurs from 77 K to 150 K before a sudden rise peaking at 210 K,

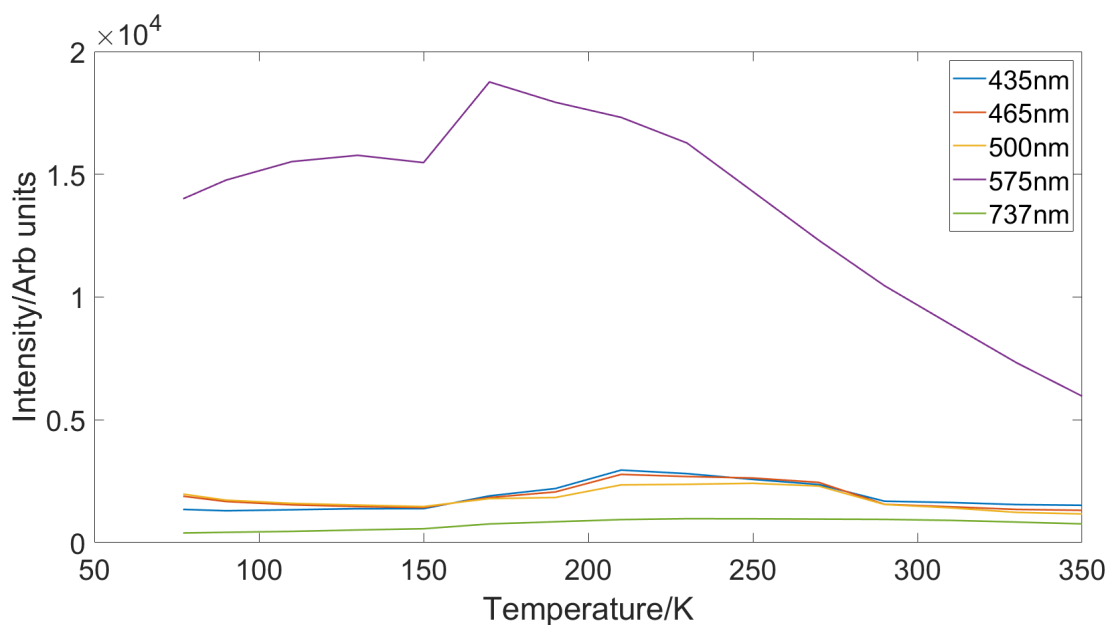


FIGURE 6.15: Spectra showing the prompt luminescence intensity vs temperature for a number of different wavelengths for the nitrogen containing sample. The 575 nm wavelength dominates the spectra at all temperatures.

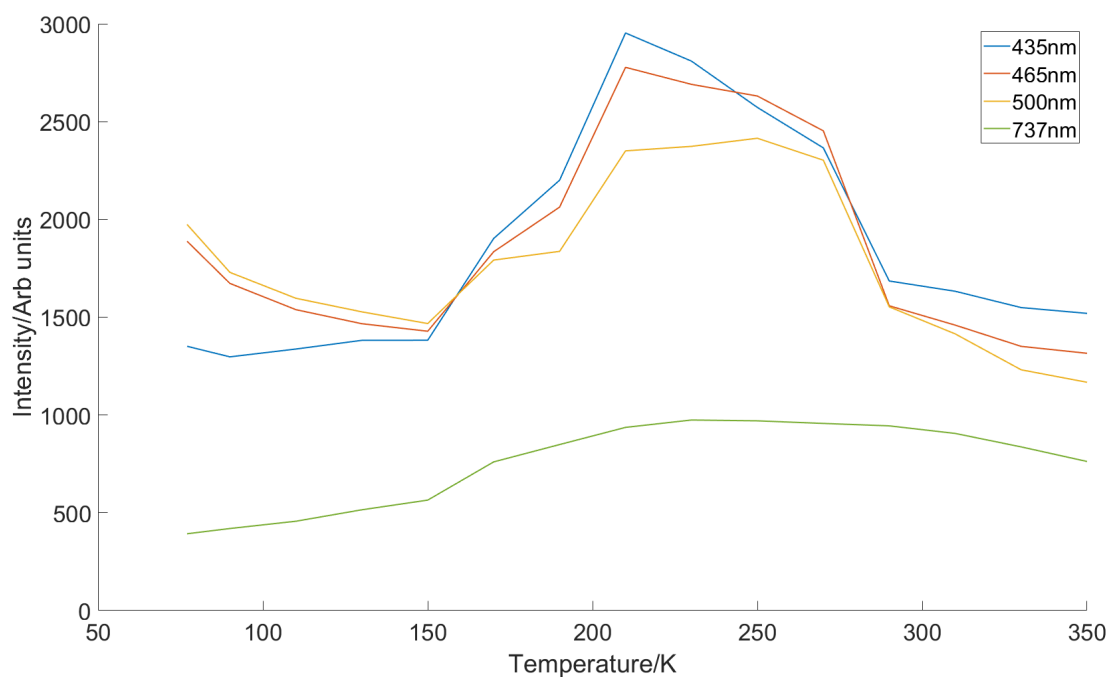


FIGURE 6.16: Zoomed in version of Figure 6.15 showing the prompt luminescence intensity vs temperature for a number of different wavelengths for the nitrogen containing sample. The 435 nm, 465 nm and 500 nm wavelengths all share a very similar profile while the 737 nm does not follow the same profile as any of the other wavelengths.

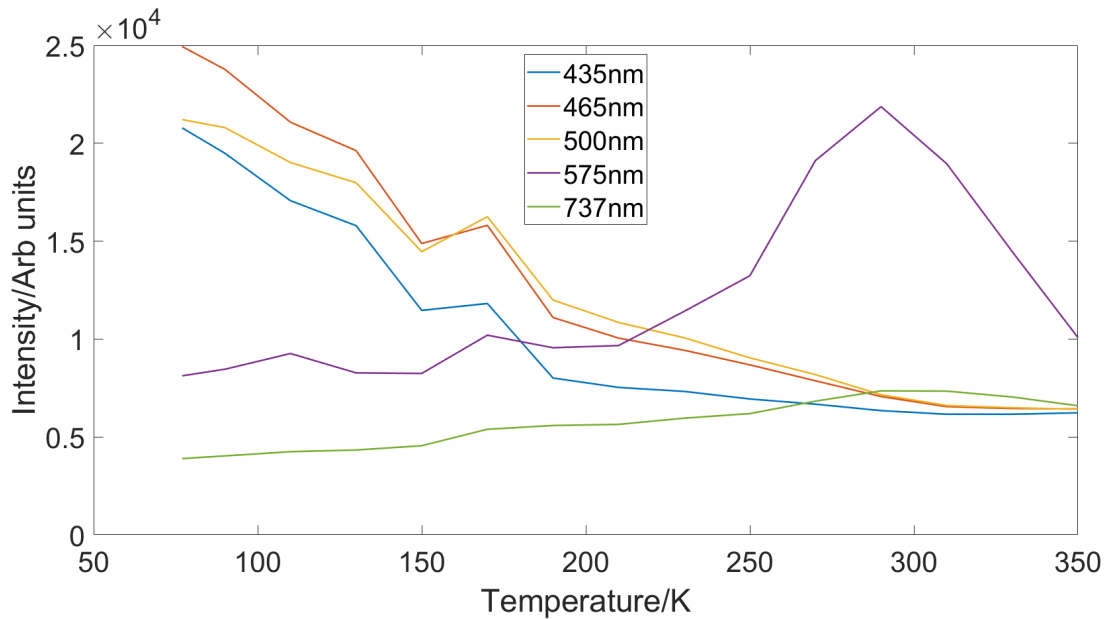


FIGURE 6.17: Spectra showing the delayed luminescence intensity vs temperature for a number of different wavelengths for the nitrogen containing sample. The 435 nm, 465 nm and 500 nm wavelengths all share a similar profile, the 575 nm wavelength and the 737 nm wavelength do not share a similar profile to each other or any of the lower wavelengths.

followed by drop at 290 K continuing to decrease gradually to the lowest point at 350 K. The intensity at 737 nm is very low as this stone had not been doped with silicon vacancy and, therefore, any silicon in the stone would be negligible meaning the 737 nm present in this data is more likely to be part of the tail of the NV^0 centre's vibronic band.

The results collected from the delayed luminescence can be seen in Figure 6.17. On delayed timescales, a clear shift can be seen between the hot and cold temperatures; the hotter regions (temperatures over 230 K) are dominated by the NV^0 centre with all other wavelengths flatlining around this region. As the NV^0 centre is much reduced at lower temperatures, this suggests that there could be a thermally activated step required in the mechanism to produce this luminescence on delayed timescales. The 435 nm, 465 nm and 500 nm features all share a very similar profile to each other, with the overall trend being a decrease in intensity from 77 K all the way to 350 K with the exception of a small rise in intensity at 170 K at all three wavelengths. Once again, a small peak is seen at 737 nm throughout this is thought to be due to the broadband from the NV^0 centre's vibronic band.

The results collected from both the prompt and delayed luminescence are not, overall, very similar. The main similarity is the prominence of the NV^0 centre at 575 nm on both the prompt and delayed luminescence. However, in the prompt luminescence this

centre dominates the whole temperature region where-as on delayed timescales, it only dominates from 230 K up to 350 K. On both prompt and delayed timescales the features at 435 nm, 465 nm and 500 nm all share the same profile as each other; however, these profiles are different from each other.

6.10 High purity sample: Intensity vs Temperature

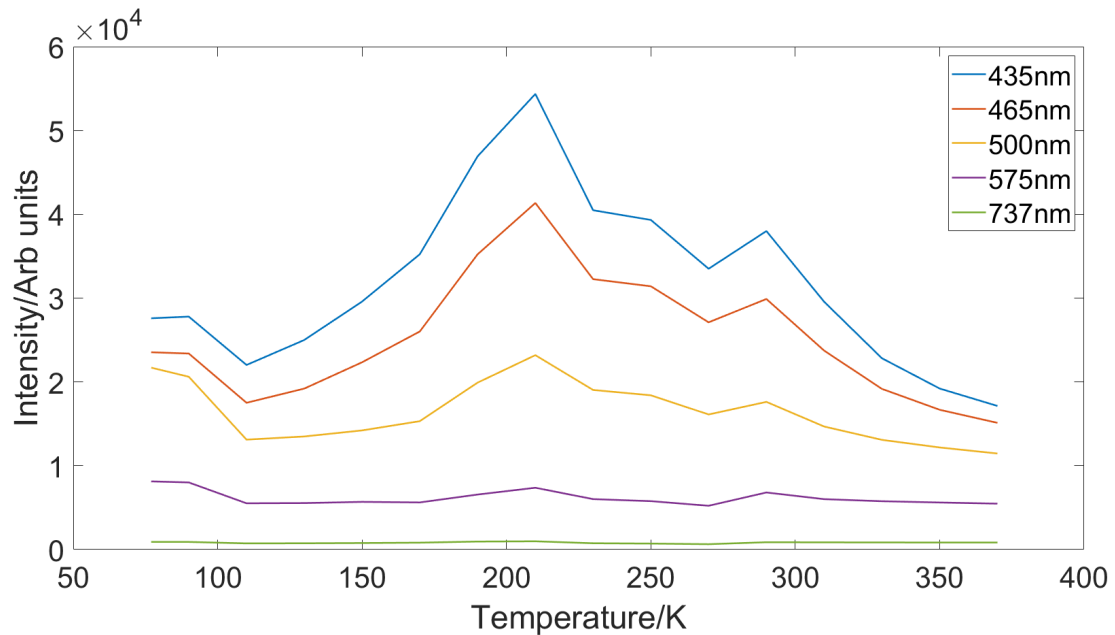


FIGURE 6.18: Spectra showing the prompt luminescence intensity vs temperature for a number of different wavelengths for the high purity sample. All the wavelengths share the same profile.

The results collected from the prompt luminescence can be seen in Figure 6.18. All the wavelengths sampled in the prompt luminescence of the high purity sample share the same profile as each other including the SiV^- centre which, although it is hard to see from the graph due to its low intensity, also shares a very similar profile to the other wavelengths. As this stone has been grown to be as close to intrinsic diamond as possible all of the wavelengths sampled, with the exception of the silicon vacancy centre, would be sampled from the same broadband and therefore would be expected to have similar profiles. This profile involves an initial drop in intensity from 77 K to 110 K, an increase in intensity to the peak intensity at 210 K, a second drop in intensity to 270 K, a further increase in intensity to a maxima at 300 K, finally followed by a drop in intensity to the lowest intensity at 370 K.

The results collected from the delayed luminescence can be seen in Figure 6.19. The 435 nm, 465 nm and 500 nm features all share a very similar profile, with a gradual

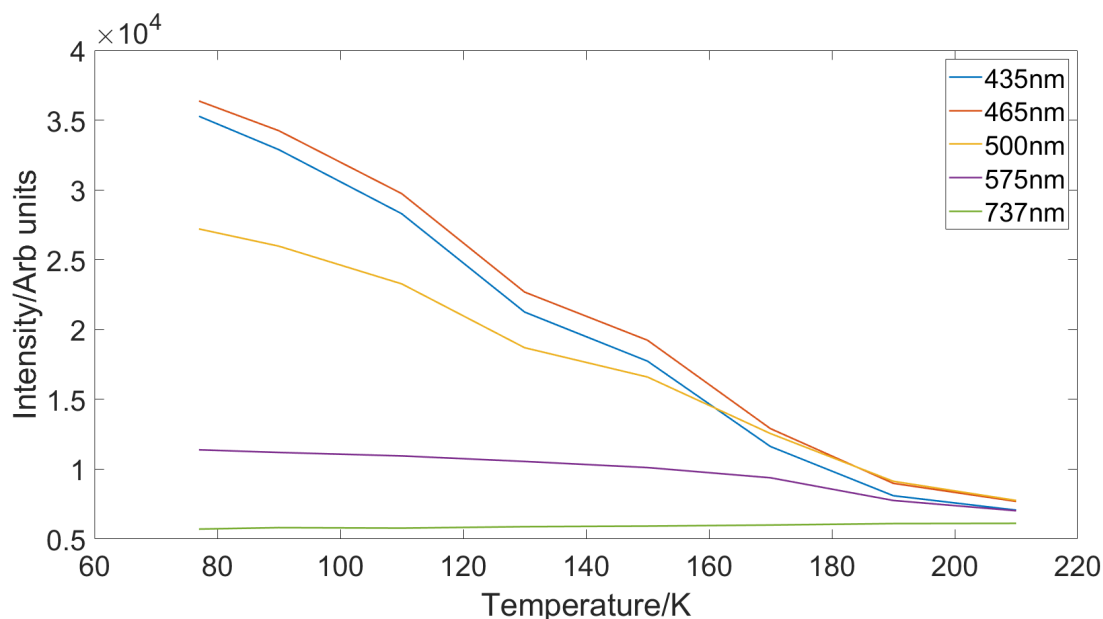


FIGURE 6.19: Spectra showing the delayed luminescence intensity vs temperature for a number of different wavelengths for the high purity sample. The 435 nm, 465 nm, 500 nm and 575 nm wavelengths all share a similar profile, the 737 nm wavelength does not share a similar profile with any of the wavelengths.

decrease in intensity from 77 K to 210 K; there are small troughs within this overall decline at 130 K (shared by all three wavelengths) and 170 K (shared by 435 nm and 465 nm). Although not as obvious on the graph, the 575 nm wavelength also shares a very similar profile to the lower wavelengths but with a much smaller overall intensity. The 737 nm wavelength, however, does not share the same trend and actually increases in wavelength from 77 K to 210 K.

Overall, the results taken from the prompt and delayed luminescence do not show many similarities; the prompt luminescence exhibited peak intensities in the mid temperature range and the delayed luminescence intensity decreased in line with temperature. The overall prominence (amplitude) of each wavelength follows the same order on both prompt and delayed timescales, with the exception of the 435 nm and 465 nm wavelengths, with the 435 nm being the most prominent on prompt timescales and the 465 nm being most prominent on delayed timescales.

6.11 Comparison of defect features in samples

Figure 6.20 shows a comparison of the effect temperature has on the prompt luminescence of certain wavelengths within the three diamond samples. The Figure is made up of a repeat of figure 6.1, 6.4 and 6.8 for ease of comparison. The nitrogen containing stone is dominated by the NV^0 centre at 575 nm, dwarfing the other wavelength features

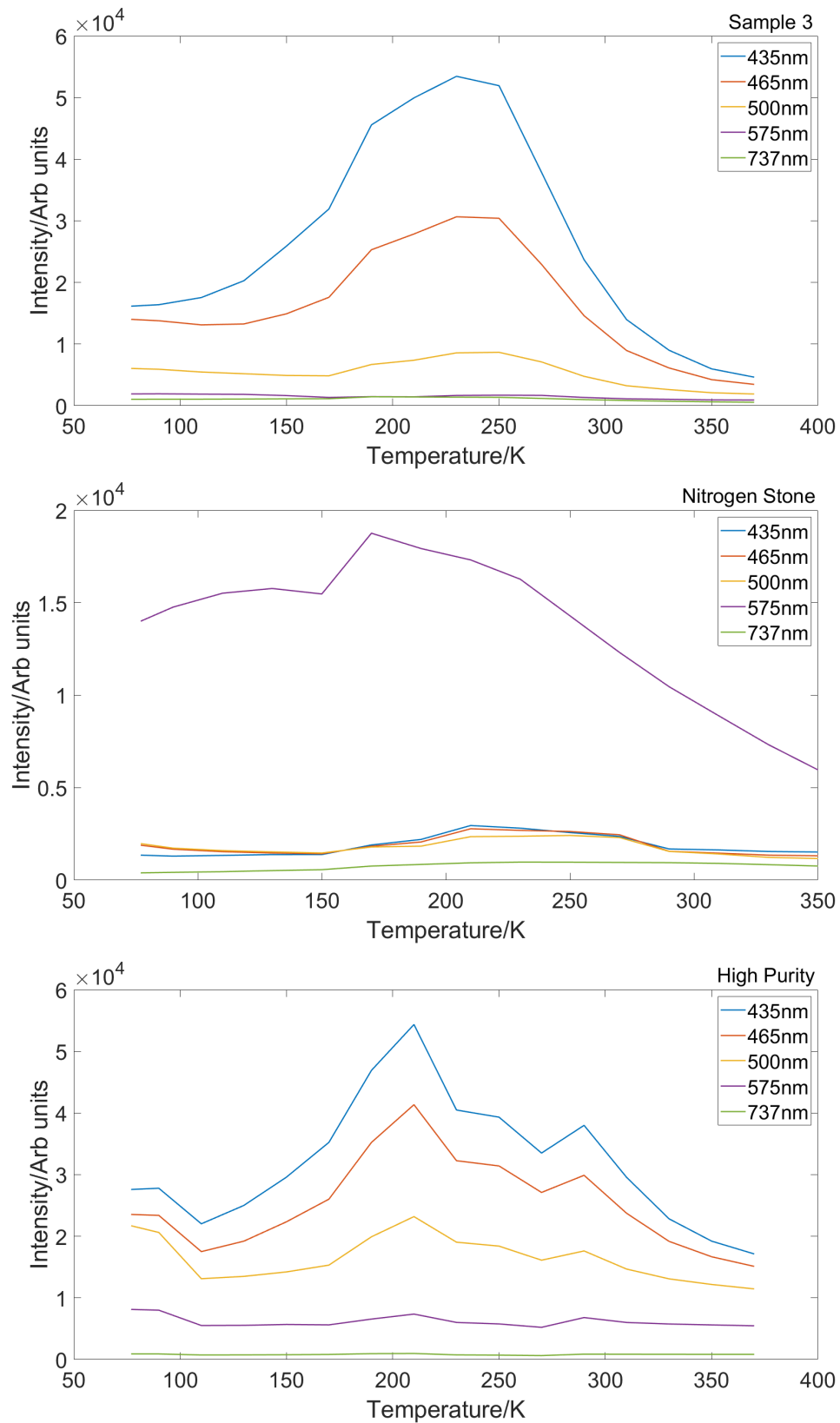


FIGURE 6.20: Comparison of the temperature dependence of the prompt luminescence between each stone, this is repeat spectra of sample 3: Figure 6.13 (top), nitrogen containing sample: Figure 6.15 (middle) and the high purity sample: Figure 6.18 (bottom) shown together for ease of comparison.

at all temperatures. However, if the 575 nm feature in the nitrogen containing stone is excluded, all the stones exhibit similar profiles. All stones show the strongest intensities for each wavelength between 170 K to 290 K. Sample 3 and the nitrogen containing stone exhibit a smooth peak between these temperatures, whereas the high purity stone has a number of peaks and troughs within this high intensity region. Within each stone, the same profile is seen for each wavelength but with varying amplitudes; the only exception to this is the NV^0 centre in the nitrogen containing stone. Additionally, all stones follow the same pattern in terms of the amplitude of the specific wavelengths studied, with the 435 nm feature being the most prominent and the 737 nm feature being the least prominent (excluding the NV^0 centre in the nitrogen containing stone).

Figure 6.21 shows a comparison of the effect of temperature on the delayed luminescence of certain wavelengths within the three diamond samples. The figure is made up of a repeat of Figures 6.2, 6.5 and 6.9 for ease of comparison. On first inspection, there does not appear to be much correlation between the samples on delayed timescales. However, as with the prompt timescales, if the dominant 575 nm feature is excluded from the nitrogen containing stone, the nitrogen and high purity stone share a very similar overall profile. It is important to note that the delayed luminescence for the high purity stone was only recorded up to 210 K as no delayed luminescence was recorded at temperatures above this. With this in mind the profile of the nitrogen stone matches very closely with the high purity stone up to these temperatures. There are no apparent similarities between the delayed luminescence in Sample 3 and the delayed luminescence of the other two stones.

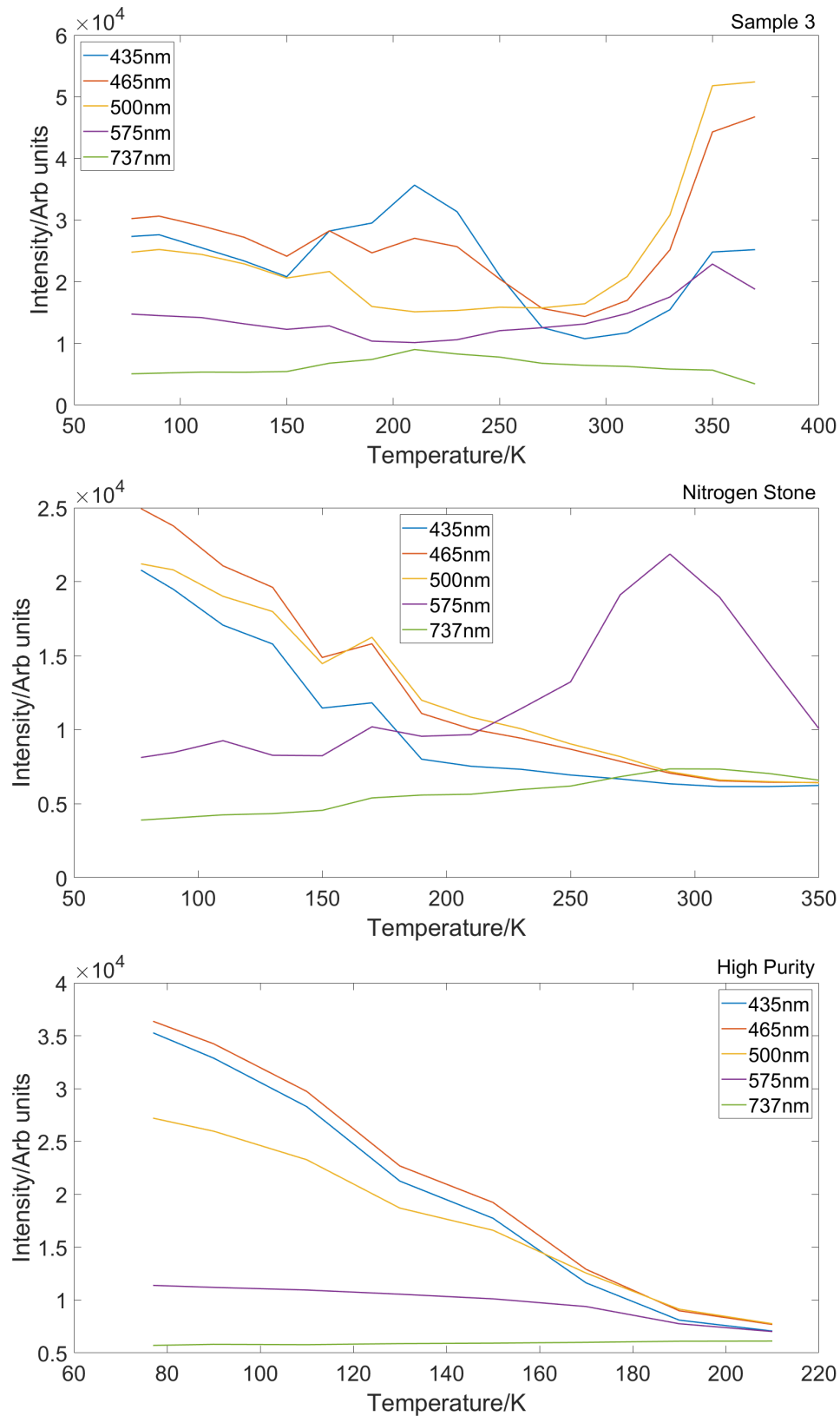


FIGURE 6.21: Comparison of the temperature dependence of the delayed luminescence between each stone, this is repeat spectra of sample 3: Figure 6.14 (top), nitrogen containing sample: Figure 6.17 (middle) and the high purity sample: Figure 6.19 (bottom) shown together for ease of comparison.

6.12 Sample 3: Lifetime studies

Temperature dependent time decay traces were recorded for Sample 3. These traces were taken at 450 nm and 510 nm; these wavelengths were chosen as 450 nm falls within the blue broadbands seen at colder temperatures in the sample's delayed luminescence and 510 nm falls within the vibronic side band of the 499 nm feature. A sample decay taken at both 450 nm and 510 nm can be seen in Figure 6.25.

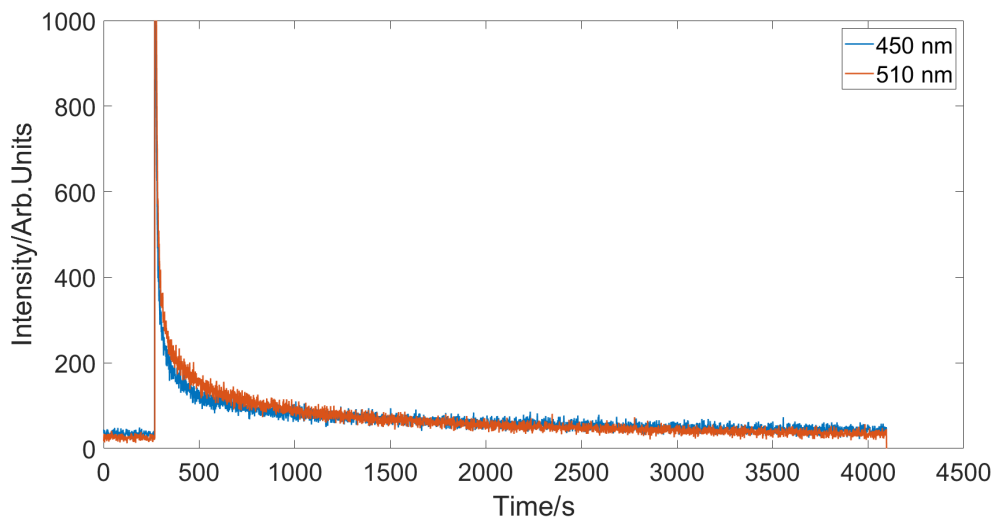


FIGURE 6.22: Spectra showing the decay traces seen for both the 450 nm and 510 nm spectral line at 290 K.

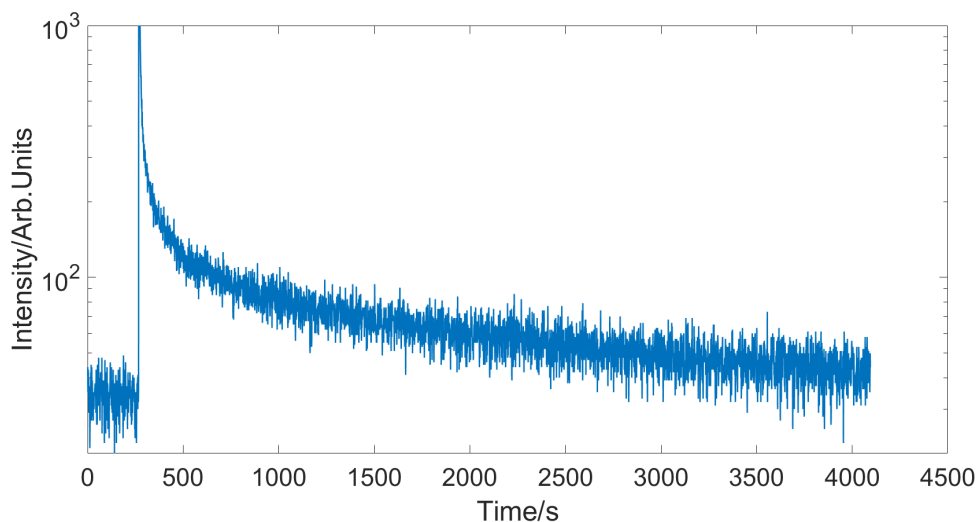


FIGURE 6.23: Spectral data of the decay trace taken at 290 K for the 450 nm line plotted on a log scale. If the spectral data was exponential you would expect a linear line once plotted on a log scale, this is not seen here.

The decay was not exponential as shown in Figure 6.23 with the log plot resulting in a non-linear trend, therefore the decay rate is not proportional to the population. This

suggests that the population dynamics are more complex, for example other defects could be feeding the upper level at different rates. Figure 6.23 shows that initially the decay rate decreases until ~ 750 s after which the trend is more linear suggesting the decay rate stabilises. The change in trend of the decay could be due to a decay channel being switched off.

In order to fit these graphs, three exponentials had to be used; this allowed for the time component to be taken from each and averaged together in order to give a quantitative value that could be used for comparing the data set and temperatures. Although the average decay time does not give us any insight into the lifetime of the features, it does allow for comparisons to be drawn from within the data. Figure 6.24 shows an example fit of the 450 nm decay time using the three exponentials, in this case the average decay time was found to be 1.58 s.

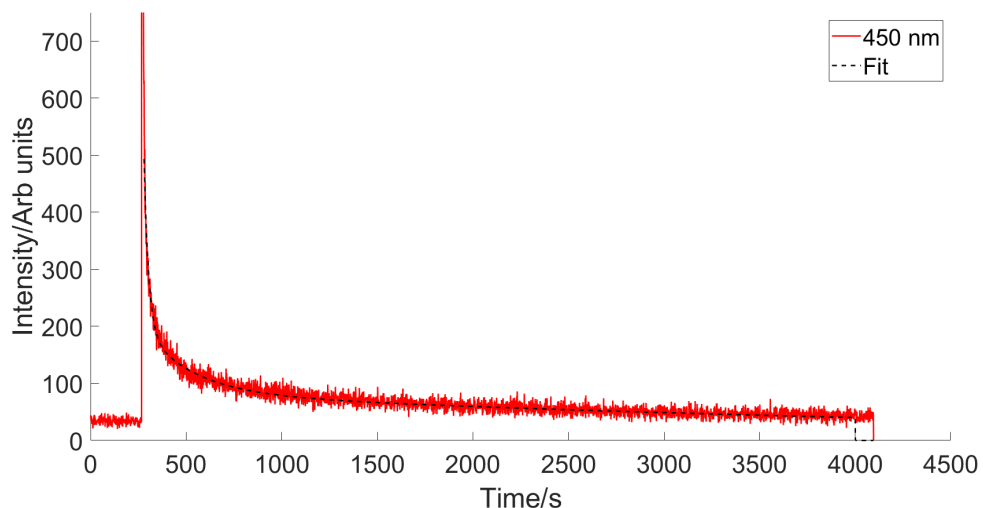


FIGURE 6.24: Spectral data showing an example fit for the 450 nm time decay. The fit is made up of three exponentials.

The average decay time was calculated for both wavelengths at a temperature range from 77 K to 370 K, the results of this can be seen in Figure 6.25. The average decay time for both wavelengths shares the same overall trend with temperature. The general trend sees an increase in average decay time from 77 K to a maxima around 110 K followed by a drop to the lowest minima at 190 K before rising to the peak at 270 K (for the 450 nm wavelength) and 290 K (for the 510 nm wavelength) followed by another rapid fall until reaching a minima at 370 K. The 450 nm wavelength has predominantly higher average decay times than the 510 nm wavelength particularly at mid-high temperatures. The average decay times for both the 450 nm wavelength and 510 nm wavelength tend towards each other at both 190 K and 370 K.

It was intended that the decay traces be recorded for all three stones at 435 nm, 465 nm, 500 nm, 575 nm and 737 nm, the wavelengths of interest studied in the rest of this chapter, in order to compare how the intensity of the wavelength changed with temperature in comparison with one another. Unfortunately, this was not able to be carried out at this time so this is proposed as future work.

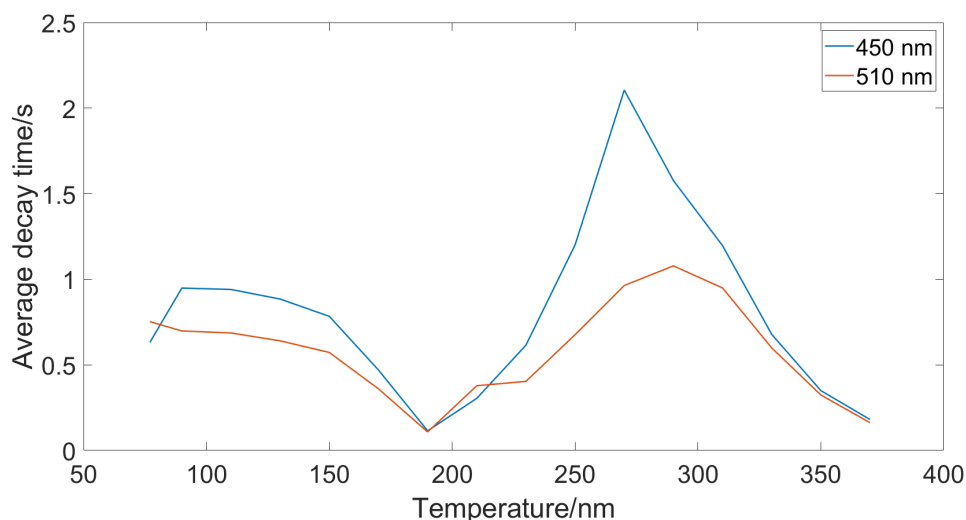


FIGURE 6.25: Spectra showing the effect of temperature on the average decay time of wavelengths at 450 nm and 510 nm. Both wavelengths share a similar trend in average decay time in response to temperature, with the lowest overall lifetime of both wavelengths being at 190 K and the highest average decay time being seen around 270 -290 K.

6.13 Discussion

One of the most interesting features observed during the temperature dependence study was a split broadband seen in the delayed luminescence of Sample 3 at 250 K, Figure 6.26 shows a repeat of this spectra for ease of the reader. This feature appears to be made up of two connected broadbands, one centred at 440 nm and the other at 465 nm, the energies of both the broadbands were calculated to be ~ 2.82 eV and ~ 2.67 eV, respectively, with a combined energy of ~ 5.48 eV. The band gap of diamond is reported as being between 5.47 eV and 5.5 eV [93, 94], due to their combined energies being ~ 5.48 eV, it is hypothesised that these two broadbands are potentially evidence for a new level within the electronic structure of the diamond. Figure 6.27 shows the two possible configurations for this level, the blue emission is 460 nm, the red emission is 440 nm and the green emission is 500 nm, their respective energies are shown on the figure. It is also proposed that this level could, in fact, be a level that is involved in filling the band that emits the 499 nm feature, also shown in Figure 6.27. If the 499 nm feature is involved with this level it is thought that the structure proposed on the

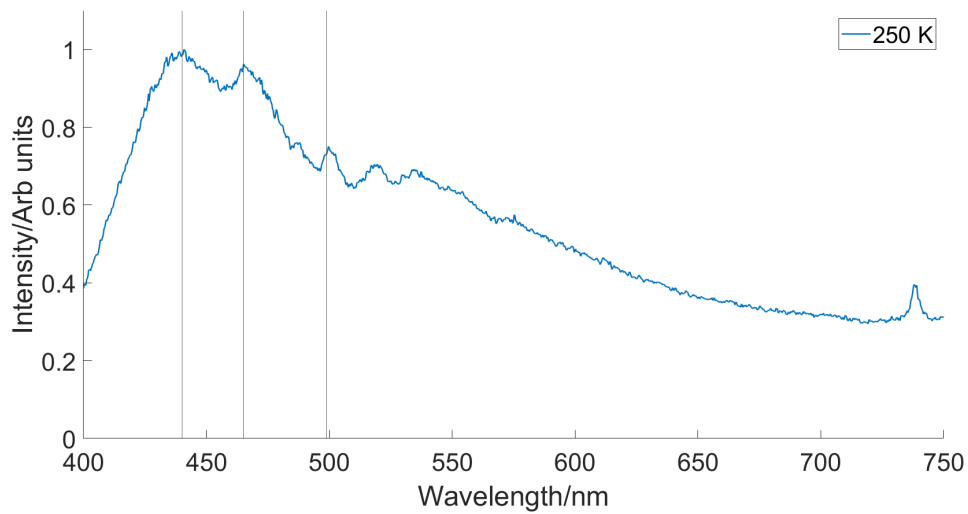


FIGURE 6.26: Repeat spectral data of delayed luminescence data for Sample 3 taken at 250 K, showing the split broadband at 440 nm and 465 nm and the 499 nm feature all marked with a black line.

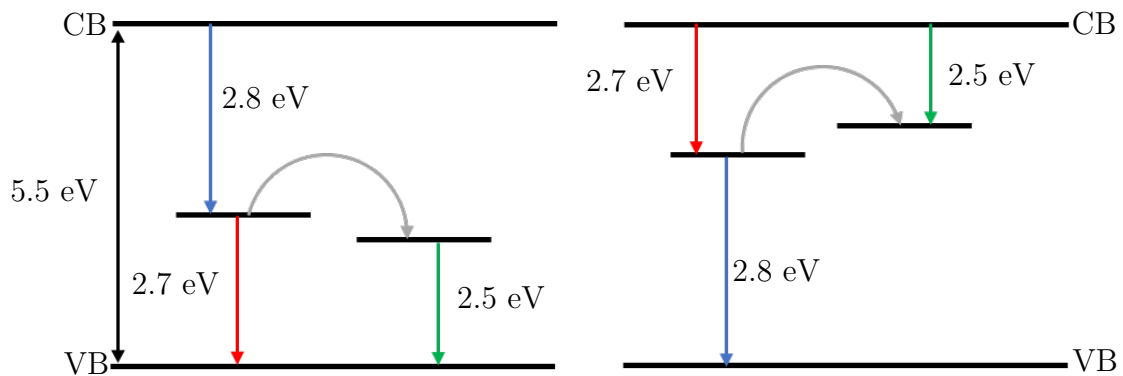


FIGURE 6.27: Schematic diagram of a proposed band structure for new defect level between the conduction band and valence band. Where the blue emission is from the 460 nm peak, the red is from the 440 nm peak and the green is from the 499 nm peak.

LHS of Figure 6.27 would be the most likely candidate as the 499 nm emission is a sharp emission usually meaning it is a level-band transition rather than a band to level transition, as shown on the RHS. There is not enough evidence to conclusively prove the level structure. However, it is hypothesised that a previously undiscovered defect level exists in these diamond samples, which could have one of two possible positions relative to the valence and conduction bands.

As discussed in Chapter 5, the 499 nm feature was originally seen on delayed timescales taken at room temperature. However, the temperature dependence studies carried out have shown that the 499 nm feature can, in fact, also be seen in the prompt luminescence at certain temperatures. The 499 nm feature is seen in delayed luminescence at temperatures above 250 K (the same temperature at which the split broadband was first

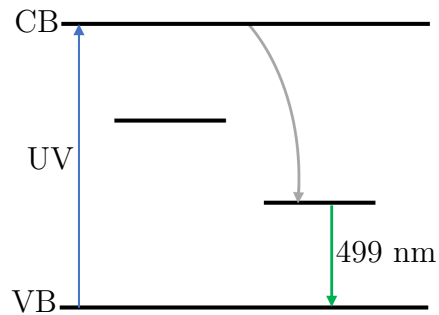


FIGURE 6.28: Schematic diagram of a proposed band structure allowing for the emission of the 499 nm feature on prompt timescales. Where the blue arrow represents the UV excitaton, grey arrow represents either phonons or potentially photons in the IR region and the green arrow the 499 nm emission.

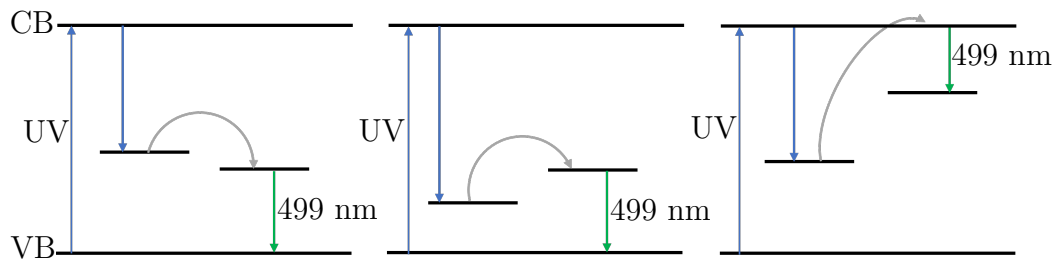


FIGURE 6.29: Schematic diagram of a proposed band structures allowing for the emission of the 499 nm feature on delayed timescales. Where the blue arrows represent the UV excitation and intial emission from the CB, grey arrows represent the presence of phonons and the green arrows represent the 499 nm emission.

recorded) and on prompt luminescence in temperatures below 110 K. The 499 nm feature has only been observed on shorter timeframes at lower temperatures (below 110 K), however, it is thought that the 499 nm feature always exists in the prompt luminescence it is just masked by another defect emission, such as the strong blue emission seen in the prompt luminescence of Sample 3. The strong blue emission is thought to be switched off at lower temperatures allowing for the 499 nm emission to be observed. Figure 6.28 suggests a mechanism for the production of the 499 nm emission in the prompt luminescence. It is thought that once the electrons have been excited by the UV light into the conduction band that either phonons or an IR photon (IR being a wavelength we couldn't investigate) could allow the electrons to fall into the 499 nm level. Once in the 499 nm level the electrons can fall straight back to the valence band allowing for 499 nm emission on fast timescales. Figure 6.29 shows some potential mechanisms for the delayed 499 nm emission seen at higher temperatures, these are much like those shown in Figure 6.27, however, show all three trap levels that we believe could occur without the specific levels hypothesised from the split broadband. The slower timescales of this emission shows the 499 nm level must be pumped from elsewhere. As shown in Figure 6.29 the UV excitation fills unknown levels and in each example the electrons become trapped in these levels. At low temperatures these electrons would remain trapped, however, at higher temperatures phonons can scatter electrons into the 499 nm level in

a thermally activated step. Therefore, once the 499 nm level has been pumped the 499 nm emission itself would be fast, however, the slower time frames occur due to the extra thermally activated step needed. Meaning overall the 499 nm emission could not occur at lower temperatures.

Observations of a defect at 460 nm were seen in all temperatures of the high purity samples prompt luminescence spectra, a feature at 460 nm was also seen at cold temperatures in Sample 3. This may also prove to be an interesting feature for further investigation as very little is currently known about it in literature.

6.14 Conclusion

Temperature dependent investigations were carried out on three CVD synthetic gemstones, with the aim of learning more about the luminescence characteristics of the stones and the electronic structures that could be causing this luminescence. The more that can be learned about the physical origin of luminescent features in diamond the more useful the features can become; whether it is for use as an identifier between synthetic and natural diamond or allowing for the growth conditions to be determined so specific defects can be grown into the diamond in order to exploit their properties. This work allowed for the luminescence of the three synthetic gemstones to be compared and contrasted, to identify similarities and differences between the stones. The 499 nm feature was seen in sample 3 but did not exist in the other two stones. Until now, it was thought that the 499 nm feature was only seen on delayed timescales; however, the 499 nm spectral line has now been recorded on prompt timescales at low temperatures. An undiscovered defect level was hypothesised that may be involved in the mechanism for the 499 nm emission. Further experimentation into this hypothesis was planned using a bespoke instrument that was designed and calibrated but unfortunately not used due to lab closures for COVID-19. It was intended that a range of samples containing the 499 nm defect be investigated to look for the presence of this undiscovered defect in order to confirm a link between the two, it is therefore left as future work.

Chapter 7

Conclusion and Future Work

7.1 Conclusion

The overall aim of this PhD thesis was to explore a new interrogation method to learn more about diamond defects and their origins, with special attention paid to a defect observed optically in diamond at 499.6 nm.

As synthetic diamond gemstones' quality is ever increasing, the task of diamond screening is becoming much more challenging. Given that it is becoming common practice for less experienced diamond appraisers to carry out this task, it is important there are less complex and time-consuming techniques that can be used to identify the origin of diamonds. There is considerable interest in research into defects found within the diamond lattice. These defects have significant impact on both the overall look and physical properties of the diamond. This interest comes not only from the scientific community, but also from industrial companies, mining companies and jewellers alike, each with a different interest in what effect the defect has on the diamond: all are of significant interest. With increasing quantities of synthetic diamonds finding their way onto the gem market, it has become more important than ever that synthetic, or treated, diamonds can be identified from natural stones. The more advanced the synthesis process of diamond becomes, the more important it is that investigation techniques continue to improve to allow for true identification of diamond samples. Research into optical properties of diamond has been carried out for well over half a century and it has now become clear that this fundamental research underpins the work carried out into diamond classification.

To gain greater understanding of the nature of colour centres in diamond, an imaging investigation technique was constructed, in the form of an imaging rig. The imaging

rig allows for information to be gathered into specific defects as well as providing a user-friendly way of differentiating between natural and synthetic stones. A survey of stones was imaged using the rig, in order to further understand the characteristics of natural, CVD synthetic and HPHT synthetic diamonds. Using the imaging rig, a CVD synthetic sample was identified as having a prompt luminescence similar to that of natural diamond. However, on delayed timescales the luminescence became green in colour, this is not a luminescence feature that has ever been recorded in natural diamond. Photoluminescence spectroscopy was carried out in order to determine the source of the green luminescence feature; a feature was observed at 499 nm which was attributed to this green colour. Observation of such a feature was originally made by Kong and Collins in 1992; since then, a feature has been observed at the same wavelength by both De Beers Technologies and the Gemological Institute of America (GIA). However, very little was known about the feature or its origin.

Luminescence spectroscopy was performed on three CVD synthetic gemstones, all of which displayed the 499 nm on delayed timescales. Further temperature dependent investigations have since shown that the defect can, in fact, be seen on both prompt and delayed timescales, however, at different temperatures. The 499 nm feature can be seen in the delayed luminescence at temperatures above 250 K and in prompt luminescence at temperatures below 110 K, mechanisms have been proposed for both prompt and delayed timescales. The 499 nm feature was also observed in a set of annealed stones that contained nitrogen and silicon; it was found that the 499 nm feature was only present in samples which had been annealed between 1600 °C and 2000 °C. Nitrogen vacancy centres are known to become mobile around 1600 °C, indicating that nitrogen could be involved in the defects structure. A comparison was carried out with a similar annealing sequence with comparable nitrogen concentration but negligible silicon concentration, the 499 nm spectral line was not observed in any of the annealed samples. This led to the conclusion that silicon could also be part of the 499 nm feature's structure. It is therefore hypothesised that both nitrogen and silicon are necessary for the formation of this colour centre.

Investigations into the electronic structure of features in diamond were carried out in regards to both the 499 nm spectral line and other luminescent features observed. A new energy level within the conduction band and valence band of diamond was proposed. It was also hypothesised that this level could be involved in filling the energy level producing the 499 nm emission. However, further work is needed in order to confirm this.

Characterisation of a defect seen at 499 nm in photoluminescence will have both scientific and industrial applications. If the lifetime is found to be long enough, this colour centre

could be a contender for use in quantum technologies. Equally, as the defect is only found in synthetic stones it can be another indicator used by jewellers and gemmologists to identify synthetic and natural stones.

7.2 Future Work

There are many aspects of this thesis which could be of interest for further study. Below is a brief list of work it was not possible to complete during the course of this PhD but which has shown promise for further study.

Much work was carried out into the characterisation of the 499 nm feature observed in the luminescence of some CVD synthetic diamond stones and many characteristics were identified. A structure was hypothesised; however, further work is required to conclusively prove or disprove the theorised structure. As previously discussed, characterisation of this defect could have both scientific and industrial applications.

Detailed EPR studies could be performed on diamonds containing the 499 nm feature in order to understand the spin state of the feature; again, this would prove useful for the characterisation of the defect.

A collaboration with Newcastle University was started using Density Functional Theory (DFT) to learn more about the structure of the 499 nm feature. Unfortunately, there was not sufficient time to complete this work but further computational modelling would be advised. Modelling of diamond lattices encompassing defects we know to be in all samples containing the 499 nm emission (e.g., silicon and nitrogen) would be very useful in theorising the identity of the 499 nm feature.

Further studies had been planned into the temperature dependence of the 499 nm feature to gain greater understanding of its electronic configuration in terms of energy levels and the mechanism for emitting the 499 nm light. These studies involved systematic study of stones known to contain the 499 nm spectral feature in order to ascertain whether the new spectral line hypothesised may be involved in the overall mechanism. Other CVD synthetics were also to be surveyed to learn more about energy levels within diamond and time dynamics of luminescence produced.

Further lifetime studies would be useful in order to understand more about the 499 nm features lifetime and whether it would be a contender for any kind of quantum application. Finding out the lifetimes of the other spectral features of interest, such as the blue luminescence features attributed to the new energy level proposed, may also

provide further information about whether this level is linked to the mechanism that produces the 499 nm emission.

Bibliography

- [1] Samuel Tolansky. *The history and use of diamond*. Methuen, 1962.
- [2] James Remington McCarthy. *Fire in the earth: The story of the diamond*. Harper & brothers, 1942.
- [3] Amanda S Barnard. *The diamond formula: diamond synthesis—a gemmological perspective*. Butterworth-Heinemann, 2000.
- [4] Antoine Laurent Lavoisier. *Premier mémoire sur la destruction du diamant par la feu*. Académie des sciences, 1772.
- [5] Christine Lehman. What is the “true” nature of diamond? *Nuncius*, 31(2):361–407, 2016.
- [6] Michael E Thomas and William J Tropsf. Optical properties of diamond. *Johns Hopkins APL Technical Digest*, 14(1):16–23, 1993.
- [7] Georg Will and Peter G Perkins. A scientific approach to hardness:: the hardness of diamond and cubic boron nitride. *Materials Letters*, 40(1):1–4, 1999.
- [8] JR Olson, RO Pohl, JW Vandersande, A Zoltan, TR Anthony, and WF Banholzer. Thermal conductivity of diamond between 170 and 1200 k and the isotope effect. *Physical Review B*, 47(22):14850, 1993.
- [9] John E. Graebner. *Thermal Conductivity of Diamond*, pages 285–318. Springer US, Boston, MA, 1995. ISBN 978-1-4615-2257-7. doi: 10.1007/978-1-4615-2257-7.7. URL https://doi.org/10.1007/978-1-4615-2257-7_7.
- [10] M Seal. Passive electronic applications. *Diamond and Related Materials*, 1(10-11): 1075–1081, 1992.
- [11] PA Nistor and PW May. Diamond thin films: giving biomedical applications a new shine. *Journal of the royal society interface*, 14(134):20170382, 2017.
- [12] Leon M Tolbert, Burak Ozpineci, S Kamrul Islam, and Madhu S Chinthavali. Wide bandgap semiconductors for utility applications. *semiconductors*, 1:3, 2003.

- [13] Paul Zimnisky. Global natural diamond production forecasted at 142m carats worth \$15.6 b. *Paul Zimnisky Diamond Analytics*, 2017.
- [14] TJ Brown, NE Idoine, CE Wrighton, ER Raycraft, SF Hobbs, RA Shaw, P Everett, EA Deady, and C Kresse. World mineral production 2015-2019. 2021.
- [15] Olya Linde, Oleg Geyler, and Ari Epstein. The global diamond industry 2018: A resilient industry shines through. 2018.
- [16] Y Spektorov, Olya Linde, and Pierre-Laurent Wetli. The global diamond industry: Portrait of growth. *Bain & Company*, 2012.
- [17] Wuyi Wang, Ulrika FS D’Haenens-Johansson, Paul Johnson, Kyaw Soe Moe, Erica Emerson, Mark E Newton, and Thomas M Moses. Cvd synthetic diamonds from gemesis corp. *Gems & Gemology*, 48(2), 2012.
- [18] Benjamin Esty. The de beers group: Launching lightbox jewelry for lab-grown diamonds. *HBS Strategy Case*, 2018.
- [19] De Beers Group of Companies. Media release: De beers group to launch new fashion jewelry brand with laboratory-grown diamonds, 2018. URL <https://www.debeersgroup.com/~media/Files/D/De-Beers-Group-V2/documents/company-news/2018/media-release-de-beers-group-to-launch-new-fashion-jewelry-brand-with-laboratory-grown-diamonds.pdf>.
- [20] Paul Zimnisky. Diamonds a not so shiny outlook. *Mining Review Africa*, 2019.
- [21] NQ Vinh, PT Greenland, K Litvinenko, B Redlich, AFG Van Der Meer, Stephen Anthony Lynch, M Warner, AM Stoneham, G Aeppli, DJ Paul, et al. Silicon as a model ion trap: Time domain measurements of donor rydberg states. *Proceedings of the National Academy of Sciences*, 105(31):10649–10653, 2008.
- [22] Alexander M Zaitsev. *Optical properties of diamond: a data handbook*. Springer Science & Business Media, 2013.
- [23] Lilian Childress and Ronald Hanson. Diamond nv centers for quantum computing and quantum networks. *MRS bulletin*, 38(2):134–138, 2013.
- [24] Stephen J Pearton, Assel Aitkaliyeva, Minghan Xian, Fan Ren, Ani Khachatryan, Adrian Ildefonsorosa, Zahabul Islam, Md Abu Jafar Rasel, Aman Haque, Alexander Y Polyakov, et al. Radiation damage in wide and ultra-wide bandgap semiconductors. *ECS Journal of Solid State Science and Technology*, 2021.

- [25] Karl E Spear and John P Dismukes. *Synthetic diamond: emerging CVD science and technology*, volume 25. John Wiley & Sons, 1994.
- [26] Thomas P Seward III and Terese Vascott. *High temperature glass melt property database for process modeling*. Wiley-American Ceramic Society, 2005.
- [27] Artem R Oganov, Russell J Hemley, Robert M Hazen, and Adrian P Jones. Structure, bonding, and mineralogy of carbon at extreme conditions. *Reviews in Mineralogy and Geochemistry*, 75(1):47–77, 2013.
- [28] Melissa B Kirkley. The origin of diamonds: Earth processes. *The nature of diamonds*. Edited by GE Harlow. Cambridge University Press, Cambridge, UK, pages 48–71, 1998.
- [29] FP Bundy, H Tracy Hall, HM Strong, and RH Wentorfjun. Man-made diamonds. *nature*, 176(4471):51–55, 1955.
- [30] M Werner and R Locher. Growth and application of undoped and doped diamond films. *Reports on Progress in Physics*, 61(12):1665, 1998.
- [31] JE Butler, Yu A Mankelevich, A Cheesman, Jie Ma, and MNR Ashfold. Understanding the chemical vapor deposition of diamond: recent progress. *Journal of Physics: Condensed Matter*, 21(36):364201, 2009.
- [32] AA Giardini and JE Tydings. Diamond synthesis: observations on the mechanism of formation. *American Mineralogist: Journal of Earth and Planetary Materials*, 47(11-12):1393–1421, 1962.
- [33] William Eversole. Synthesis of diamond, 1958.
- [34] John C Angus, Herbert A Will, and Wayne S Stanko. Growth of diamond seed crystals by vapor deposition. *Journal of Applied Physics*, 39(6):2915–2922, 1968.
- [35] Satoshi Koizumi, Christoph Nebel, and Milos Nesladek. *Physics and applications of CVD diamond*. John Wiley & Sons, 2008.
- [36] W Müller-Sebert, E Wörner, F Fuchs, C Wild, and P Koidl. Nitrogen induced increase of growth rate in chemical vapor deposition of diamond. *Applied Physics Letters*, 68(6):759–760, 1996.
- [37] J Barjon, E Rzepka, F Jomard, J-M Laroche, D Ballutaud, T Kociniewski, and J Chevallier. Silicon incorporation in cvd diamond layers. *physica status solidi (a)*, 202(11):2177–2181, 2005.

- [38] Martin Fischer, Stefan Gsell, Matthias Schreck, R Brescia, and Bernd Stritzker. Preparation of 4-inch ir/ysz/si (001) substrates for the large-area deposition of single-crystal diamond. *Diamond and related materials*, 17(7-10):1035–1038, 2008.
- [39] Richard F Mould. Sir william crookes (1832–1919) biography with special reference to x-rays. *Nowotwory. Journal of Oncology*, 67(1):79–88, 2017.
- [40] W Kaiser and WL Bond. Nitrogen, a major impurity in common type i diamond. *Physical Review*, 115(4):857, 1959.
- [41] WV Smith, PP Sorokin, IL Gelles, and GJ Lasher. Electron-spin resonance of nitrogen donors in diamond. *Physical Review*, 115(6):1546, 1959.
- [42] Ichiro Watanabe and Ken Sugata. Esr in diamond thin films synthesized by microwave plasma chemical vapor deposition. *Japanese journal of applied physics*, 27(10R):1808, 1988.
- [43] James E Shigley and Christopher M Breeding. Optical defects in diamond: A quick reference chart. *Gems & Gemology*, 49(2):107–111, 2013.
- [44] Simone Salustro, Giuseppe Sansone, Claudio M Zicovich-Wilson, Yves Noël, Lorenzo Maschio, and Roberto Dovesi. The a-center defect in diamond: quantum mechanical characterization through the infrared spectrum. *Physical Chemistry Chemical Physics*, 19(22):14478–14485, 2017.
- [45] Hsiao-Chi Lu, Meng-Yeh Lin, Sheng-Lung Chou, Yu-Chain Peng, Jen-Iu Lo, and Bing-Ming Cheng. Identification of nitrogen defects in diamond with photoluminescence excited in the 160–240 nm region. *Analytical chemistry*, 84(21):9596–9600, 2012.
- [46] MF Thomaz and G Davies. The decay time of n3 luminescence in natural diamond. *Proceedings of the Royal Society of London. A. Mathematical and Physical Sciences*, 362(1710):405–419, 1978.
- [47] AT Collins. Vacancy enhanced aggregation of nitrogen in diamond. *Journal of Physics C: Solid State Physics*, 13(14):2641, 1980.
- [48] AT Collins and SC Lawson. Cathodoluminescence studies of isotope shifts associated with localised vibrational modes in synthetic diamond. *Journal of Physics: Condensed Matter*, 1(39):6929, 1989.
- [49] Yoshimi Mita. Change of absorption spectra in type-ib diamond with heavy neutron irradiation. *Physical Review B*, 53(17):11360, 1996.

- [50] Chih-Kai Lin, Huan-Cheng Chang, M Hayashi, and SH Lin. Excitation properties of the h3 defect center in diamond: A theoretical study. *Chemical Physics Letters*, 475(1-3):68–72, 2009.
- [51] VS Vavilov and A Gippius. Investigation of the cathodoluminescence of epitaxial diamond films. *Sov. Phys. Semicond.*, 14(9):1078–1079, 1980.
- [52] U. F. S. D’Haenens-Johansson, A. M. Edmonds, B. L. Green, M. E. Newton, G. Davies, P. M. Martineau, R. U. A. Khan, and D. J. Twitchen. Optical properties of the neutral silicon split-vacancy center in diamond. *Phys. Rev. B*, 84:245208, Dec 2011. doi: 10.1103/PhysRevB.84.245208.
- [53] Jonas Nils Becker and Elke Neu. Chapter seven - the silicon vacancy center in diamond. In Christoph E. Nebel, Igor Aharonovich, Norikazu Mizuochi, and Mutsuko Hatano, editors, *Diamond for Quantum Applications Part 1*, volume 103 of *Semiconductors and Semimetals*, pages 201–235. Elsevier, 2020. doi: <https://doi.org/10.1016/bs.semsem.2020.04.001>.
- [54] Jonas Nils Becker and Elke Neu. The silicon vacancy center in diamond. 2020.
- [55] Igor I Vlasov, EA Ekimov, AA Basov, E Goovaerts, and AV Zoteev. On the origin of the raman scattering in heavily boron-doped diamond. *arXiv preprint arXiv:0801.1611*, 2008.
- [56] Christiane Albrecht. Joseph r. lakowicz: Principles of fluorescence spectroscopy, 2008.
- [57] N Ferrer and JM Nogues-Carulla. Characterisation study of cut gem diamond by ir spectroscopy. *Diamond and related materials*, 5(6-8):598–602, 1996.
- [58] James E Shigley and Christopher M Breeding. Visible absorption spectra of colored diamonds. *Gems & Gemology*, 51(1):41–43, 2015.
- [59] Marcello Picollo, Maurizio Aceto, and Tatiana Vitorino. Uv-vis spectroscopy. *Physical Sciences Reviews*, 4(4), 2018.
- [60] Qi Lu, Huaiyu Gong, Qingfeng Guo, Xuren Huang, and Jiayi Cai. Gemological characteristic difference between colorless cvd synthetic diamonds and natural diamonds. *Materials*, 14(20):6225, 2021.
- [61] Sally Eaton-Magana and Christopher M Breeding. An introduction to photoluminescence spectroscopy for diamond and its applications in gemology. *Gems & Gemology*, 52(1), 2016.

- [62] Yuri N Palyanov, Yuri M Borzdov, Alexander F Khokhryakov, and Igor N Kupriyanov. Effect of rare-earth element oxides on diamond crystallization in mg-based systems. *Crystals*, 9(6):300, 2019.
- [63] CM Welbourn, M Cooper, PM Spear, et al. De beers natural versus synthetic diamond verification instruments, 1996.
- [64] Colin D McGuinness, Amber M Wassell, Peter MP Lanigan, and Stephen A Lynch. Separation of natural from laboratory-grown diamond using time-gated luminescence imaging. *Gems & Gemology*, 56(2), 2020.
- [65] Vasilica Tucureanu, Alina Matei, and Andrei Marius Avram. Ftir spectroscopy for carbon family study. *Critical reviews in analytical chemistry*, 46(6):502–520, 2016.
- [66] AA Khomich, AN Dzeraviaha, ON Poklonskaya, AV Khomich, RA Khmelnsky, NA Poklonski, and VG Ralchenko. Effect of neutron irradiation on the hydrogen state in cvd diamond films. In *Journal of Physics: Conference Series*, volume 1135, page 012019. IOP Publishing, 2018.
- [67] Jong-Rang Kim, Shoo-Hack Shon, Su-Hun Kim, Ye-Won Lim, Jong-Gun Kim, Jeong-Jin Kim, and Yun-Deuk Jang. Application of ftir on the study of natural, synthetic and irradiated diamonds. *Journal of the Mineralogical Society of Korea*, 20(3):175–180, 2007.
- [68] Barry R Masters. A brief history of spectral analysis and astrospectroscopy. *Optics and Photonics News*, 20(11):34–39, 2009.
- [69] J.N. Miller. Fluorescence — instrumentation. In Paul Worsfold, Alan Townshend, and Colin Poole, editors, *Encyclopedia of Analytical Science (Second Edition)*, pages 106–112. Elsevier, Oxford, second edition edition, 2005. ISBN 978-0-12-369397-6. doi: <https://doi.org/10.1016/B0-12-369397-7/00163-1>.
- [70] VINCENT J COATES. A simple grating-prism dispersive arrangement which provides improved resolution over a wide spectral range. In *Advances in Molecular Spectroscopy*, pages 1270–1280. Elsevier, 1962.
- [71] Arthur B Shafer, Lawrence R Megill, and Leann Droppleman. Optimization of the czerny–turner spectrometer. *JOSA*, 54(7):879–887, 1964.
- [72] Andra Naresh Kumar Reddy and Dasari Karuna Sagar. Half-width at half-maximum, full-width at half-maximum analysis for resolution of asymmetrically apodized optical systems with slit apertures. *Pramana*, 84(1):117–126, 2015.
- [73] Christopher Palmer and Erwin G Loewen. Diffraction grating handbook. 2005.

- [74] Daniel J Schroeder. *Astronomical optics*. Elsevier, 1999.
- [75] Paul Spear and Christopher Welbourn. Distinguishing natural from synthetic diamonds, 1994.
- [76] Hannah Ponders Feist. Diamonds aren't always a consumer's best friend: Considering the need for regulation in the diamond grading industry. *Ga. J. Int'l & Comp. L.*, 46:261, 2017.
- [77] John M King, Ron H Geurts, Al M Gilbertson, and James E Shigley. Color grading "d-to-z" diamonds at the gia laboratory. *Gems & gemology*, 44(4), 2008.
- [78] Gion Calzaferri and Ruedi Rytz. The band structure of diamond. *The Journal of Physical Chemistry*, 100(26):11122–11124, 1996.
- [79] Alexandre Douplik, Guennadi Saiko, Irina Schelkanova, and Valery V Tuchin. The response of tissue to laser light. In *Lasers for Medical Applications*, pages 47–109. Elsevier, 2013.
- [80] David F Edwards and HR Philipp. Cubic carbon (diamond). In *Handbook of Optical Constants of Solids*, pages 665–673. Elsevier, 1997.
- [81] Philip Martineau, Mike Gaukroger, Riz Khan, and Dave Evans. Effect of steps on dislocations in cvd diamond grown on {001} substrates. *physica status solidi c*, 6(8):1953–1957, 2009.
- [82] Kenji Watanabe, Simon C Lawson, Junichi Isoya, Hisao Kanda, and Yoichiro Sato. Phosphorescence in high-pressure synthetic diamond. *Diamond and Related Materials*, 6(1):99–106, 1997.
- [83] YL Khong and AT Collins. Temperature dependence of cathodoluminescence from cvd diamond. *Diamond and Related Materials*, 2(1):1–5, 1993.
- [84] Hiroshi Kawarada, Takahiro Tsutsumi, Hiroki Hirayama, and Akira Yamaguchi. Dominant free-exciton recombination radiation in chemical vapor deposited diamonds. *Applied physics letters*, 64(4):451–453, 1994.
- [85] Hiroshi Kitawaki, Masahiro Yamamoto, Mio Hisanaga, Makoto Okano, and Kentaro Emori. Undisclosed samples of large cvd synthetic diamond, 2013.
- [86] Amber M Wassell, Colin D McGuinness, Chris Hodges, Peter MP Lanigan, David Fisher, Philip M Martineau, Mark E Newton, and Stephen A Lynch. Anomalous green luminescent properties in cvd synthetic diamonds. *physica status solidi (a)*, 2018.

- [87] JP Goss, PR Briddon, and MJ Shaw. Density functional simulations of silicon-containing point defects in diamond. *Physical Review B*, 76(7):075204, 2007.
- [88] BG Breeze, CJ Meara, XX Wu, CP Michaels, R Gupta, PL Diggle, MW Dale, BL Cann, T Ardon, UFS D’Haenens-Johansson, et al. Doubly charged silicon vacancy center, si-n complexes, and photochromism in n and si codoped diamond. *Physical Review B*, 101(18):184115, 2020.
- [89] Christopher M Breeding and Wuyi Wang. Occurrence of the si-v defect center in natural colorless gem diamonds. *Diamond and Related Materials*, 17(7-10):1335–1344, 2008.
- [90] UFS D’Haenens-Johansson, AM Edmonds, BL Green, ME Newton, G Davies, PM Martineau, RUA Khan, and DJ Twitchen. Optical properties of the neutral silicon split-vacancy center in diamond. *Physical Review B*, 84(24):245208, 2011.
- [91] Vladimir Nadolinny, Andrey Komarovskikh, and Yuri Palyanov. Incorporation of large impurity atoms into the diamond crystal lattice: Epr of split-vacancy defects in diamond. *Crystals*, 7(8):237, 2017.
- [92] VS Varichenko, AM Zaitsev, and VF Stelmakh. Luminescence of natural iia diamond implanted with nitrogen ions. *Physica Status Solidi. A, Applied Research*, 95(1):K25–K28, 1986.
- [93] Jasprit Singh. *Physics of Semiconductors and their Heterostructures*. McGraw-Hill College, 1993.
- [94] Simon M Sze, Yiming Li, and Kwok K Ng. *Physics of semiconductor devices*. John wiley & sons, 2021.